Study of Neutrino Oscillations in NOvA/DUNE experiments
(JINR Participation)
Project extension for the period 2021-2023

Project NOvA/DUNE

02-2-1099-2010/2023 Study of Neutrino Oscillations

N.Anfimov[1], A.Antoshkin[1], N.Balashov[3], A.Baranov[3], S.Bilenky[2], I.Butorov[1], V.Chalyshev[1], A.Chetverikov[1], A.Chukanov[1], A.Dolbilov[3], D.Fedoseev[1], V.Gromov[1], I.Kakorin[2], A.Kalitkina[4], O.Klimov[1], L.Kolupaeva[1], D.Korablev[1], V.Korsunov[4], C.Kullenberg[1], N.Kutovskiy[3], K.Kuzmin[2], E.Kuznetsov[3], K.Kuznetsova[1], V.Matveev[2], A.Morozova[1], V.Naumov[2], A.Olshevskiy[1], M.Petropavlova[4], O.Petrova[1], A.Rybnikov[1], O.Samoylov[1], A.Selyunin[1], V.Sharov[1], A.Sheshukov[1], S.Sokolov[1], A.Sotnikov[1], S.Vasina[1],

[1] Dzhelepov Laboratory of Nuclear Problems (DLNP)
[2] Bogolyubov Laboratory of Theoretical Physics (BLTP)
[3] Laboratory of Information Technologies (LIT)
[4] University Center (UNC)

Project Leader: **A.Olshevskiy**
Project Deputy Leader: **O.Samoylov**

Date of submission of proposal of project to SOD: **30/04/2020**

Date of the Laboratory STC: **23/04/2020** Document Number: **2020-6**

Date of Seminar on Physics of the Project: **03/04/2020, 07/04/2020, 09/04/2020, 10/04/2020**

Starting Date of Project: **2021**

(For Extension of Project — Date of its First Approval): **2015**

PROJECT ENDORSEMENT LIST

Study of Neutrino Oscillations in NOvA/DUNE experiments
(JINR Participation)
Project extension for the period 2021-2023

Project NOvA/DUNE

02-2-1099-2010/2023 Study of Neutrino Oscillations

A.Olshevskiy

APPROVED BY JINR DIRECTOR _____ _____

ENDORSED BY

JINR VICE-DIRECTOR _____ _____

CHIEF SCIENTIFIC SECRETARY _____ _____

CHIEF ENGINEER _____ _____

HEAD OF SCIENCE ORGANIZATION DEPARTMENT _____ _____

LABORATORY DIRECTOR _____ 6.05.2020

LABORATORY CHIEF ENGINEER _____ 06.05.2020

PROJECT LEADER 29/04/2020

PROJECT DEPUTY LEADER 29/04/2020

ENDORSED

RESPECTIVE PAC _____ _____

2

Schedule proposal and resources required for the implementation of the **project NOvA/DUNE**

Expenditures, resources, financing sources		Costs (k$) Resource Requirements	Proposals of the Laboratory on the distribution of finances and resources		
			1st year	2nd year	3rd year
Expenditures	1. ROC-Dubna upgrade, computer and equipment exchange, network, materials	25.0	15.0	5.0	5.0
	2. Laboratory equipment for measurements and tests (cryogenic and electronic), scintillators, etc.	45.0	15.0	15.0	15.0
	3. Materials and Equipment for the construction of the 2x2 prototype of Light Collection system for the DUNE Near Detector Liquid Argon modules (SiPM, fibers, cables, other components), electronic crates and modules.	250	100	100	50
	4. Computer Infrastructure (servers, disk storage)	300.0	100.0	100.0	100.0
Required resources	*Hours* — Experimental Workshop Design Bureau	2100 2400	700 800	700 800	700 800
	k$) — Travel money for NOvA and DUNE tasks in USA, CERN, Bern. Participation in Conferences and Collaboration meetings	300.0	100.0	100.0	100.0
Financing sources	Budget — Budget	**920.0**	**330.0**	**320.0**	**270.0**
	External — Additional contributions by collaborators, grants, etc. .	**30.0**	**10.0**	**10.0**	**10.0**

PROJECT LEADER:

Estimated expenditures for the **Project NOvA/DUNE**

Expenditure items	Full cost	1st year	2nd year	3rd year…
Direct expenses for the Project				
1. Accelerator, reactor	-	-	-	-
2. Computers	-	-	-	-
3. Computer connection k$	6.0	2.0	2.0	2.0
4. Design bureau (hours)	2400	800	800	800
5. Experimental Workshop (hours)	2100	700	700	700
6. Materials k$	54	18	18	18
7. Equipment k$	560	200	200	160
8. Construction/repair of premises	-	-	-	-
9. Payments for agreement-based research	-	-	-	-
10. Travel allowance (k$), including:	300	100	100	100
Total direct expenses	**920**	**320**	**320**	**280**

PROJECT LEADER:

LABORATORY DIRECTOR:

LABORATORY CHIEF ENGINEER-ECONOMIST:

Study of Neutrino Oscillations in NOvA/DUNE experiments

(JINR Participation)

Project extension for the period 2021-2023

Contents

1. Executive summary

The unique phenomenon of neutrino oscillations is well established by now and its parameters were measured in experiments of different types. However, the neutrino mass ordering (hierarchy) and lepton CP violation still remain unknown and are of the first priority in neutrino oscillation physics. Both questions can be addressed in accelerator-type long baseline experiments through the measurement of matter effects in atmospheric-regime neutrino oscillations.

NOvA is such an experiment studying oscillations in the beam from the Fermilab accelerator complex and using Near Detector at the Fermilab site and Far Detector placed 810 km away. Both detectors are of similar construction based on a large-volume liquid scintillator tracking calorimeter, and both are situated 14.6 mrad off-axis to the neutrino beam, optimizing the signal to background ratio. An important feature of experiment is the possibility to run with neutrino and antineutrino beams, which significantly improves sensitivity to the (generally degenerate) measured parameters.

At present the Fermilab accelerator complex is producing (anti)neutrinos from the proton beam of the record power of 700kW, which resulted in a large exposure used by NOvA in a recent analysis: 8.85e20 POT nu and 12.33e20 POT antinu. This is only a small part of the total statistics (36e20 POT nu and 36e20 POT antinu) expected to be taken for the approved period of running until 2025 in parallel with the beam power upgrade up to 900kW.

Further on, oscillation measurements will be continued in the DUNE project, which is planned to start operation in 2026 with 1.2MW (upgraded later to 2.4MW) beam power, longer baseline of 1300km and large volume Liquid Argon FAR detectors. Larger statistics, longer baseline and fine grained detectors of DUNE will provide significantly better sensitivity for oscillation parameters measurement.

The JINR group in NOvA is contributing significantly to the NOvA results and is well visible in the Collaboration.

The Remote Operation Center (ROC-Dubna) developed at JINR provides the possibility to fully participate in the data taking and quality monitoring. The computer infrastructure developed for NOvA at JINR on the basis of GRID and Cloud technologies is efficiently used for the home-based running of jobs and is also a part of the NOvA distributed computing resources system for the use at peak loads (e.g., before conferences). The NOvA electronics and scintillator test benches were set up at JINR and provide important measurements for simulation and calibration.

Members of the JINR group are deeply involved in the ongoing analyses and in the preparation of new ones. This comprises the 3-Flavor oscillation, Supernova, Slow monopole, Cosmic Ray and Near Detector physics teams. The JINR people are also involved in the development of simulation and analysis software, serving as a Detector Simulation convener, Offline and DAQ Software Release Managers, DAQ, DDT and ROC experts, etc.

While the successful involvement of JINR in NOvA will be continued, the JINR group is also planning to extend the scope of the present project to the preparation of DUNE. On the detector side a very good opportunity was developed by the R&D results in the framework of the Argoncube

Collaboration. The JINR group in Argoncube has developed the Light Collection System of Liquid Argon modules, which are approved by DUNE Collaboration as a Near Detector option.

By this project we are planning to contribute to the 4-module Argoncube demonstrator, which is expected as a next step of approval process by the DUNE Collaboration. We are also planning to contribute to the simulation and software development of different options of DUNE ND and extrapolate our NOvA analyses to the framework and conditions of DUNE.

The concurrent to the NOvA is the T2K experiment, running at KEK with ~3 times lower neutrino beam energy and baseline, and Super Kamiokande as a water cherenkov Far Detector. This measurement, being conceptually very similar to the NOvA one, has quite different sensitivity to the oscillation parameters due to different energy, baseline and detection techniques. At present NOvA and T2K results are compatible within the precision, dominated by statistics, and the work on preparing the NOvA and T2K combination is in progress with the JINR participation.

The T2K experiment also proposes continuation of measurements in the T2HK project, which will be competitive to DUNE in timescale and sensitivity. Our choice of DUNE is motivated by the continuity of our program from NOvA to DUNE and the very distinct and visible role we already achieved in analysis and detector techniques for NOvA and DUNE.

Finally, one should also mention another method of neutrino mass hierarchy determination in the JUNO reactor neutrino experiment, which should come with ~3-4 sigma sensitivity in 6 years after the startup in 2022. Such competition is positively considered, since the comparison of different results provide not only the cross check of each other, but being properly combined, introduce new features than a single result.

The work of NOvA/DUNE at JINR attracts a lot of attention from students and young staff. This provides a very good potential for growing and extending the JINR participation in this excellent physics with a good visibility.

2. Introduction

Recent discovery of a non-zero (and not so small) θ_{13} mixing angle has confirmed the possibility of studying neutrino mass hierarchy and lepton CP violation in accelerator-type long baseline experiments through the measurement of matter effects in atmospheric-regime neutrino oscillations.

NOvA is such a new generation experiment studying oscillations of muon to electron flavor neutrinos and antineutrinos. The NOvA apparatus consists of a Near Detector at the Fermilab site, where the muon neutrinos are produced by the NuMI facility, and a Far Detector placed 810 km away. Both detectors are of similar construction based on a large-volume liquid scintillator tracking calorimeter, and both are situated 14.6 mrad off-axis to the neutrino beam, optimizing the signal to background ratio.

Detector exposure in accelerator neutrino experiments is counted in terms of a number of protons delivered to the target (POT). In case of NOvA the proton NuMI beam at Fermilab with 120 GeV energy hits the carbon target. This interaction produces mesons, which decay into leptons and

neutrinos. The resulting neutrino beam composition in $1 - 5$ GeV region is: 95% ν_μ, 4% $\overline{\nu}_\mu$, 1% ν_e(93% $\overline{\nu}_\mu$, 6% ν_μ, 1% ν_e in the case of an antineutrino beam). The type of the beam depends on the polarity of the magnetic horns, which are focusing mesons of a particular sign.

Total amount of protons delivered to the target and accelerator beam power is shown in Figure 2.1. So far, a record beam power over 700 kW has been reached by the Fermilab accelerator complex. This beam power will be steadily increased up to 900 kW during NOvA operation approved until 2025. After that the DUNE project is planned to start operation with 1.2 MW beam power, and later upgrade it up to 2.4 MW. The DUNE project will also have a larger baseline of 1300 km and large volume fine grained liquid argon Far Detector.
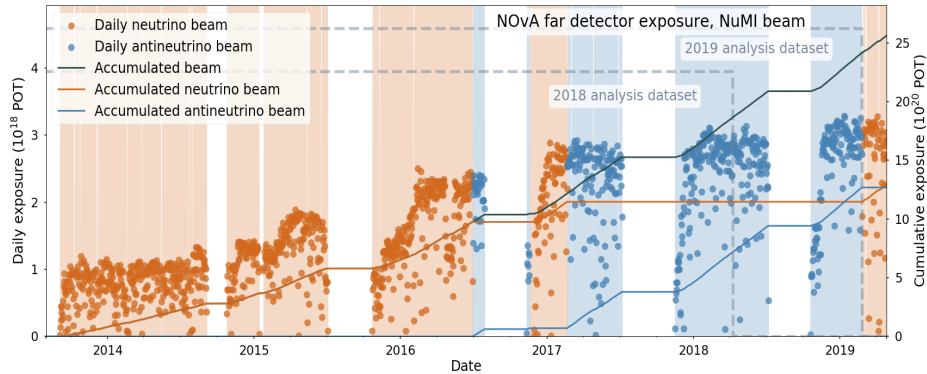

Figure 2.1. Exposure in POT recorded by the NOvA Far Detector.

Continuing the data collection NOvA can unambiguously resolve the neutrino mass hierarchy at >95% C.L. for about 2/3 of possible values of δ. For other values of this CP violation parameter, NOvA will provide δ-dependent hierarchy determination plus improved measurements of θ_{13}, θ_{23}, $|\Delta m^2_{23}|$, and δ itself, which is also very important for global analysis of the neutrino oscillation data.

During previous periods of the project the JINR group in NOvA has contributed significantly to the NOvA results. The Remote Operation Center (ROC-Dubna) was developed at JINR, giving the possibility to fully participate in the data taking and quality monitoring. The JINR computer infrastructure on the basis of GRID and Cloud technologies was developed. It is efficiently used for the home-based running of jobs and is also a part of the NOvA distributed computing resources system for the use at peak loads (e.g., before conferences). The NOvA electronics and scintillator test benches were set up at JINR and provided important measurements for simulation and calibration.

Members of the JINR group are deeply involved in the ongoing analyses and in the preparation of new ones. This comprises the ν_μ, ν_e, Supernova, Slow monopole, Cosmic Ray and Near Detector physics teams. The work is planned to be continued in the framework of the proposed prolongation of the project.

In addition, the JINR group is also planning to extend the scope of the present project to the preparation for the DUNE experiment. On the detector side a very good opportunity was already developed by our R&D results in the framework of the Argoncube Collaboration.

The JINR group in Argoncube has developed the Light Collection System of Liquid Argon Modules, which were recently approved by DUNE Collaboration as a Near Detector option.

In the present project we are planning to continue this R&D effort and, in particular, contribute to the construction and running of the ArgonCube 2x2 Demonstrator. The details of this work are presented below. We are also planning to contribute to the simulation and software development of different options of DUNE ND and extrapolate our NOvA analyses to the framework and conditions of DUNE.

In the next sections we present the status of the project work and plans for the project extension. Some more details are provided in the Appendix section.

3. Project Results and Plans

3.1. ROC-Dubna

The NOvA experiment at both the ND and FD sites have storages and file transfer systems to accumulate detector data. While this is safely done at the FD and ND locally, it is more efficient to monitor the operation of both systems from one location simultaneously, which can be accomplished from a Remote Operation Center (ROC).

Currently twenty five ROCs are operating for the NOvA experiment at different locations. The first non-US Remote Operation Center, ROC-Dubna, has been developed at JINR and started operation in October 2015. It has all of the necessary features and allows for full monitoring and control of FD and ND operation, as well as communication with FNAL services and other ROCs.

NOvA data storage and transfer software based on Linux-nodes collect information from NOvA DAQ system. ROCs connect to control and operation nodes on both FD/ND sites via VNC-tunneling under secure protocols. Basic idea is that a VNC server transfers a VNC session to many VNC viewers at ROCs with control. In total there are 5 active Scientific Linux based VNC-sessions are connected directly to Near/Far Detectors' nodes at FNAL and through GateWays to another World. System includes 1 Linux node for Web-monitoring of the
operated systems (Beam, ND/FD Cameras, Data transfer control, Ganglia, Nearline) and 1 Windows node for communication (NOvA electronic logbook, latest version of expert contact and Bulletin board, Polycom via Vidyo, Slack-chat, Skype, Zoom).

ROC-Dubna at JINR has developed infrastructure for 8 hours (a shift period) continuous   work (stable internet, international land-lines, kitchen, ROC is also a public JINR area). Computing monitoring system on Zabbix controls local Linux-nodes, internet connection, server conditions and notifies JINR experts in case of troubles.

ROC-Dubna is also a very popular public place for the excursion visits by Scholars, Teachers, Students, Journalists and other JINR guests. Its presence at JINR has significantly increased the interest in the NOvA experiment by young people.

3.2. Computing Infrastructure

NOvA and DUNE are the large-scale neutrino experiments which require a huge amount of computing resources to process all of its data. While the major amount of computing resources both experiments get from the local infrastructure at Fermilab - Fermigrid - they also rely on contributions from other participating organizations via the global distributed computing infrastructure Open Science Grid (OSG). DUNE, being an international collaboration, plans on gathering ~5000 CPU cores and 12 PB of data storage as a general collaboration contribution. JINR already has an established Multifunctional Information and Computing Complex (MICC) at the Laboratory of Information Technology (LIT), two components (Tier-2 cluster and JINR Cloud) of which were set up and extended to provide computing support to the NOvA, Mu2e and DUNE experiments through the OSG.

Specially for the NOvA experiment 24 new servers were purchased and added to the JINR Cloud extending its resources by 540 CPU cores and ~3 TB RAM. These servers were used to host VMs of the new batch cluster and the OSG-site, that allowed to process jobs from both local JINR NOvA team and the NOvA jobs coming from the OSG, contributing directly to the NOvA collaboration. In this system every component of a Grid-site is virtualized, which is a first-time experience for the JINR Grid-sites and is an important step for further development of computing models at JINR.

With the growth of the virtual computing cluster development of the local data storage for storing a copy of the most requested experimental data becomes the most urgent task. Creation of such a storage system is crucial for the efficiency of local data analysis performance. To form the storage backend 4 storage servers were purchased, added to the cloud's Ceph storage system. The already existing dCache storage at JINR was registered in the Sequential Access via Metadata (SAM) data handling system and a dedicated cloud virtual machine with a large Ceph block-device was created and configured to join the NOvA dCache pool extending its 3 TB NOvA quota by 50 TB. Grid jobs use the GridFTP door to transfer data via the GridFTP protocol.

Participation of JINR in the DUNE experiment analysis is expected to increase the load on both the data storage and computing cluster, therefore, the overall capacity of the JINR computing infrastructure will need to be increased.

The DUNE experiment plans to build a tiered distributed computing infrastructure (similar to CERN) to strengthen international cooperation. Current estimate is to have ~5000 CPU cores and 24 PB disk storage by 2022 (split 25/75 % between Fermilab and the rest of Collaboration) and a serious contribution is considered to be 5-10 %.

In terms of CPU it is already possible for JINR to fulfil the DUNE "Tier-2" requirements by the joint use of existing NOvA (and other neutrino experiments) shared resources, but the DUNE dedicated disk storage has to be purchased.

For the moment the DUNE Tier-2 node at JINR seems appropriate for the planned activities, but larger contributions can be discussed, particularly, in connection with the use of High Performance Computing technologies (the JINR "Govorun" super-computer) and possibility to have a joint DUNE computing effort agreement with russian institutes.

3.3. 3-Flavor Oscillation Analysis

An exposure used by NOvA in a recent analysis [3.3.1] was: 8.85×10^{20} POT (ν) and 12.33×10^{20} POT ($\bar{\nu}$). The experiment observed in the Far Detector 113 ν_μCC (102 $\bar{\nu}_\mu$ CC) candidates with a background expectation $4.2^{+0.8}_{-0.6}$ selected events with neutrino beam and $2.2^{+0.4}_{-0.4}$ events with an antineutrino beam. There were also 58 ν_e CC (27 $\bar{\nu}_e$ CC) candidate events with an expected background of $15.0^{+0.8}_{-0.9}$ and $10.3^{+0.6}_{-0.5}$ events for neutrino and antineutrino beam, respectively. This observation provides 4.4σ evidence of $\bar{\nu}_e$ appearance in an initially predominantly $\bar{\nu}_\mu$ beam.

In order to extract the oscillation parameters, a joint fit of ν_μ and ν_e spectra was performed. Solar oscillation parameters θ_{12} and Δm^2_{12} were fixed to the PDG values [3.3.2], while θ_{23}, Δm^2_{32}, δ_{CP} and neutrino mass hierarchy were varied. The value of θ_{13} was constrained by reactor experiment measurements. Analysis of NOvA is frequentist with profiled systematics and penalty terms. The details of analysis and results are presented in the Appendix section of this document.

The best fit of NOvA is: $\delta_{CP} = 0\pi, \sin^2\theta_{23} = 0.56^{+0.04}_{-0.03}, \Delta m^2_{32} = +2.48^{+0.11}_{-0.06} \times 10^{-3}\ eV^2$, which corresponds to the Normal neutrino mass hierarchy and upper octant of $\theta_{23} (> \pi/4)$.

Inverted mass hierarchy is disfavored at 1.9σ for all values of δ_{CP} and a large region in the Inverted hierarchy at $\delta_{CP} = \pi/2$ was ruled out at $> 4\sigma$.

Upper octant of θ_{23} is preferred at 1.6σ, but the result is still consistent with maximal mixing at 1.2σ.

All values of δ_{CP} in the Normal hierarchy and Upper octant of θ_{23} are allowed at 1.1σ.

New analysis with an increased exposure of 14×10^{20} POT (ν) and 12.33×10^{20} POT ($\bar{\nu}$) is planned to be ready by this summer for the Neutrino2020 conference. The JINR group was involved in different steps of NOvA three-flavor analysis procedure: cut tuning and event selection, extrapolation and predictions in the Far Detector, experiment sensitivities calculation and final data fits.

The NOvA experiment is expected to run until 2025, which implies approximately 36×10^{20} POT (ν) and 36×10^{20} POT ($\bar{\nu}$) POT collected during full operation. Figure 3.3.1 shows sensitivity to measure neutrino mass hierarchy after full run.
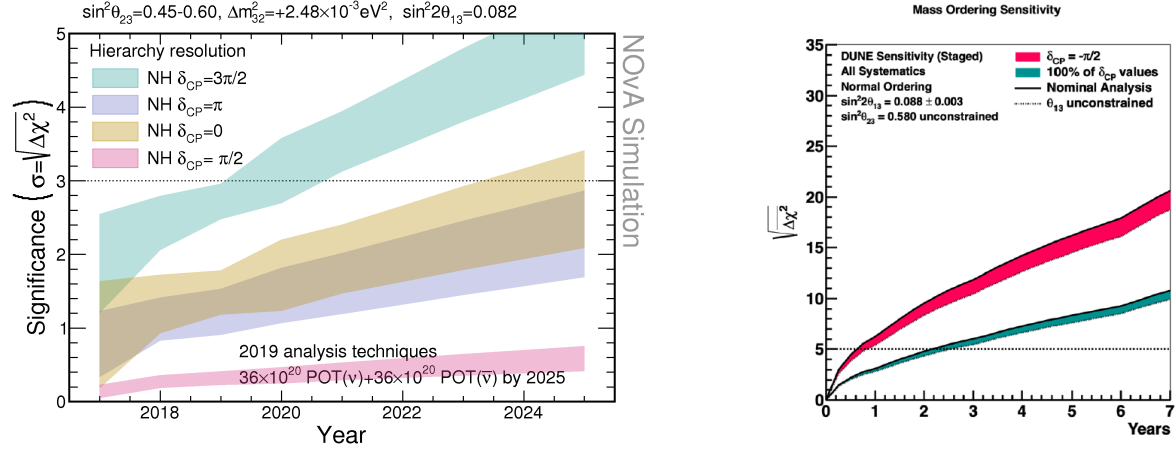
Figure 3.3.1. Projected sensitivities for upcoming years to measure neutrino mass hierarchy for NOvA (left) and DUNE (right)

NOvA is capable of measuring neutrino mass hierarchy up to 4σ and δ_{CP} up to 2σ depending on true δ_{CP} value in Nature (there are unlucky regions with $\delta_{CP} = 0, \pi$).

In 2021 NOvA and T2K (Japan) are planning to present the first joint data analysis. Several common groups were organized for the preparation of this work. This analysis can enhance the sensitivity to oscillation parameters.

The DUNE experiment is expected to start operations in 2025 with further beam and detector upgrades. First year of data taking will be with atmospheric neutrinos. Upgraded accelerator will start operations in 2026. Higher beam intensity, large detector volume, and long oscillation baseline make this experiment one of the best tools to probe neutrino oscillation parameters.

It is expected to have 5σ sensitivity to mass hierarchy after 2 years of DUNE beam running for any value of δ_{CP} (Figure 3.3.1) and 5σ sensitivity to 50% of δ_{CP} values after 10 years of beam running. More details on the comparison with other competitive projects are given in the Appendix section of this document.

3.4. Development of nuN Monte Carlo

For the recent NOvA analysis [3.4.1], neutrino interactions were modeled using the latest version of GENIE 3.0.6 [3.4.2] updated with new models, which allows a user to test several predefined sets of the generator parameters (so-called "tunes"). In particular, GENIE 3 includes completely updated quasielastic scattering (QES) event generation procedure and well-known Valencia models for charged current (CC) QES and meson exchange currents (MEC) processes with fixed bugs [3.4.3], which improve the agreement of MC-simulation with ND data significantly and lead to the partial elimination of reweighting.

To describe the cross section of CC0π-processes (process without any meson in final state) with bound nucleons in any kind of nuclei at all energies of interest we propose an empirical notion of the effective ("running") axial-vector mass of the nucleon as a simple recipe for calculating the

cross sections within the relativistic Fermi-gas model [3.4.4]. The approach allows describing one-particle-one-hole (1p1h) processes along with the effects beyond impulse approximation (short- and long-range nucleon correlation, MEC, etc). It is applicable to any nuclear target at all energies of interest and makes it possible to describe all available accelerator data on the total, differential, and double differential quasielastic cross sections by using only two adjustable parameters. Our previous analysis based on "running" axial-vector mass model [3.4.5, 3.4.6] (so-called "JINR-model") shows quite good agreement with ND data. In this analysis, we used Berger-Sehgal model for single pion production (SPP) simulation, while official NOvA one used Rein-Sehgal model [3.4.7, 3.4.8]. In the recent NOvA analysis, Berger-Sehgal model is also used, but unlike it we use for resonance axial mass value obtained from a global fit to available deuterium data, which is equal to 1.18 GeV.

As the empirical "running axial mass" enters in GENIE 3 among other models, it is quite easy to implement all settings for our analysis as a tune. We intend to include it in the official tunes list [3.4.9] to generate a small batch of events (mini-production) with JINR-model in the full data tuning and processing chain of the NOvA experiment and use it for both modeling and interpretation of the data in the ND and FD.

The SPP models currently implemented in GENIE does not account for interference between resonances and background contribution, which can result in additional uncertainties in simulation that requires additional studying. To clarify this issue, we are planning to implement MK-SPP model [3.4.10], which utilizes an alternative non-resonance background model and takes into account interference between resonances. The model allows defining the angular distribution of the final state pions that can be studied in the DUNE experiment.

A superscaling model SuSAv2+MEC [3.4.11] will be included in the future version of GENIE soon. It is an alternative to the Valencia model to describe the CC0π channel in neutrino interactions and the full regime in (e, e′) reactions. In collaboration with Granada University we intend to implement in GENIE another superscaling model − SuSAM* [3.4.12] using a scaling function extracted from a selection of the (e, e′) cross section data, and an effective nucleon mass inspired by the relativistic mean-field model of nuclear matter. This is a phenomenological model, which is technically much easier to implement, than SuSAv2+MEC and therefore we expect that such implementation will require less computing resources.

3.5. Detection of supernova signal

Detection of neutrino signals from the core-collapse supernova SN would be a valuable source of knowledge about both neutrino properties and the supernova explosion process. The NOvA experiment is sensitive to such signals if the supernova occurs within our galaxy. However, since the estimated rate of such events in our galaxy is 1-3 SN/century, an experiment expecting to detect SN neutrino signals should implement a real-time triggering system, continuously monitoring the detector data and measuring the significance of presence of SN neutrino bursts.

A dedicated software package named "GenieSNova" was developed to simulate interactions of supernova neutrinos inside the NOvA detectors. This new package generates neutrinos according to a supernova neutrino flux distribution including both the time structure and energy distributions. It then simulates neutrino interactions on the NOvA materials according to the detectors' geometry.

NOvA's Data-Driven Trigger (DDT) system is used to perform fast data reconstruction online in order to decide which time ranges of data should be saved for further offline analyses. To achieve this, the data stream from the detector is sliced into 5 ms chunks and subjected to background rejection and neutrino interaction candidates' reconstruction procedures in parallel DDT processes on NOvA Detectors.

After the parallel DDT processes have performed searches for IBD interaction candidates, the data on the candidate rate per 5 ms are sorted and accumulated in a time series. In order to decide if this time series contains a signal from a supernova, we use the log likelihood ratio function to discriminate between the "background-only" and "signal + background" hypotheses. This log likelihood ratio, depending on the signal hypothesis enhances the significance of the supernova signal detection and allows the SN triggering system to probe supernova models.

The trigger alert is issued when the significance exceeds the threshold corresponding to an average false triggering rate of one per week.

This threshold allows detection of the 27 M_{sun} at the distance 10.58 kpc (9.6 M_{sun} at 6.23 kpc) with at least 50% efficiency using the Far Detector of NOvA.

The plans for the future work on the supernova trigger include several directions.

Using the fact that the SN trigger system in NOvA is sensitive to the signal shape, we plan to estimate the sensitivity of NOvA to the neutrino oscillation parameters, in particular, neutrino mass hierarchy.

An improvement in the system sensitivity can be achieved by performing a meta analysis, combining the significance measurements from two NOvA detectors. Development of a real-time system for the significance combination and commissioning it on the NOvA detectors can also be used for the upgrade of the global SuperNova Early Warning System.

Also current work on the SN detection system can be applied for the future DUNE experiment, which is expected to be sensitive to the core-collapse SN neutrino up to ~ Mpc distance. This could provide the opportunity to study the effects of the neutrino oscillations, core-collapse shockwave instabilities, neutrino collective effects, and others.

Moreover, DUNE will feature several detectors with various detection techniques, which would allow to study flavour composition of the SN neutrino signal, providing additional capabilities to study the core-collapse process and neutrino properties. In view of this, the development of the real-time combination system should also be useful, when applied to DUNE.

3.6. Search for Monopole

The NOvA neutrino detector was designed to search for the transition of muon neutrinos to electron neutrinos. Its Far Detector is a 14 kt segmented liquid scintillator detector on the surface.We report on a search for a slow magnetic monopole component of the cosmic ray flux in 95 days of live time. No events consistent with monopoles were observed. Because NOvA lacks significant overburden, a new limit of $<2\times10^{-14}$ cm^2 s^{-1} sr^{-1}at 90% C.L. is set on the flux of monopoles with $6\times10^{-4} < \beta < 5\times10^{-3}$ and mass $>5\times10^{8}$ GeV, a previously unexplored region of phase space.

The NOvA detectors were designed to measure energy deposition of particles with β near 1, which traverse each cell in the detector in under a nanosecond. No consideration was given in the design phase to particles depositing energy over as much as a microsecond, as monopoles at the lower end of our sensitivity would. In order to verify our simulation of the detector response to such slow signals, we performed a dedicated test stand measurement which simulated monopole signals using light pulses generated by LEDs. The ratio of the measured signal to the simulation was 1.0±0.1.

While this indicates no trouble, to conservatively account for the possibility that signals from slow energy depositions are overmodeled in our detector simulation, we reduce the signal by 10% in our simulation.

By virtue of a large fine-grained detector on the Earth's surface, NOvA is uniquely sensitive to slow intermediate-mass monopoles which would not reach previous detectors such as MACRO. We have constrained the flux of this population of monopoles in a large region of speed-mass space which had previously been unconstrained. For heavier monopoles, our result confirms previous limits.

The results obtained in NOvA represent less than 10% of the data collected so far by the NOvA Far Detector. The data following October 2015 was taken at a higher APD gain, allowing collection of fainter signals and, therefore, an improved mass reach. We plan to continue the slow monopole analysis with a high APD gain period of data taking.

3.7. Physics with Cosmic Muons

The Far Detector of the NOvA experiment is located on the surface and due to large dimensions it detects 10^5 atmospheric muons per second. Based on this, NOvA Collaboration provides several researches connected to atmospheric muons, and has opportunities for some more. JINR team already participates in the measurement of the East-West asymmetry of secondary cosmic rays and in the study of very high-energetic muon events in the Far Detector. Also, NOvA members study seasonal variations of atmospheric muon flux (multi-muon event research was finished and printed in [3.7.1]) and events with high multiplicity parallel cosmic muons from Extensive Air Showers in the NOvA Far Detector.

High-energy cosmic-ray muons

Analysis of muons with the energies higher than 100 GeV, produced in the upper atmosphere, can provide information about the spectrum and composition of primary cosmic rays and the details of the interaction of hadrons with nuclei at energies inaccessible to current accelerators.

It is possible to estimate the energy spectrum of these high-energy muons using the method named "parmeter" [3.7.2]. It is one of the methods of muon energy reconstruction, based on measuring the specific components of energy loss.

Muon energy loss can be defined as *-(dE/dx)=a+bE*, where *a* is the ionisation energy (delta-electrons) loss and *bE* is the sum of e-pair production, bremsstrahlung, and photonuclear contributions (*a* and *b* are slowly varying function of the muon energy). Above 1 TeV energy loss is almost proportional to *E*.

The key point of the implementation of this method is the separation of relatively mild fluctuating loss on the e-pair formation and catastrophic collisions in the processes of bremsstrahlung and nuclear interactions. So far we are concentrating on the trigger conditions and MC studies. When we manage this, we will be able to estimate the muon energy from its energy loss.

East-west asymmetry

East-West asymmetry of atmospheric muons is defined as A=(W-E)/(W+E), where W is muon flux coming from West, E is one from East. The phenomenon is based on the Lorentz force, that incline charged particles, moving in a geomagnetic field. East-west asymmetry measurements can improve the knowledge about the geomagnetic field and primary cosmic rays.

The study of east-west asymmetry in the Far Detector of NOvA is complicated by the fact that the overburden covering the detector and the rock surrounding it are also asymmetrical.

East-west asymmetry of atmospheric muon fluxes, detected in the NOvA Far Detector, was so far measured on 122 millions reconstructed tracks. The contribution of the anisotropic detector environment was previously estimated by using MC-generator CRY, where the geomagnetic effect of East-West asymmetry is not implemented.

As a first step, the reconstruction efficiency of muons stopping in the detector was estimated depending on the arrival direction: according to the expectation, the reconstruction efficiency of tracks aligned with the planes that make up the detector structure turned out to be significantly lower: about 60% and 50% for muons moving in +/-10 degrees from the vertical and horizontal, respectively, with efficiency in other areas of about 80%. Initial energy reconstruction of a stopped muon was made by four methods. To describe the absorption of muons in matter and the efficiency of muon parameter reconstruction, a Monte Carlo simulation of 10 million muon tracks has been created. In the future we are going to use the regularization of the inversion procedure according to the Tikhonov method.

3.8. NOvA hardware results and plans

During the years of the NOvA experiment operation a comprehensive understanding of the NOvA detectors performance was achieved, in particular, due to important additional measurements of electronics and scintillator parameters performed at JINR test benches.

The NOvA electronics test bench (Fig.3.8.1) was developed at JINR using Avalanche PhotoDiodes and Front-End Board of the actual NOvA electronics.
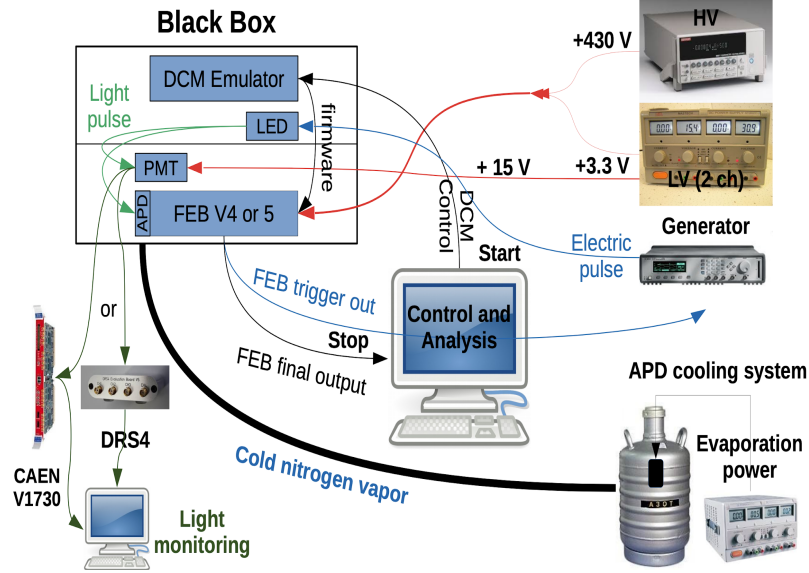
Figure 3.8.1. Scheme of the NOvA electronics test bench at JINR.

There were several measurements performed at this electronics test bench:

- An important parameter of electronics operation is a cross-talk between different channels. The effect of the cross-talk is particularly important for large signals, which resulted in NOvA electronics by the, so-called, flashes: clusters with high hit multiplicity, the origin of which was unknown. It was found in our measurements that this effect is due to the capacitance coupling of APDs in the common bias voltage supply and quantitative characteristics of this effect were introduced in the detector simulation.
- The setup was also adapted to check the response of the electronics to the long signals. By adding to the setup PMT and standalone ADC we were able to monitor the shape of the initial light pulse and study the NOvA electronics channel response to the long signals of different shapes. The results of measurements were introduced in the NOvA detector simulation. This was important for studying the sensitivity of the NOvA detector to the detection of the exotic slow monopoles.
- There was a general request to measure precisely all of the NOvA electronics shaping parameters. The scheme of the measurement was the same as aforementioned. We have found that the fall time of the output signal depends linearly on the input signal amplitude and the rise time variation is negligible. The results of measurements were included in the NOvA detector simulation.

Another challenge in simulating the NOvA detector response is the scintillator light output to different particles. In particular, the light from a scintillator is known to be saturated for particles with high density of ionization losses (so-called, Birks law). In the case of NOvA it was necessary to measure Birks coefficients for protons of MeV energy scale. The scheme of the setup is presented in Fig.3.8.2. The protons from the NOvA scintillator in the cuvette (Sc) are hit by the neutrons from the Pu-Be source. Selecting neutrons with different energies we can extract recoil proton spectrum and its edge is equal to the primary neutron energy, which we know from TOF measurement between NaI and Sc.
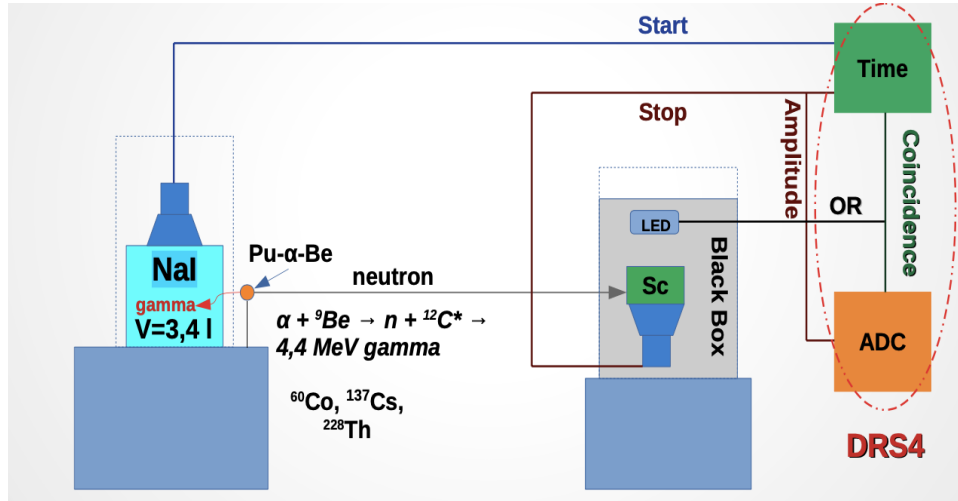
Figure 3.8.2. Scheme of scintillator light output measurements.

Response from protons was calibrated with respect to gamma-sources ^{137}Cs, ^{60}Co, ^{228}Th assuming negligible quenching effect for fast electrons. Finally, data were analysed by using NOvA simulation software based on GEANT deposit energies and custom simulation for light output. The results were found to be in good agreement with each other and cross-checks performed. This validated the full chain of the NOvA simulation software.

In addition, we also measured the actual density and density temperature dependence of the NOvA scintillator.

Our future plan is to measure the contribution of the Cherenkov light in the NOvA LS, which is also important for the NOvA detector simulation. We will set up a new measurement scheme, which will use the monochromatic γ-source (e.g., ^{137}Cs). We have to prepare a radioactive premise to perform this measurement and purchase PMTs, NaI-crystals, radioactive sources and other materials.

4. Light Collection System for the DUNE ND

The DUNE is a next generation project of accelerator long baseline neutrino facility at Fermilab (LBNF), which the JINR is considering to pursue after NOvA at NuMI. In addition to the continuation of analyses, developed for NOvA, we are planning to contribute to the DUNE Near Detector (ND) and its physics since the start of the project.

One of the main neutrino detection systems in the ND is a modular structure one-phase Liquid Argon TPC, dubbed ArgonCube. The total system will be a 5x7 array of the TPC modules with a size of $1.0 \times 1.0 \times 3.5 \text{m}^3$. To confirm the modular operation a 2x2 demonstrator is being constructed

for tests at the Fermilab NuMi beam. The demonstrator contains 4 prototypes of smaller TPC modules with dimensions of $0.67 \times 0.67 \times 1.81 m^3$.

ArgonCube offers true 3D tracking information using a pixelated charge readout. The charge readout window (drift time) of 137µs is long compared to the 10µs beam spills at NuMI and LBNF beams. Neutrino interactions overlap and individual energy deposits cannot be easily associated with a specific neutrino vertex. This problem can be solved by incorporating fast timing information from the prompt scintillation light emitted by the charged particles in LAr at ~127 nm wavelengths along with ionization. The module's opaque cathode and walls contain scintillation light within each TPC (half module), improving the detection efficiency of the prompt component of the scintillation light. The solution developed by the ArgonCube effort (Fig.4.1) is a Light Collection Module (LCM) (or another option: ArcLight), which is a compact dielectric light trap allowing for light collection from a large area and inside high electric fields.
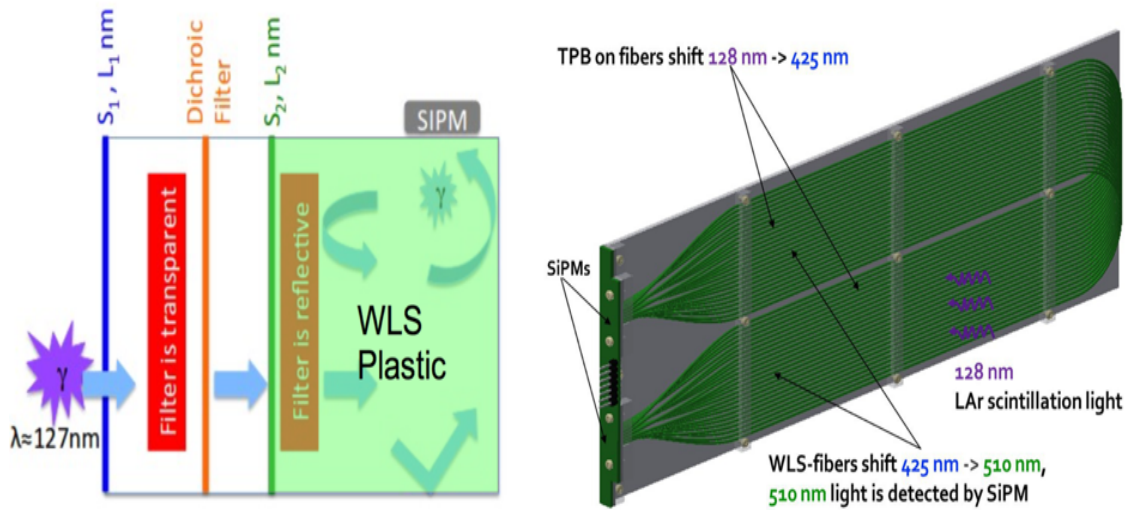
Figure 4.1.: Scheme of the operation for ArcLight (left) and LCM (right).

Both approaches are based on the two-stage wavelength shifting: first is from 127 nm (VUV) to 425 nm (blue) to increase the light penetration and then trap the blue light in a plastic bulk with dichroic mirror or in a fiber core by shifting it to green light (~510 nm). Finally, the green light is read out by Silicon Photomultipliers.

In the ArgonCube collaboration, JINR took responsibility to provide and produce the complete light readout system. This includes: LCM/ArcLight modules, Front-End electronics (preamplifiers), ADC, power supply system, signal/power lines, DAQ and Slow Control. Our joint effort is also to implement light readout with charge readout by using time and data synchronization between two systems.

The readout chain is as follows. The light signal is read out by SiPMs sitting on a PCB. The PCB interfaces to E-shape PCB that supplies power for six SiPMs and drives their responses to long coax signal lines out of the TPC cryostat. Then the signals are adjusted and transformed to differential signal lines by Variable-Gain Amplifiers and sent thereafter to the ADCs. The ADCs are 100 MHz sampling converters designed at JINR (VBLHEP) for NICA/MPD ECAL readout and adapted for our needs.

As a part of R&D for ArgonCube we have constructed at JINR (DLNP) a cryogenic stand, which allowed numerous tests of the light readout system: light detection efficiency of different light collection modules, electronics, mechanical stresses, etc. The prototype of the readout chain (right) and the setup for cryogenic tests (left) are shown in Fig.4.2.

For the power supply system, we are considering two options. Option "A" is to bias SiPM with a single operating voltage. This option is provided by the HVSYS company, which has long experience working with JINR in producing power supplies for SiPM (e.g., COMPASS ECAL0). Option "B" is to use common bias on one side and deliver additional bias by Digital-to-Analog Converters (DAC). We are aiming to implement option "B" leaving "A" as a backup solution. We have already demonstrated a prototype of the power supply using TI DAC81416 DAC with a prototype of the slow control software.
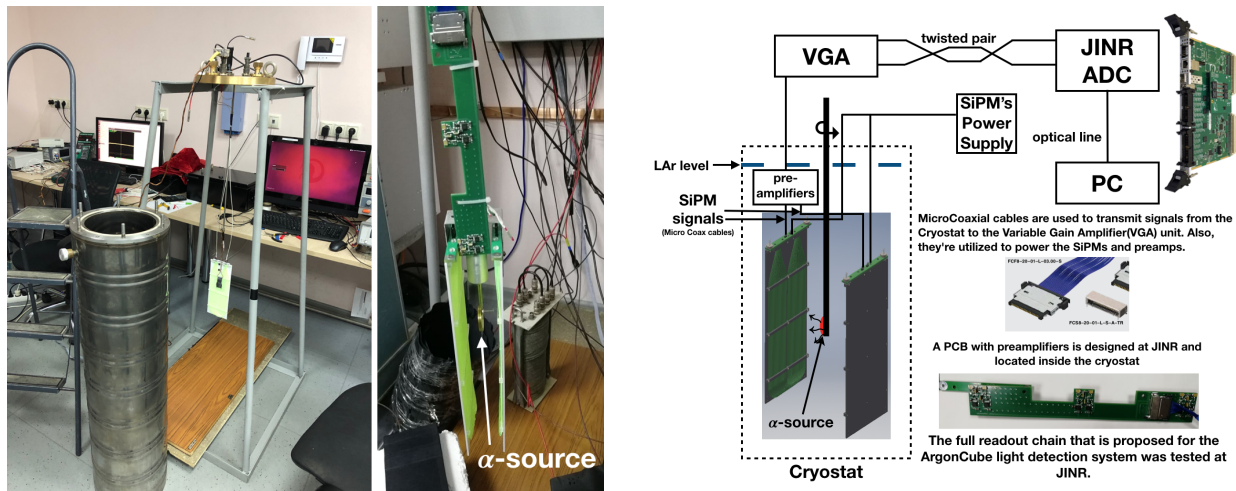
Figure 4.2.: Cryogenic standt (left) and scheme of readout chain (right).

In total, to provide the 2x2 demonstrator tests we need to supply ~250 LCM modules ~(5 km of optical fiber), ~500 SiPMs, 500 channels of power supply, 10 ADC, ~100 E-Shape PCB with 6 preamplifiers each, ~100 micro coaxial 20-line cable assemblies, ~600 VGAs, 300 m of 32-twisted pair cables. This will require ~200 kUSD for purchase of materials, equipment and production contracts.

The next step will be to prototype full size (50 cm long) LCM and ArcLight modules. This will need extra materials, equipment and contracts of ~50 kUSD.

5. Tasks and Manpower at JINR

#	Name	Laboratory	Tasks	FTE
1	Anfimov Nikolay	DLNP	Methodical group leader	0.6
2	Antoshkin Alexander	DLNP	Test bench measurements; Slow monopole analysis; ROC-liaison;	1.0
3	Balashov Nikita	LIT	Computing	0.3
4	Baranov Alexander	LIT	Computing, cloud	0.1
5	Bilenky Samoil	BLTP	Oscillation theory	0.1
6	Butorov Ilya	DLNP	Software/analysis	0.5
7	Chalyshev Vyacheslav	DLNP	Mechanics	0.5
8	Chetverikov Alexey	DLNP	Mechanics/electronics engineering	0.7
9	Chukanov Artem	DLNP	Det., Light R/O Simulations	0.3
10	Dolbilov, Andrey	LIT	Computing, network support	0.1
11	Fedoseev Dmitry	DLNP	Mechanics/electronics engineering	0.7
12	Gromov Vasiliy	DLNP	Slow-Control software	0.5
13	Kakorin Igor	BLTP	Det simulation, GENIE	1.0
14	Kalitkina Anastasia	UNC	Master student, data analysis, NOvA software release manager	1.0
15	Klimov Oleg	DLNP	Reconstruction, proton ID	0.6
16	Kolupaeva Liudmila	DLNP	PhD student, 3-flavor oscillation analysis	1.0
17	Korablev Denis	DLNP	Light R/O DAQ expert	0.4
18	Korsunov Vladislav	UNC	Bachelor student, sterile neutrino analysis	1.0
19	Kullenberg Christopher	DLNP	ND Physics, coh pion	0.6

20	Kutovskiy Nikolay	LIT	Computing hardware support	0.3
21	Kuzmin, Konstantin	BLTP	Det sim, cross sec theory	0.1
22	Kuznetsov Evgeny	LIT	Computing hardware	0.1
23	Kuznetsova Ksenia	DLNP	Analysis/measurements	0.7
24	Matveev Victor	BLTP	Theory, Coll management	0.1
25	Morozova Anna	DLNP	PhD student, Exotics, CR muons	1.0
26	Naumov, Vadim	BLTP	Osc and cross sec theory	0.3
27	Olshevskiy Alexander	DLNP	Coll and JINR tasks management, IB-rep	0.5
28	Petropavlova Maria	UNC	Master student, Supernova analysis	1.0
29	Petrova Olga	DLNP	Exotics, CR muons	1.0
30	Rybnikov Arseniy	DLNP	Software/analysis/measurements	0.7
31	Samoylov Oleg	DLNP	Det sim, co-convener; Det control, ROC-manager; JINR ana coordinations; Coll manag, deputy at JINR;	1.0
32	Selyunin Alexander	DLNP	Methodical group deputy: software, hardware, analysis, measurements	0.8
33	Sharov Vladislav	DLNP	Software/analysis	0.5
34	Sheshukov Andrey	DLNP	DAQ: software dev/support; DDT: supernova trigger; Exotics: SN detection; Detector control: ROC software;	1.0
35	Sokolov Sergey	DLNP	Mechanics/machinery	0.5
36	Sotnikov, Albert	DLNP	Hardware measurements and analysis	0.3
37	Vasina Svetlana	DLNP	Detector simulation	0.3
	TOTAL			**21.2**

The average age of the JINR NOvA team is ~35 years. There are: 1 bachelor, 2 master and 2 PhD students; 14 young research scientists also preparing PhD (5 of them are ready to present their thesis in the near future), 10 engineers, 4 staff members with PhD degrees and 4 professors.

6. Plans and Requested resources

During the whole project extension period we are planning to maintain and further develop NOvA data analyses presented above and update their results on the basis of available data sets. In addition, we will start to adapt those analysis tools for use in the DUNE environment and continue to work on general and analysis software development.

During 2021-2023 the JINR ROC-Dubna and computer infrastructure will be upgraded to cope with the demand of further NOvA operation and an estimate of the DUNE computing request for Tier 2.

As a major hardware task of the project we plan to construct the whole Light Collection System of the 2x2 ArgonCube Demonstrator, which is planned to be tested at Fermilab as a prototype of the liquid argon part of DUNE Near Detector. We also plan to perform additional measurements of the NOvA scintillator light output and include our results in the detector simulation.

The following resources are requested for the proposed extension of the NOvA/DUNE project at JINR for the period of 2021-2023:

1. 25K$ - Maintenance and upgrade of the ROC-Dubna. Office equipment (ageing desktop and laptop computer replacement) for team members.

2. 45K$ - Laboratory equipment for tests. Additional hardware for tests, including DAQ and analysis computers.

3. 250K$ - Construction of the Liquid Argon Light Collection system for the 2x2 ArgonCube DUNE ND Demonstrator.

4. 300K$ - Computing infrastructure extension. We plan to add ~2PB of disk storage to the common NOvA/DUNE resources in the framework of the JINR neutrino experiments platform.

5. 300K$ - money for visiting the NOvA and DUNE collaborating laboratories, participating in conferences and meetings.

7. SWOT Analysis

	Helpful	Harmful
Internal	**STRENGTHS** • Already fully operational NOvA experiment with the detector and beam parameters confirmed • Possibility to improve significantly in the next several years our knowledge on the neutrino Mass Hierarchy, CPV determination and other oscillation parameters, including θ_{23} octant determination • Rich non-oscillation program	**WEAKNESSES** • Failure to deliver in time flux expected from NuMI for NOvA (and DUNE) • Low sensitivity in certain cases of Neutrino Hierarchy and CPV combinations • Systematic error sources depending on unknown cross sections and detector features
External	**OPPORTUNITIES** • Supernova burst, new physics existence • Systematic errors reduction due to new measurements or theory improvement • Approved NOvA running until 2025 and changeover to DUNE after that	**THREATS** • Major accident with detector or beam hardware • Unexpected change in Fermilab plans due to significant budget cuts or major changes in the world situation

For the period until 2025 NOvA has a very good chance to be the first in many aspects of Mass Hierarchy, CPV and θ_{23} octant determination. This statement is highly reliable because NuMI complex, NOvA detectors and software tools are already used and have confirmed projected performance and sensitivities. New analyses have been developed and some more are in progress.

An opportunity of running NOvA until 2025 has been approved at Fermilab along with the upgrade of NuMI to ~900kW beam power, which will provide a significant increase in sensitivity and good opportunity for the world leadership. After that the DUNE experiment will take over with significantly extended possibilities.

The sensitivity of the NOvA experiment is actually dependent on a particular value of Mass Hierarchy and CPV phase, realized in Nature. The probability to distinguish between degenerate regions of (NH, $\pi/2$) and (IH, $3\pi/2$) is the lowest and significant data statistics collection becomes crucial. Some of the systematic errors of the experiment depend on the external information and modelling of the cross sections and detector response. Being a weakness, this, at the same time, represents an opportunity for improvement if the corresponding measurements in NOvA/DUNE itself or elsewhere will be successful.

The major opportunity for many of the experiments will be the Supernova burst in our galaxy or existence of a new physics. The ability of NOvA to detect such events was confirmed and all

necessary components are in place. It is expected that this opportunity will be even more pronounced in DUNE.

8. References

[3.3.1] M. Acero et al. [NOvA Collaboration] "First Measurement of Neutrino Oscillation Parameters using Neutrinos and Antineutrinos by NOvA", Phys.Rev.Lett. 123 (2019) 15, 151803
[3.3.2] M. Tanabashi et al. [Particle Data Group], Phys. Rev. D 98, no. 3, 030001 (2018).
[3.4.1] K. Bays. Internal report. DocDB # 43581.
[3.4.2] C. Andreopoulos et al., The GENIE Neutrino Monte Carlo Generator, Nucl. Instrum. Meth. A614, 87 (2010).
[3.4.3] https://hep.ph.liv.ac.uk/~costasa/genie/releases.html
[3.4.4] I.D. Kakorin, K.S. Kuzmin and V.A. Naumov. An unified empirical model for quasielastic interactions of neutrino and antineutrino with nuclei (Accepted in PEPAN Letters).
[3.4.5] I.D. Kakorin, K.S. Kuzmin and V.A. Naumov. Internal report. DocDB # 38061.
[3.4.6] I.D. Kakorin, K.S. Kuzmin and V.A. Naumov. Internal report. DocDB # 23018.
[3.4.7] P. Adamson et al. (NOvA Collaboration), Phys.Rev.Lett. 118, 151802 (2017), ibid. 118, 231801 (2017).
[3.4.8] D. Rein and L.M. Sehgal. Annals Phys. 133, 79 (1981).
[3.4.9] https://hep.ph.liv.ac.uk/~costasa/genie/tunes.html
[3.4.10] M. Kabirnezhad. Phys.Rev.D 97, 013002 (2018).
[3.4.11] S. Dolan et al. Phys.Rev.D 101, 033003 (2020).
[3.4.12] I. Ruiz Simo et al. Phys.Rev. D 97, 116006 (2018).
[3.7.1] NOvA Collaboration (M.A. Acero (U. Atlantico, Barranquilla) et al.) Observation of seasonal variation of atmospheric multiple-muon events in the NOvA Near Detector // Phys.Rev. D99 (2019) no.12, 122004.
[3.7.2] R. P. Kokoulin, A. A. Petrukhin, Phys. Part. Nucl. (Zh. Fiz. Elem. Chast. Atom. Yadra) (In russian), 21, no. 3, 774 (1990).

9. Recent conference reports and seminars

1. A.Antoshkin, Slow monopole bench work, NOvA Collaboration Meeting, 21-24 February 2019.
2. A.Antoshkin, Electronic test stand at Dubna, NOvA Collaboration Meeting, 21-24 February 2019.
3. A.Antoshkin, Slow monopole bench work, NOvA Collaboration Meeting, 3-7 June 2019.
4. A.Antoshkin, Electronic test stand, NOvA Collaboration Meeting, 3-7 June 2019.
5. A.Antoshkin, E. C. Dukes, R. Ehrlich, M. J. Frank, E. Song, Subluminal Magnetic Monopole Search with NOvA, Madison, USA, 24 July - 1 August, ICRC 2019.
6. N.Anfimov. Light Readout System of the ArgonCube Liquid Argon Modular TPC for the Near Detector of the DUNE experiment. DLNP seminar, JINR, Dubna, Russia, 09 April 2020.

7. Nikolay Anfimov, Oleg Samoylov, Adam Aurisano, Alexander Antoshkin, Albert Sotnikov, Improvements in the NOvA Detector Simulationbased on JINR stand measurements, INSTR2020, Novosibirsk, Russia, 24-28 February 2020.

8. N. Anfimov. NOvA Benchmarking at Dubna. NOvA Collaboration Meeting, Irvine, USA, 13-16 February 2020.

9. N. Anfimov. Light Readout System. DUNE Collaboration meeting, CERN, January 27 - 31 2020.

10. N. Anfimov. Status of Measurements for the NOvA Liquid Scintillator. Sussex, Great Britain, June 3-7 2019

11. N. Anfimov. Light Readout System for ArgonCube prototype, DUNE ND workshop, Fermilab, May 25-27, 2019.

12. N. Anfimov. Photon Detection System: Electronics and Status. ArgonCube Collaboration Meeting, Bern, Switzerland, March 21-23, 2019.

13. Oleg Samoylov, Adam Aurisano, Nikolay Anfimov, Alexander Antoshkin, Albert Sotnikov, Improvements in the NOvA Detector Simulation based on JINR stand measurements, Boston, USA, 29 July - 2 August, DPF 2019.

14. A.Antoshkin, Slow monopole bench work, NOvA Collaboration Meeting, 10-13 October 2019.

15. Oleg Samoylov, Adam Aurisano, Nikolay Anfimov, Alexander Antoshkin, Improvements in the NOvA Detector Simulation based on JINR stand measurements, Nuclear Electronics and Computing 2019 (NEC-2019), 30 September — 4 October, 2019, Montenegro.

16. Oleg Samoylov, Adam Aurisano, Nikolay Anfimov, Alexander Antoshkin, Albert Sotnikov, Shiqi Yu, Improvements in the NOvA Detector Simulationbased on JINR stand measurements, Adelaide, Australia, 4-8 November, CHEP 2019.

17. О.Б.Самойлов, Изучение нейтринных осцилляций в эксперименте NOvA, Сессия-конференция Секции ядерной физики ОФН РАН, Новосибирск, 10-12 марта 2020.

18. N.Balashov, I. Kakorin, V. Naumov Accelerating personal computations with HTCondor: generating large numbers of events with GENIE, Nuclear Electronics and Computing 2019 (NEC-2019), 30 September — 4 October, 2019, Montenegro.

19. N.Balashov JINR Computing Infrastructure Status, NOvA Collaboration Meeting, 13-16 February 2019.

20. N.Balashov JINR Computing Sites Status, NOvA Collaboration Meeting, 12-16 June 2017.

21. N.Balashov JINR Computing Resources, NOvA Collaboration Meeting, 28-31 January 2016.

22. A.Olshevskiy, Invited Neutrino Physics Lecture, JINR Summer school, 15 July 2019.

23. A. Sheshukov, Detecting neutrinos from the next galactic supernova in the NOvA detectors, Cape Town, South Africa, 21-28 February, 2020, CNNP2020

24. A.Sheshukov,Real-time detection of supernova neutrino signal, 127th session of the JINR Scientific Council, 20 February 2020

25. A.Sheshukov,Real-time detection of supernova neutrino signal, 52th JINR PAC on Particle Physics, 3 February 2020

26. A. Sheshukov, Supernova triggering and signals combination for the NOvA detectors, Sudbury, Canada, June 2019, Supernova Neutrinos in the Multi-Messenger Era workshop (SNEWS 2.0)

27. A. Sheshukov, Detecting neutrinos from the next galactic supernova in the NOvA detectors, April 2019, Baksan school on Astroparticle physics

28. A. Sheshukov, Supernova trigger status, NOvA Collaboration Meeting, 21-24 February 2019.

29. A. Sheshukov, Supernova trigger performance, NOvA Collaboration Meeting, 21-24 February 2019.

30. A. Sheshukov, Supernova trigger upgrade: combining the detectors, NOvA Collaboration Meeting, 3-7 June 2019.

31. A. Sheshukov, Supernova trigger status & updates, NOvA Collaboration Meeting, 3-7 June 2019.

32. A. Sheshukov, SN trigger status, NOvA Collaboration Meeting,10-13 October 2019.

33. A. Sheshukov, Supernova DDT, NOvA Collaboration Meeting,10-13 October 2019.

34. M. Petropavlova, A. Sheshukov, Simulation of the Supernova Neutrino Signal in NOvA Detectors, 51th JINR PAC on Particle Physics, 19-20 June 2019.

35. O. Petrova, East-West Asymmetry of Cosmic Ray Muons in the Far Detector of NOvA, 48th JINR PAC on Particle Physics, 31 January 2018.

36. O. Petrova, East-West Asymmetry of Cosmic Ray Muons in the Far Detector of NOvA, ISAPP-Baikal, Bolshie Koty, Russia, 12-21 July 2018.

37. O. Petrova, East-West asymmetry: an update, NOvA Exotics WG Meeting, 15 January 2019.

38. O. Petrova, A. Sheshukov, East-west asymmetry effect in atmospheric muon flux in the Far Detector of NOvA, 50th JINR PAC on Particle Physics, 21 January 2019.

39. O. Petrova, EWA update: reweighting uncertainties, NOvA Collaboration Meeting, 21-24 February 2019.

40. O. Petrova, East-west asymmetry effect in atmospheric muon flux in the Far Detector of NOvA, 22 February 2019, 125th session of the JINR Scientific Council.

41. O. Petrova, East-west asymmetry effect in atmospheric muon flux in the Far Detector of NOvA, 16th Baksan School on Astroparticle Physics "Particles and Cosmology", 10-18 April 2019.

42. O. Petrova,EWA update: efficiencies, NOvA Collaboration Meeting, 3-7 June 2019.

43. O. Petrova, EWA update: plans for regularization, NOvA Collaboration Meeting, 10-13 October 2019.

44. O. Petrova, East-West asymmetry: Tikhonov regularization, NOvA Exotics WG Meeting, 13 February 2020.

45. <u>A. Selyunin. Development of the light collection module for the Liquid Argon TPC. INSTR2020, Novosibirsk, Russia, 24-28 February 2020.</u>

46. A. Selyunin. Light Readout System. ArgonCube Collaboration Meeting, Bern, Switzerland, 9-10 December 2019.

47. A. Selyunin. Results from Light Collection Module (LCM) tests. ArgonCube Collaboration Meeting, Bern, Switzerland, 12-13 June 2018.

48. <u>L. Kolupaeva "NOvA's nue+numu oscillation analysis", PHYSTAT-nu 2019, CERN (22-25.01.2019)</u>

49. L. Kolupaeva "Cross-checks for the particle-identification algorithm in nue analysis by the means of muon removal procedure at the NOvA experiment", AYSS-2019, 17.04.19

50. <u>L. Kolupaeva "Latest three-flavor neutrino oscillation results from NOvA", EPS-HEP 2019, 12.07.19</u>

51. L. Kolupaeva "Neutrino oscillation analysis in the NOvA experiment", 51st meeting of the Programme Advisory Committee for Particle Physics, 19.06.2019

52. <u>L. Kolupaeva "Neutrino oscillation analysis in the NOvA experiment", 126th session of the Scientific Council, 20.09.2019</u>

53. L. Kolupaeva "2019 joint fit summary", 3flavor working group meeting

54. L. Kolupaeva "Fake data studies for 2019 joint analysis", 3flavor working group meeting

55. L. Kolupaeva "Decomp/Extrapolation with extra events study", 3flavor working group meeting

56. L. Kolupaeva "2019 nue+numu goodness of fit", 3flavor working group meeting

10. APPENDIX: Details of the Project

10.a ROC setup and operation

10.a.1 Data Taking and Quality Checking

The NOvA experiment at both the ND and FD sites have storages and file transfer systems to accumulate detector data. While this is safely done at the FD and ND locally, it is more efficient to monitor the operation of both systems from one location simultaneously, which can be accomplished from a Remote Operation Center (ROC). This policy was anticipated from the very beginning for all neutrino experiments at FNAL, and now all of the NuMI experiments are developing ROCs. The Main Remote Operation Center, ROC-West, is located in the Wilson Hall at FNAL.

Currently twenty five ROCs are operating for the NOvA experiment at different locations. The first non-US Remote Operation Center, ROC-Dubna, has been developed at JINR and started operation in October 2015. It has all of the necessary features and allows for full monitoring and control of FD and ND operation, as well as communication with FNAL services and other ROCs.
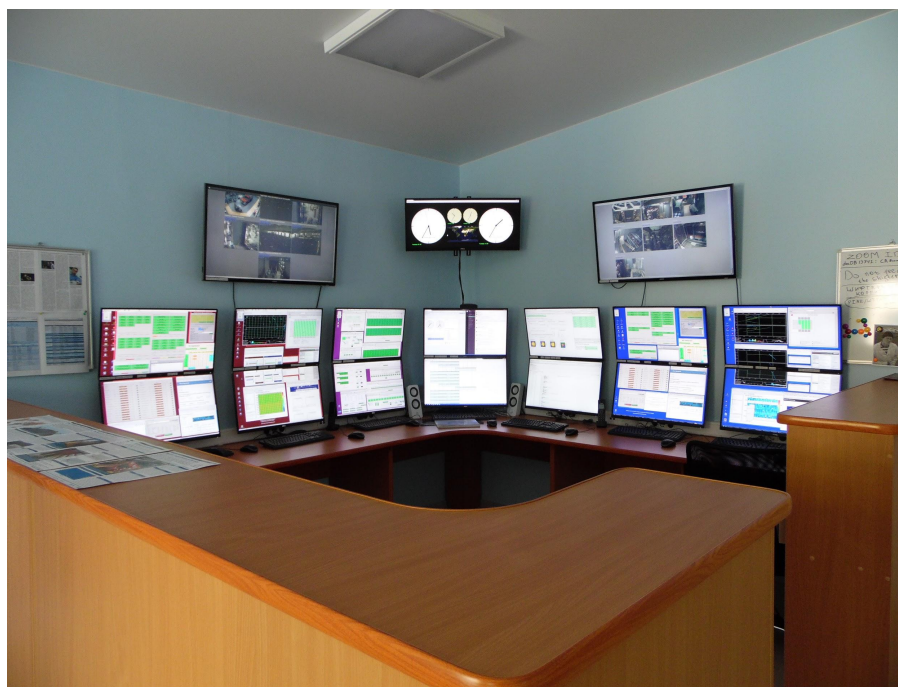
Figure10.a.1. ROC-Dubna view.

The NOvA experiment is operating 24/7 over its lifetime. (According to the project plan NOvA will run at least until the end of 2025). All of the ROCs together ensure continuous monitoring and control of detector systems on both sites, as well as monitoring of the beam status.

This work is managed by several Run coordinators changing every 2 weeks, which communicate with Shifters, ROC Contacts, System Experts and FNAL and Ash river On-site Crews. Such an

organization allows for the smooth operation and monitoring of all system components: beam, detector, electronics, DAQ, data transfer, safety matters, etc.

NOvA data storage and transfer software based on Linux-nodes collect information from NOvA DAQ system. ROCs connect to control and operation nodes on both FD/ND sites via VNC-tunneling under secure protocols. Basic idea is that a VNC server transfers a VNC session to many VNC viewers at ROCs with control. In total there are 5 active Scientific Linux based VNC-sessions are connected directly to Near/Far Detectors' nodes at FNAL and through GateWays to another World. System includes 1 Linux node for Web-monitoring of the operated systems (Beam, ND/FD Cameras, Data transfer control, Ganglia, Nearline) and 1 Windows node for communication (NOvA electronic logbook, latest version of expert contact and Bulletin board, Polycom via Vidyo, Slack-chat, Skype, Zoom).

ROC-Dubna at JINR has developed infrastructure to 8 hours (a shift period) continues work (stable internet, international land-line, kitchen, ROC is also public JINR area). Computing monitoring system on Zabbix controls local Linux-nodes, internet connection, server conditions and notifies JINR experts in case of troubles.

10.a.2 Hardware and software setup

All PCs, storages, UPSs, monitoring based on Linux-nodes and hardware from backup Internet connections have been moved to the special server room with an excellent and stable cooling system. On the top (main ROC area) we have only monitors with keyboards and mice.

Backup Internet connections are extremely important because we have to be online and monitor the NOvA detectors working state during all the shifts without any drops. For these purposes in addition to the main JINR network we have made two backup connections mobile (4G) and sky-fi ones.
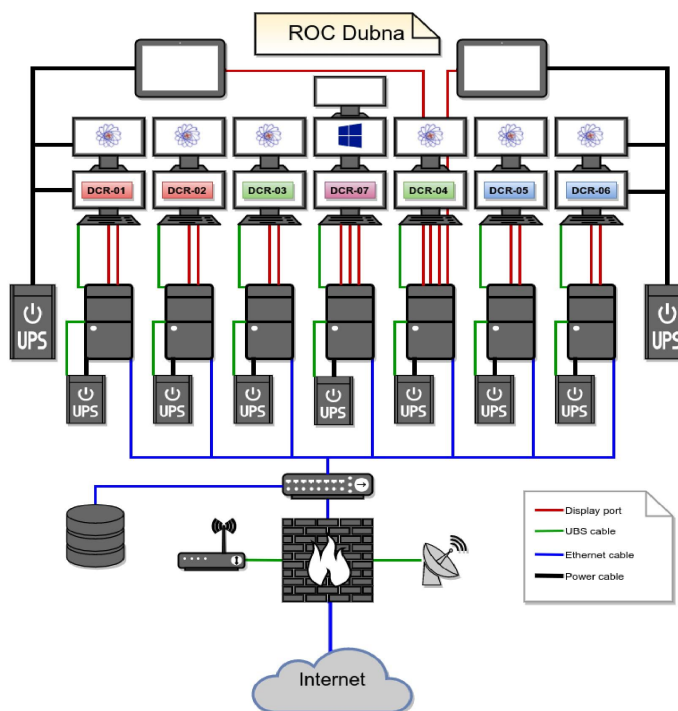
Figure 10.a.2. ROC-Dubna internet connection system.

All of these improvements allow ROC-Dubna to operate as stable as possible and to be ready for any possible hardware and software issues.

10.a.3 Advantages for JINR

1. ROC-Dubna amends people's time while shifting for both JINR and FNAL sides. We can control Detectors during day time for the Night shifts.

2. Taking shifts at home ROC-Dubna saves a budget of about 30k$/year. In addition, real time demonstration of the work attracts new people to the JINR team.

3. ROC-Dubna is a public place for excursions visiting by Scholars, Teachers, Students, Journalist and other JINR guests. Its presence at JINR has significantly increased the interest in the NOvA experiment by young people.

10.a.4 ROC upgrade

We plan to make an upgrade of the hardware part of the ROC during 2020. This upgrade includes all PCs and maybe UPSs replacement for newer ones. Approximate requested budget is 15 k$ during first year and 5 k$/year subsequently.

10.b Computing support

NOvA and DUNE are the large-scale neutrino experiments which require a huge amount of computing resources to process all of its data. While the major amount of computing resources both experiments get from the local infrastructure at Fermilab - Fermigrid - they also rely on contributions from other participating organizations via the global distributed computing infrastructure Open Science Grid (OSG). DUNE, being an international collaboration, plans on gathering ~5000 CPU cores and 12 PB of data storage as a general collaboration contribution. JINR already has an established Multifunctional Information and Computing Complex (MICC) at the Laboratory of Information Technology (LIT), two components (Tier-2 cluster and JINR Cloud) of which were set up and extended to provide computing support to the NOvA, Mu2e and DUNE experiments through the OSG.

Because the Tier-2 cluster initially was built for the CERN experiments support they continue to be the main consumers of the cluster and NOvA and Mu2e are limited to 200 slots (which equals to 200 CPU cores) for running simultaneous jobs. On the contrary, a dedicated NOvA virtual cluster was deployed in the JINR Cloud and was later configured to also support Mu2e and DUNE experiments. Since the Tier-2 cluster is used in opportunistic mode and its configuration didn't change much from its original (except for some small software adjustments), only the JINR Cloud cluster development will be described in detail.

To support local JINR collaborators a set of 6 Virtual Machines (VM) was prepared and deployed in JINR Cloud, each VM having 4 CPU cores, 8 GB RAM and 160 GB local disk storage. All the required software to perform physical analysis was installed manually, the VMs have JINR

Kerberos configured to simplify user management and an office-class storage system was connected to store and share the data between these VMs. Later the number of improvements were made: CernVM-FS was installed and became the primary experimental software distribution system, a 20 TB cloud storage based on Ceph replaced the old storage system and the VMs were configured as submit nodes for the HTCondor virtual cluster.

Specially for the NOvA experiment 24 new servers were purchased and added to the JINR Cloud:
- Dell PowerEdge R430 2xE5-2650v3, 6x8GB, 2x2TB NL SAS, 4x1Gb Ethernet - 5 servers;
- Dell PowerEdge R430 2xE5-2650v3, 6x16GB, 4x4TB NL SAS, 4x1Gb Ethernet - 4 servers;
- Dell PowerEdge R430 2xE5-2650v4, 8x16GB, 2x4TB NL SAS, 4x1Gb Ethernet - 5 servers;
- Dell PowerEdge R440 2xSilver 4116, 8x16GB, 2x120GB SSD, 4x1Gb Ethernet, 2x10Gb Ethernet - 5 servers;
- Dell PowerEdge R440 2xSilver 4214, 4x32GB, 2x120GB SSD, 4x1Gb Ethernet, 2x10Gb Ethernet - 5 servers;

Later the 2 port 10 Gb ethernet cards were added to the servers that lacked them and the RAM amount was increased in all of the servers to 128 GB. The cluster has 540 CPU cores and ~3 TB RAM in total.
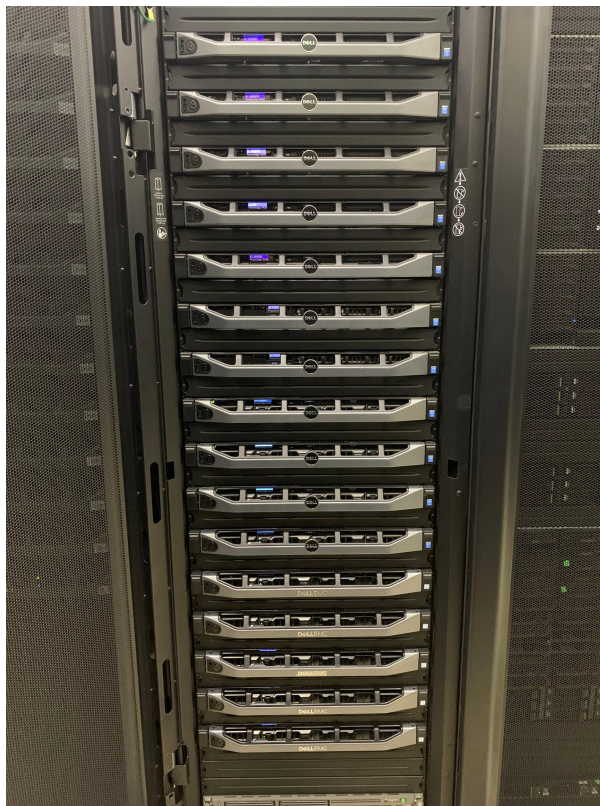
Figure 10.b.1. NOvA cloud cluster.

These servers were used to host VMs of the new batch cluster and the OSG-site, that allowed to process jobs from both local JINR NOvA team and the NOvA jobs coming from the OSG, contributing directly to the NOvA collaboration. In this system every component of a Grid-site is virtualized, which is a first-time experience for the JINR Grid-sites and is an important step for further development of computing models at JINR. Building the system in the cloud gave us a

possibility to dynamically scale the batch-cluster to add up opportunistic resources to the batch-system or to give out some resources to supplement other activities.

The basic setup of the virtual Grid-site (see Figure 10.b.1) consists of the Computing Element (CE) and a batch-system. The HTCondor batch-system was used to handle worker-nodes and distribution of jobs across them, and HTCondor-CE - a modified version of HTCondor - as a CE playing the role of a gatekeeper that handles authentication and translates jobs coming from the Grid-environment into the local batch-system's format. This setup has proven to be stable and in the period from January, 1 2018 to March 26, 2020 made a significant contribution to the NOvA experiment (statistics can be seen on the Figure 10.b.2).
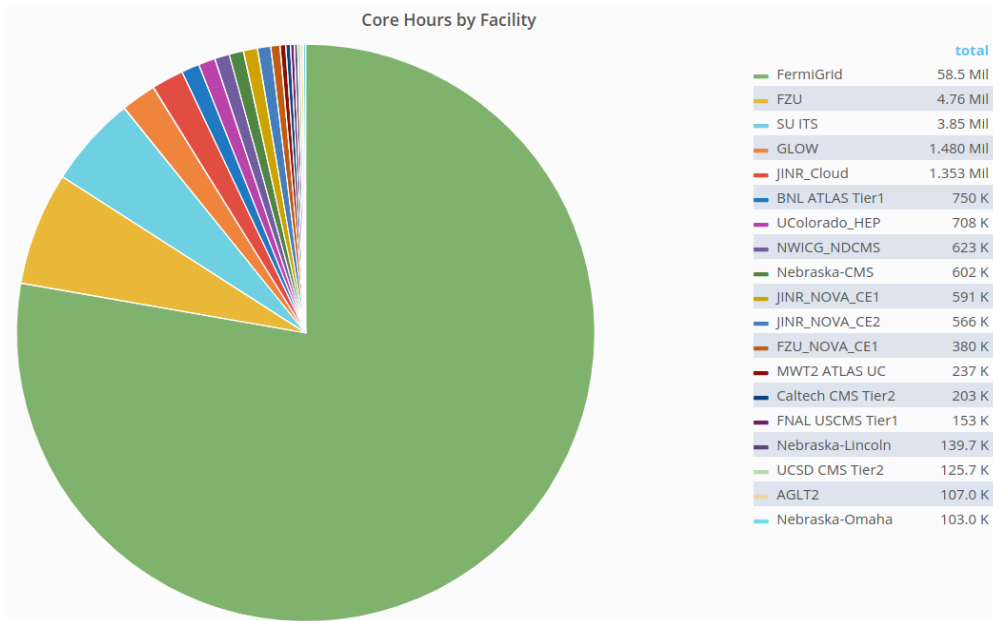
Figure 10.b.2. CPU hours spent by computing clusters in the period of January, 1 2018 to March 26, 2020 to process NOvA jobs.

With the growth of the virtual computing cluster development of the local data storage for storing a copy of the most requested experimental data becomes the most urgent task. Creation of such a storage system is crucial for the efficiency of local data analysis performance.

To form the storage backend the following servers were purchased to the cloud Ceph system:
- Dell PowerEdge R730xd, 2xE5-2620v4, 8x16 GB RAM, 2x400 GB SSD, 16x8 TB HDD, 2x10 GB Ethernet
- Dell PowerEdge R740xd, 2xSilver 4114, 8x16 GB RAM, 2x120 GB SSD, 12x10 TB HDD, 2x10 GB Ethernet
- Dell PowerEdge R740xd, 2xSilver 4114, 8x16 GB RAM, 2x400 GB SSD, 10x10 TB HDD, 2x10 GB Ethernet
- Dell PowerEdge R740xd, 2xSilver 4114, 8x16 GB RAM, 2x400 GB SSD, 10x10 TB HDD, 2x10 GB Ethernet

Figure 10.b.3. NOvA cloud storage servers.

The Ceph is a modern software defined storage system that joins storage servers into a single storage space which then can be split into virtual block devices (VBD). VBDs are used as network-attached disk devices for all of the cloud VMs. It provides automatic triple data replication to ensure data integrity and can be easily scaled up and down according to the emerging needs.

The already existing dCache storage at JINR was registered in the Sequential Access via Metadata (SAM) data handling system, JINR members were given required permission to register new datasets and a number of test data transfers were done. A dedicated cloud virtual machine with a large Ceph block-device was created and configured to join the NOvA dCache pool extending its 3 TB NOvA quota by 50 TB. Grid jobs use the GridFTP door to transfer data via the GridFTP protocol.
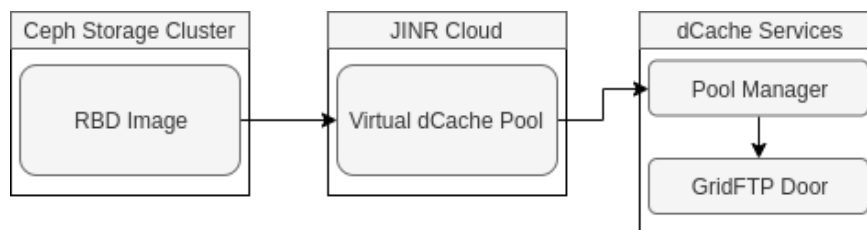
Figure 10.b.4. dCache pool structure.

Participation of the JINR in DUNE experiment analysis is expected to significantly increase the load on both the data storage and computing cluster, therefore, the overall capacity of the JINR computing infrastructure will need to be increased.

The DUNE experiment plans to build a tiered distributed computing infrastructure to strengthen international cooperation. Currently, it's proposed to forms 4 types of data centers (similar to CERN's tiering system, but may become less "tiered" eventually), distributed worldwide:

- Tier-0: host lab (FNAL);
- Tier-1: CPU, Disk and tape services ("pledged");
- Tier-2: offer CPU and Disk ("pledged");
- Tier-3: any other site which will contribute but does not meet Tier-1 or Tier-2 criteria.

The DUNE experiment plans on having an order of 5000 CPU cores by 2022 as a general contribution of all collaborators. Besides the CPU, disk storage is required for the Tier-2 sites, the total resource need is 24 PB by 2022. The goal is to have 25 % / 75 % resource split between FNAL and the rest of the collaborators, but a serious contribution is considered to be 5-10 % of the planned capacity.

Taking into account the NOvA resources, and the possibility to unite all resources of the JINR neutrino projects into one shared system (e.g. JUNO acquired ~2000 CPU cores), CPU capacity of the combined Neutrino Platform should be enough to form the Tier-2 site for the DUNE. The disk resource can't be shared between experiments and additional ~2.5 PB storage needs to be dedicated to DUNE.

Dedicating a Tier-2 site at JINR for the DUNE is sufficient to give noticeable computing contribution, but a larger contribution to the DUNE is possible and may be discussed additionally, for example, using High Performance Computing technologies (super computer "Govorun" at JINR) and an agreement of joint effort with russian institutes to represent the national contribution.

10.c 3-flavour oscillation analysis and results

NOvA's three-flavor oscillation analysis consists of two main interaction channels: electron neutrino appearance and muon neutrino disappearance. In order to identify and classify neutrino events a Convolutional Visual Network [10.c.1] is used along with classical cuts.

In the case of muon neutrino disappearance analysis, we split the ND reconstructed energy spectrum into 4 quartiles based on the reconstructed hadronic energy fraction to the full reconstructed neutrino energy ($E_{had\ frac} = E_{had}/E_\nu$). Quartile no.1 has the best energy resolution (~6%) and the lowest hadronic energy fraction. Whereas quartile no.4 has the worst energy resolution (~12%) and the highest hadronic energy fraction. The resulting measured spectra of ND ν_μ Charged Current (CC) candidates are shown in Figures 10.c.1-10.c.2.
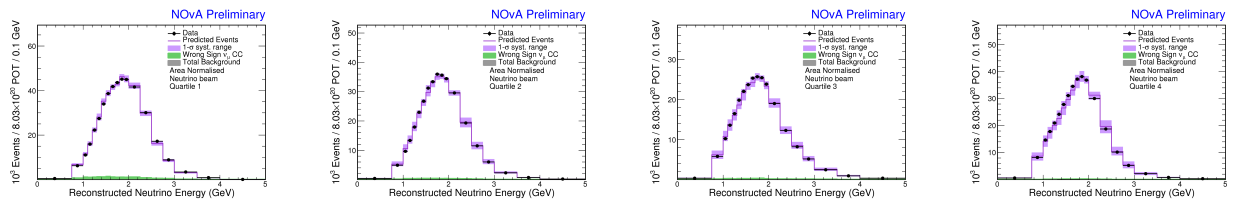
Figure 10.c.1. Measured reconstructed energy spectra of ND ν_μ CC events (dots) compared to the ND simulation (violet line). Good agreement between simulation and data.

Figure 10.c.2. Measured reconstructed energy spectra of ND $\overline{\nu}_\mu$ CC events (dots) compared to the ND simulation (violet line). Good agreement between simulation and data.

Similar detector construction allows for the application of the so-called extrapolation procedure (Figure 10.c.2): a data-driven technique for producing predictions in the FD. The high statistics of the ND data are used for constraining the simulations. Corrected simulated prediction is extrapolated to the FD and is used for the data fit. This method helps to reduce the size of cross-section and flux systematic uncertainties.
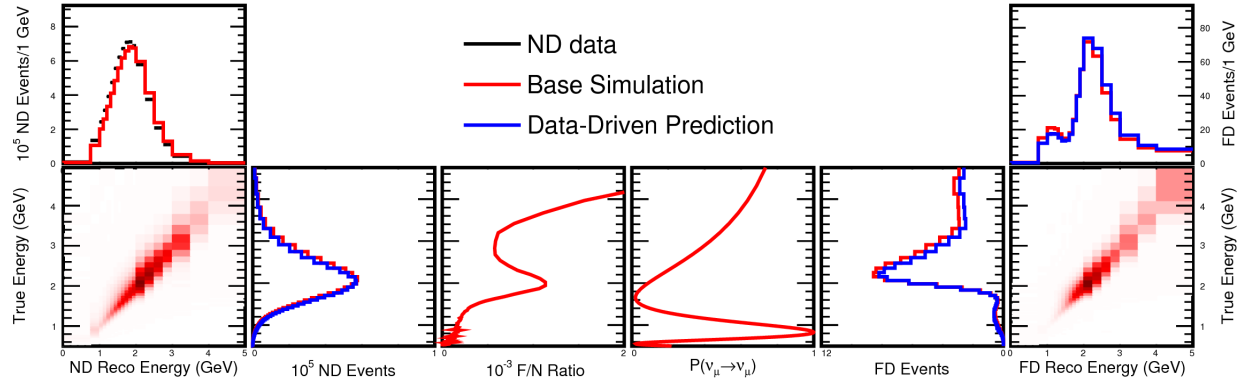
Figure 10.c.3. Schematic view of ND/FD extrapolation procedure.

The main steps of the extrapolation procedure (from top left) are:
1. Estimate the true energy distribution of selected ND events.
2. Multiply by expected FD/ND event ratio and oscillation probability as a function of true energy.
3. Convert the FD true energy distribution into a predicted FD reconstructed energy distribution.

Systematic uncertainties are assessed by varying all MC-based steps.

Each ν_μ quartile is separately extrapolated to the far detector. ND selected ν_μ ($\overline{\nu}_\mu$) events are used in the data-driven prediction of both ν_μ ($\overline{\nu}_\mu$) and ν_e ($\overline{\nu}_e$) signal events in the FD. Similarly, the ND selected ν_e ($\overline{\nu}_e$) CC events are a source of background in the FD. Measured spectra of these events are shown in Figure 10.c.4. We split these data into two regions of high and low ν_e ($\overline{\nu}_e$) purity based on their PID score.
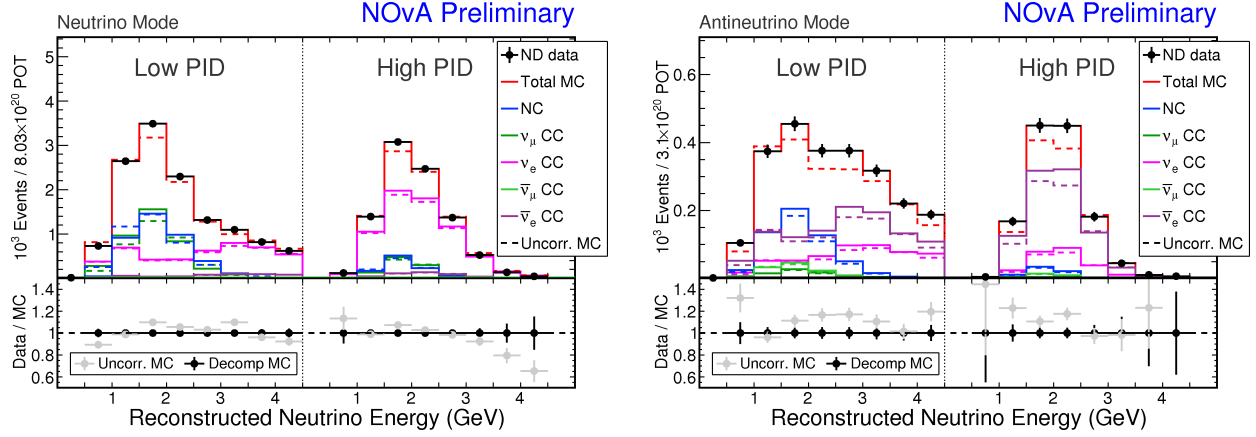
Figure 10.c.4. Measured reconstructed energy spectra of ND ν_e CC (left) and $\overline{\nu}_e$ CC (right) events (dots) compared to the ND simulation (color lines). Data-driven techniques are used to correct predictions in order to match the data. Uncorrected simulation before the procedure is shown by dashed lines. Each category of background is extrapolated separately to the FD.

The final spectra in the FD are shown in Figures 10.c.5-10.c.6, expected and observed number of events is shown in Table 10.c.1. This observation provides 4.4σ evidence of $\overline{\nu}_e$ appearance in an initially predominantly $\overline{\nu}_\mu$ beam.
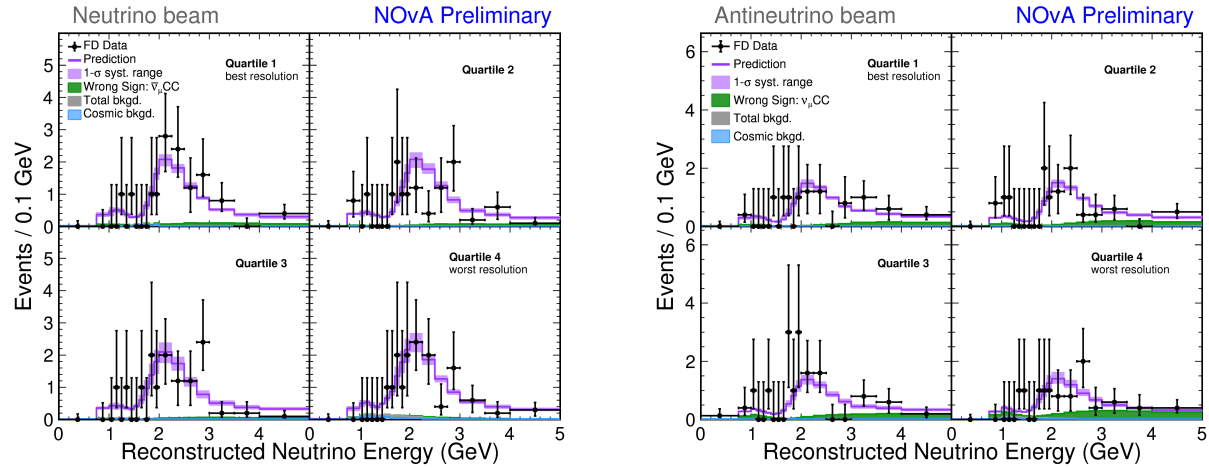
Figure 10.c.5. Measured reconstructed energy spectra of FD ν_μ CC (left) and $\overline{\nu}_\mu$ CC (right) events (dots) split into four quartiles. Color lines show the FD prediction at the best fit value after the extrapolation procedure.
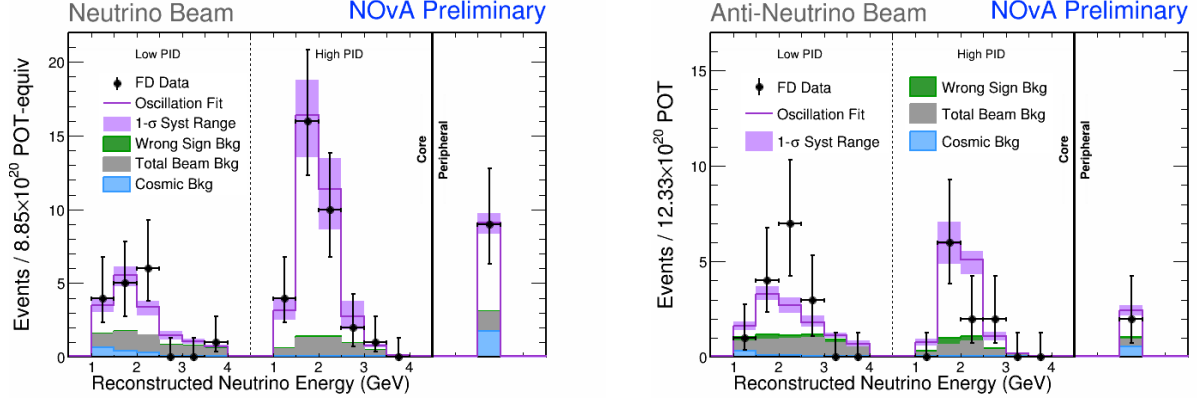
Figure 10.c.6. Measured reconstructed energy spectra of FD ν_e CC (left) and $\bar{\nu}_e$ CC (right) events (dots) split into two CVN PID bins and one additional Peripheral bin which collected all uncontained events included in the analysis.

	Neutrino beam		Antineutrino beam	
	ν_μ CC	ν_e CC	$\bar{\nu}_\mu$ CC	$\bar{\nu}_e$ CC
$\nu_\mu \to \nu_\mu$	112.5	0.7	24.0	0.1
$\bar{\nu}_\mu \to \bar{\nu}_\mu$	7.2	0.0	70.0	0.1
$\nu_\mu \to \nu_e$	0.1	44.3	0.0	2.2
$\bar{\nu}_\mu \to \bar{\nu}_e$	0.0	0.6	0.0	16.6
Beam $\nu_e + \bar{\nu}_e$	0.0	7.0	0.0	5.3
NC	1.3	3.1	0.8	1.2
Cosmic	2.1	3.3	0.8	1.1
Others	0.7	0.4	0.6	0.3
Signal	$119.7^{+10.2}_{-11.8}$	$44.3^{+3.5}_{-4.0}$	$93.9^{+8.1}_{-8.2}$	$16.6^{+0.9}_{-1.0}$
Background	$4.2^{+0.5}_{-0.6}$	$15.0^{+0.8}_{-0.9}$	$2.2^{+0.4}_{-0.4}$	$10.3^{+0.6}_{-0.5}$
Best fit	123.9	59.3	96.2	26.8
Observed	113	58	102	27
No Oscillations	$730.2^{+51.8}_{-60.5}$	—	$475.6^{+34.0}_{-37.0}$	—

Table 10.c.1. Event counts at the FD, both observed and predicted at the best fit point

A full list of systematic uncertainties for the measured parameters is shown in Table 10.c.2.

Source of Uncertainty	$\sin^2\theta_{23}$	δ_{CP}/π	Δm^2_{32} ($\times 10^{-3}$ eV^2)
Beam Flux	+0.00041 / -0.00089	+0.0042 / -0.0042	+0.0013 / -0.0013
Detector Calibration	+0.0054 / -0.0092	+0.026 / -0.025	+0.022 / -0.026
Detector Response	+0.0019 / -0.0032	+0.051 / -0.054	+0.0039 / -0.0046
Muon Energy Scale	+0.0023 / -0.003	+0.003 / -0.0016	+0.0099 / -0.011
Near-Far Differences	+0.001 / -0.004	+0.061 / -0.074	+0.0017 / -0.0019
Neutrino Cross Sections	+0.0041 / -0.0077	+0.063 / -0.071	+0.01 / -0.011
Neutron Uncertainty	+0.006 / -0.013	+0.01 / -0.00051	+0.0053 / -0.013
Normalization	+0.0013 / -0.0027	+0.023 / -0.026	+0.0013 / -0.0018
Systematic Uncertainty	+0.0097 / -0.02	+0.11 / -0.12	+0.026 / -0.032
Statistical Uncertainty	+0.024 / -0.038	+0.25 / -0.28	+0.052 / -0.049

Table 10.c.2. Systematic uncertainties for the joint $\nu_e + \nu_\mu$ analysis with neutrino and antineutrino beams.

In order to extract the oscillation parameters, a joint fit of the spectra in Figures 10.c.6 was performed. Solar oscillation parameters θ_{12} and Δm^2_{12} were fixed to the PDG values [10.c.2], while θ_{23}, Δm^2_{32}, δ_{CP} and neutrino mass hierarchy were varied. The value of θ_{13} was constrained by reactor experiment measurements. Analysis of NOvA is frequentist with profiled systematics and penalty terms.

The best fit of NOvA is: $\delta_{CP} = 0\pi$, $\sin^2\theta_{23} = 0.56^{+0.04}_{-0.03}$, $\Delta m^2_{32} = +2.48^{+0.11}_{-0.06} \times 10^{-3}\ eV^2$, which corresponds to the Normal neutrino mass hierarchy and upper octant of $\theta_{23} (> \pi/4)$.

Inverted mass hierarchy is disfavored at 1.9σ for all values of δ_{CP}.

The 1σ, 2σ, 3σ contours in $\sin^2\theta_{23} - \Delta m^2_{32}$ and $\sin^2\theta_{23} - \delta_{CP}$ surfaces are shown in Figure 10.c.7. A large region in the Inverted hierarchy at $\delta_{CP} = \pi/2$ was ruled out at $> 4\sigma$. The exclusion significances where each of δ_{CP}, Δm^2_{32} and $\sin^2\theta_{23}$ values are disfavored are shown in Figure 10.c.8. All values of δ_{CP} in the Normal hierarchy and Upper octant of θ_{23} are allowed at 1.1σ.

Upper octant of θ_{23} is preferred at 1.6σ, but the result is still consistent with maximal mixing at 1.2σ (Figure 10.c.8).

New analysis with an increased exposure of 14×10^{20} POT (ν) and 12.33×10^{20} POT ($\overline{\nu}$) is planned to be ready by this summer for the Neutrino2020 conference.

JINR group was involved in different steps of NOvA three-flavor analysis procedure: cut tuning and event selection, extrapolation and predictions in the Far Detector, experiment sensitivities calculation and data fits shown in this document.
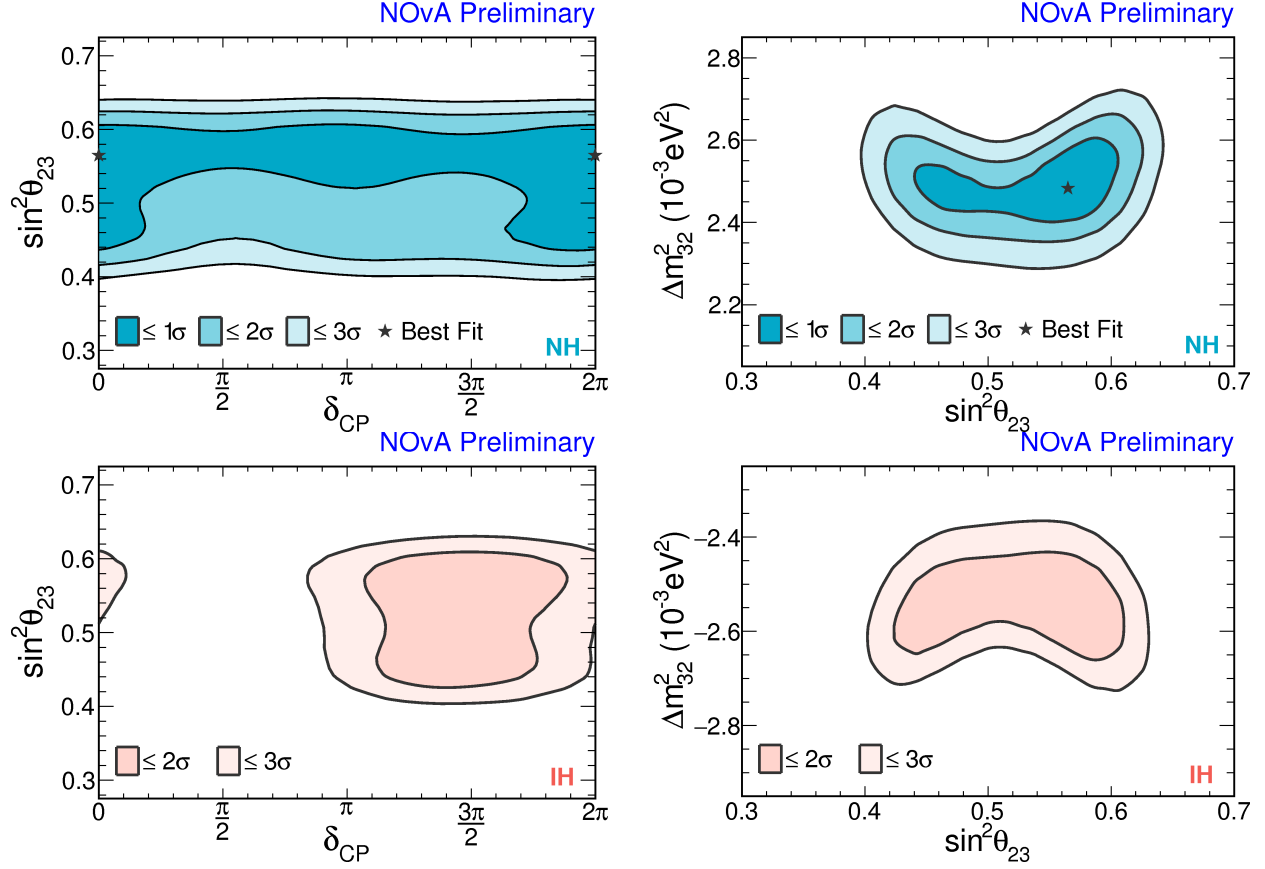
Figure 10.c.7. The 1σ, 2σ, 3σ contours in $sin^2\theta_{23} - \delta_{CP}$ (left) and $sin^2\theta_{23} - \Delta m^2_{32}$ (right) in Normal (up row) and Inverted (bottom row) hierarchy. Feldman-Cousins corrections are applied. Best fit is shown by star marker.
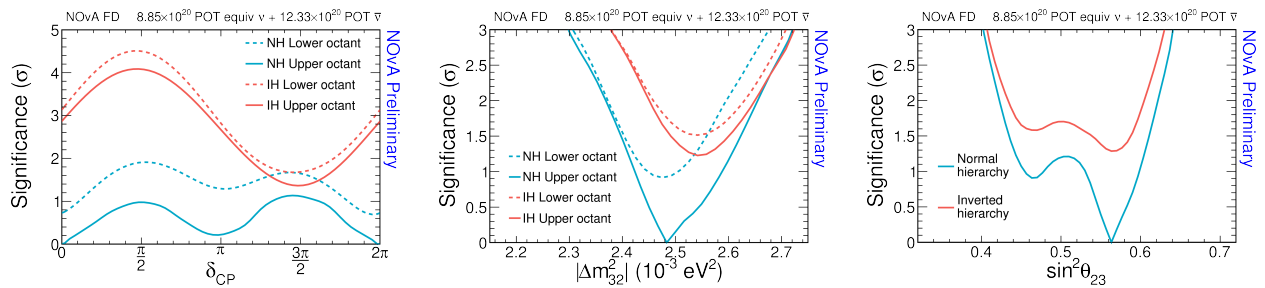

Figure 10.c.8. The exclusion significance for each value of δ_{CP} (left), Δm^2_{32} (middle) and $sin^2\theta_{23}$ (right) in Normal (blue) and Inverted (orange) mass hierarchy, dashed lines denote the octant (when it's applied).

10.c.ref References

[10.c.1] A. Aurisano et al., "A Convolutional Neural Network Neutrino Event Classifier," JINST 11, no. 09, P09001 (2016)
[10.c.2] M. Tanabashi et al. [Particle Data Group], Phys. Rev. D 98, no. 3, 030001 (2018).

10.d Prospects for NOvA and DUNE sensitivities

The NOvA experiment is expected to run until 2025 which implies approximately 36×10^{20} POT (ν) and 36×10^{20} POT ($\overline{\nu}$) collected during full operation. Figures 10.d.1-10.d.2 show sensitivity to measure neutrino mass hierarchy and CP violation phase after full run. NOvA is capable to measure neutrino mass hierarchy up to 4σ and δ_{CP} up to 2σ depending on true δ_{CP} value in nature (there are "unlucky" regions with $\delta_{CP} = 0, \pi$).
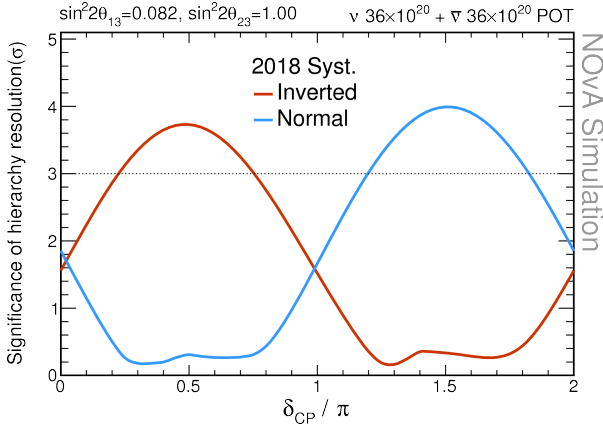
Figure 10.d.1. NOvA's sensitivity to neutrino mass hierarchy after $36 \times 10^{20} + 36 \times 10^{20}$ POT.
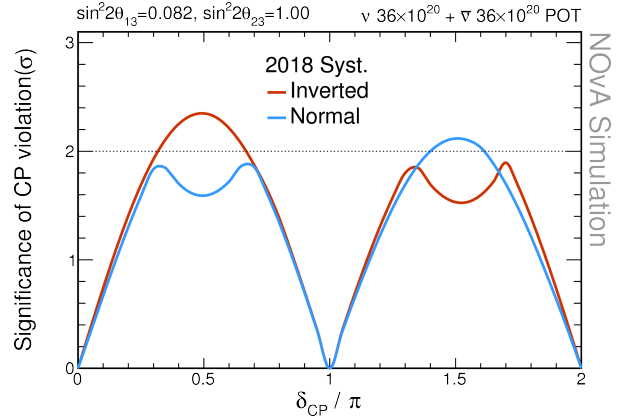
Figure 10.d.2. NOvA's sensitivity to δ_{CP} after $36 \times 10^{20} + 36 \times 10^{20}$ POT.

There is a plan to increase the accelerator beam power by upgrading and tuning existing accelerators up to ~900 kW in the years 2020-2024. These modernizations are included in the following sensitivity projections (Figure 10.d.3).

Three flavor oscillation group is planning various analysis updates in forthcoming years. A few new fitting concepts are being developed for the various steps of data fit.

Currently, NOvA uses Near Detector data for Monte-Carlo prediction extrapolation to the Far Detector. All systematics are treated in the same way. In the Far Detector, NOvA's fit is a frequentist with pull terms for systematics in a log-likelihood function. In general, Near Detector data can be used in simultaneous fit with Far Detector data. It could be a replacement for the current extrapolation method. One more possible update is a log-likelihood function and systematics

treatment for the actual fit. Instead of using a pull-term method, we can use covariance matrices for the fit. A few updates could be required for the common method since NOvA has Poissonian event statistics. An alternative method for Feldman-Cousins corrections is Bayesian fit. Many experiments use both methods for presenting their results. NOvA is considering incorporating Bayesian fit with the Markov Chain Monte-Carlo and Stan library as a fitter.

Right now there is no cross-check analysis that is developed with the main one. In upcoming years there is a plan to elaborate such a group with independent software infrastructure and analysis concepts.

NOvA's test beam at FNAL which is starting data taking this year could help to reduce important systematics such as a detector response. It also could serve as a good test for the convolutional neural networks that we use heavily for particle identification.

In 2021 NOvA and T2K (Japan) are planning to present the first joint data analysis. Several common groups were organized for the preparation works. This analysis can enhance the sensitivity to oscillation parameters.
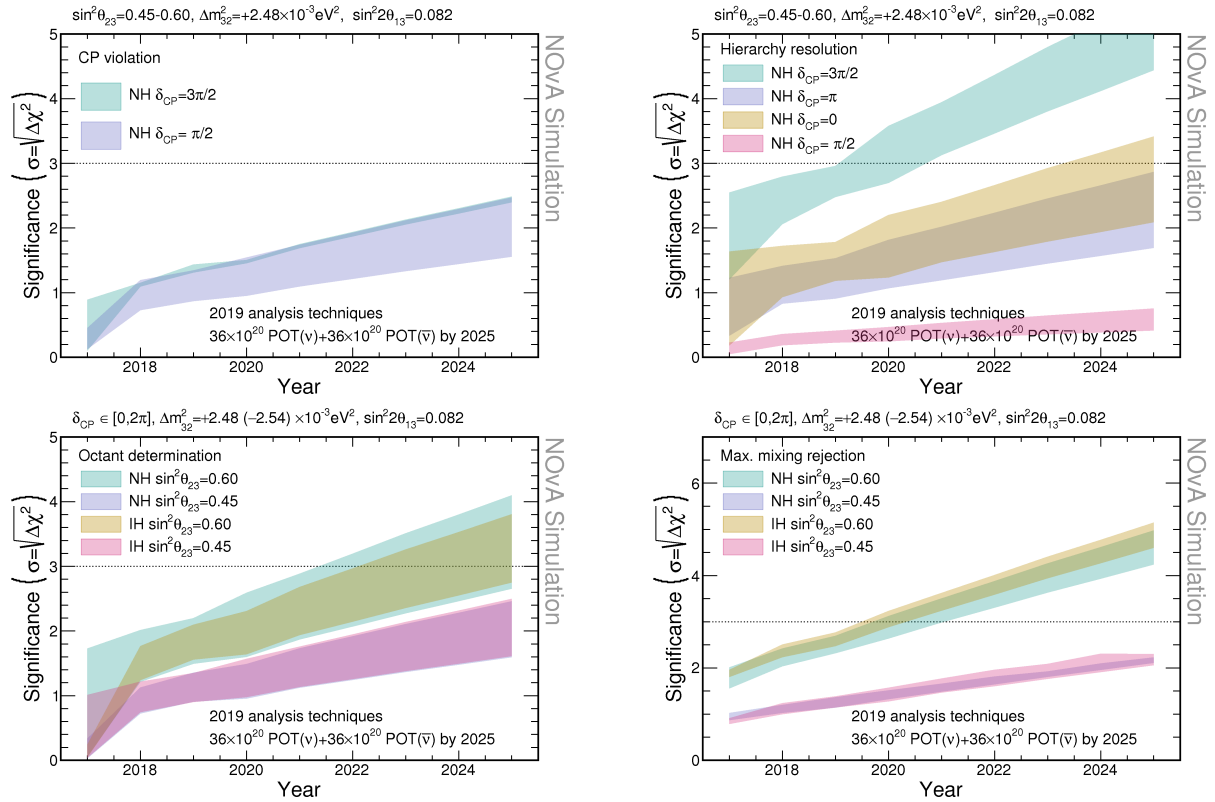
Figure 10.d.3. Projected sensitivities for upcoming years to reject: CP conservation, wrong hierarchy, wrong octant of θ_{23} and maximal mixing of θ_{23}. The width of the band shows the impact of varying the true value of $sin^2\theta_{23}$ (for δ_{CP} and mass hierarchy plots) and the true value of δ_{CP} (for wrong octant and maximal mixing plots).

The DUNE experiment is expected to start operations in 2025 with further beam and detector upgrades. First year of data taking will be with atmospheric neutrinos. Upgraded accelerator will start operations in 2026. Higher beam intensity, large detector volume, and long oscillation baseline make this experiment one of the best tools to probe neutrino oscillation parameters. Great statistics in the far detector (thousands of neutrino events in 7 years of data taking) will provide good sensitivity [10.d.1] to neutrino mass hierarchy and δ_{CP} violation (Figure 10.d.4). It is expected to have 5σ sensitivity to mass hierarchy after 2 years of beam running for any value of δ_{CP}, 5σ sensitivity to 50% of δ_{CP} values after 10 years of beam running.
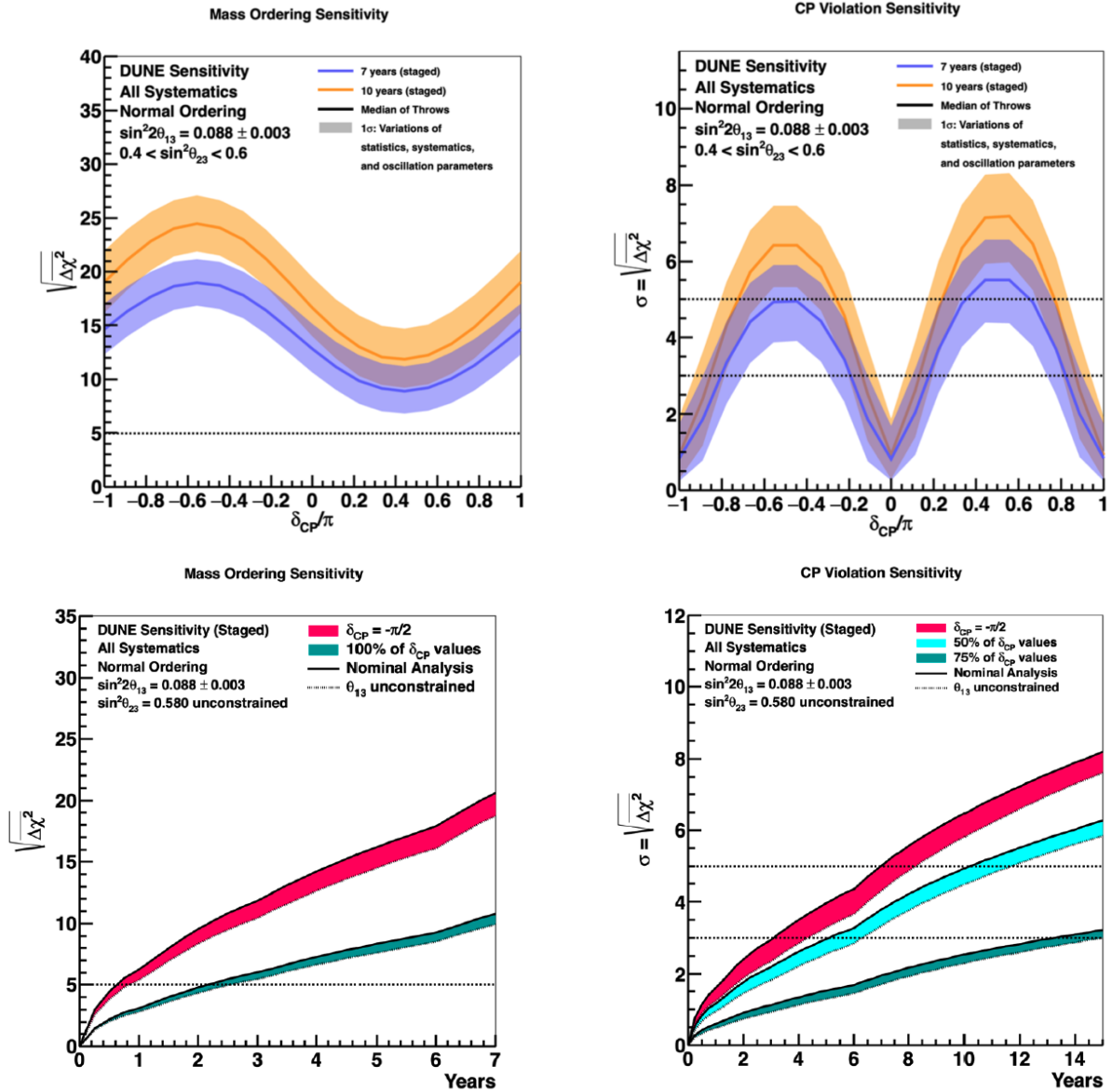
Figure 10.d.4. Upper two plots show the sensitivity to neutrino mass hierarchy and δ_{CP} after seven and ten years of running data taking. Two bottom plots show the significance of DUNE determination of mass hierarchy and δ_{CP} as a function of the calendar year.

10.d.ref References

[10.d.1] The DUNE Collaboration "Deep Underground Neutrino Experiment (DUNE), Far Detector Technical Design Report, Volume II: DUNE Physics" , arXiv:2002.03005

10.e. Current physical landscape and perspective for the next 10 years

Nowadays there are two accelerator neutrino experiments in the world – NOvA and T2K. NOvA results and prospects for NOvA and DUNE were discussed above. Here we will highlight other experiments that aim to measure neutrino mass hierarchy or/and CP-violating phase in the next ~10 years.

The latest T2K results [10.e.1] are the following: with detector exposure 14.9×10^{20} POT (neutrino) and 16.4×10^{20} POT (antineutrino) there were found 243 ν_μ CCQE, 75 ν_e CCQE, 15 ν_e CC1π, 140 $\overline{\nu}_\mu$ CCQE and 15 $\overline{\nu}_e$ CCQE. The best fit value of these spectra is in the point $sin^2\theta_{23} = 0.53^{+0.03}_{-0.04}$, $\Delta m^2_{32} = (+2.45 \pm 0.07) \times 10^{-3} \ eV^2$, $\delta_{CP} = -1.89^{+0.70}_{-0.58}$. Normal neutrino mass hierarchy is favorable with 2σ significance. The points $\delta_{CP} = 0, \pi$ are excluded at 95% confidence level.
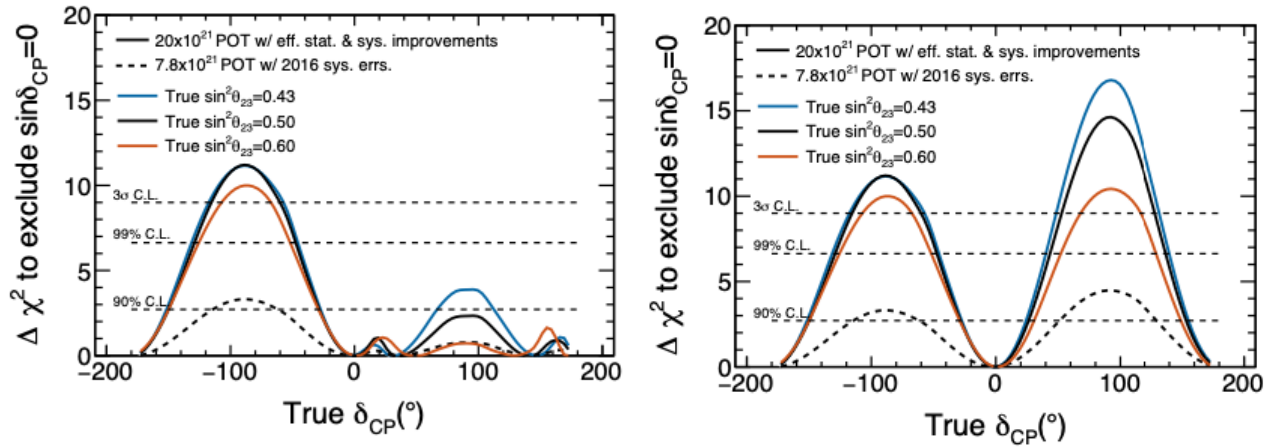
Figure 10.e.1. Sensitivity to CP violation as a function of true δ_{CP} with three values of $sin^2\theta_{23}$ (0.43, 0.50, 0.60) and normal hierarchy for the full T2K-II exposure of 200×10^{20} POT compared with designed value and reduced systematic errors in comparison with current T2K errors. Left plot shows sensitivity in case of unknown mass hierarchy and right plot shows sensitivity in case of external MH measurement.

The T2K experiment has a proposal for an extended run [10.e.2] until 200×10^{20} POT of full statistics is collected (T2K-II). With this statistical increase they aim to measure CP violation with 3σ or higher (for the case of maximum CP violation) (see Figure 10.e.1), θ_{23} with a precision 1.7 degrees or better and Δm^2_{32} with 1%. That means prolonged data taking period until 2025-2026 and implies beam upgrades up to 1.3 MW as well as the near detector and analysis developments. Due to shorter baseline T2K is not expected to have high sensitivity to neutrino mass ordering.

Current Super - Kamiokande experiment measurements with atmospheric neutrino only provide about 1σ preference for Normal Hierarchy [10.e.3].

The JUNO experiment has a wide variety of physics goals including neutrino mass hierarchy measurement [10.e.4]. The detector of the experiment is expected to be ready for the data taking in 2021-2022. With 6 years of operations, the MH sensitivity can achieve the 3-4σ level with JUNO only data. There are several possible joint analysis combinations with other experiments (the one with IceCube/PINGU is described below).

The Precision IceCube Next Generation Upgrade (PINGU) is a proposal for IceCube Neutrino Observatory upgrade [10.e.5]. Due to huge 6 Mton effective mass and high statistic sample of atmospheric neutrinos, PINGU can provide competitive measurements of θ_{23} and Δm_{32}^2 oscillation parameters as well as determine neutrino mass hierarchy at ~4σ median significance after 5 years of experiment operations. The status of this project is not clear yet. Currently, there are works on IceCube upgrades scheduled for deployment in 2022/2023 which could provide 1.5-2σ sensitivity to MH in 3 years. There is a proposal for joint analysis with the JUNO experiment after 6 years of data taken by both projects [10.e.6]. Which considers several scenarios of both experiment status. In the best case, 5σ sensitivity can be achieved after 2 years of data taking and full combined fit (Figure 10.e.2).
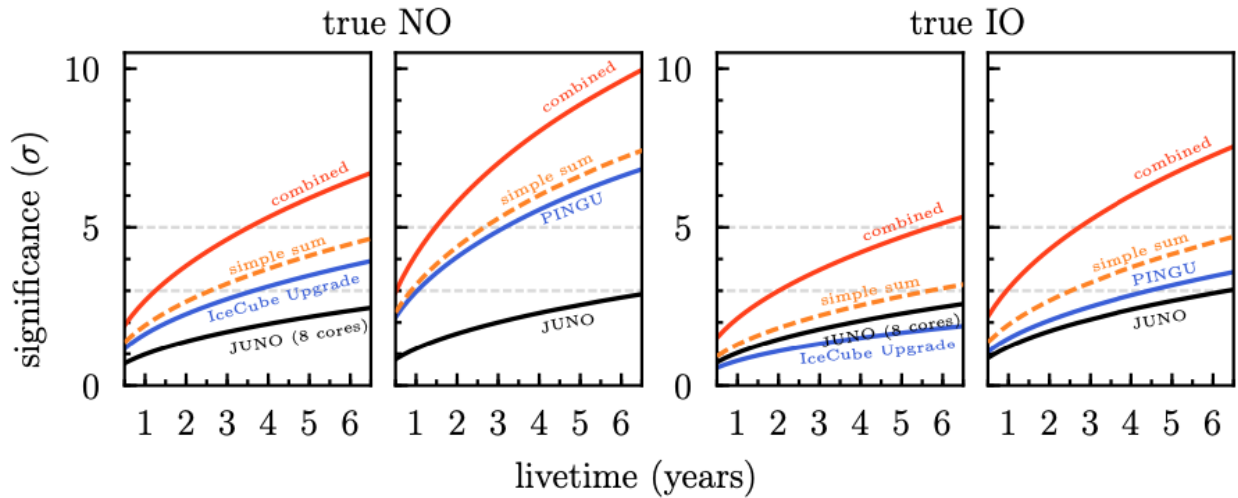
Figure 10.e.2. Evolution of the MH sensitivity by year of each considered pair of experiments. Results for the nominal JUNO configuration and PINGU are shown side-by-side with the 8-core JUNO configuration (labeled as "JUNO (8 cores)") and the IceCube Upgrade.

The KM3NeT experiment [10.e.7] is the next-generation large-volume neutrino telescope at the bottom of the Mideterranean sea. The first KM3NeT-Orca strings were deployed in 2017. Currently, four detection units are operating out of 115 planned. Neutrino mass hierarchy sensitivity after 3 years of data taking can reach 2.2-5σ depending on true parameters in Nature [10.e.8]. An interesting possibility was mentioned recently to send the neutrino beam from IHEP (Protvino) to KM3NET-Orca detector [10.e.9], but the status and timescale of this project is unclear.

The Hyper-Kamiokande experiment [10.e.10] is expected to start work in 2027-2028. It will replace Super-K as an atmospheric neutrino experiment and serve as a far detector for the accelerator neutrino beam from J-PARC (T2HK experiment). With a combined fit of the accelerator and atmospheric neutrinos, it is expected to reach 5σ sensitivity during 6-10 years of data taking

(depends on θ_{23} angle) (Figure 10.e.3). Accelerator neutrinos will provide high sensitivity to reject $\delta_{CP} = 0, \pi$. After 10 years of data taking it can achieve 8σ sensitivity to δ_{CP} in case of maximal CPV (for known neutrino mass hierarchy) (Figure 10.e.4).
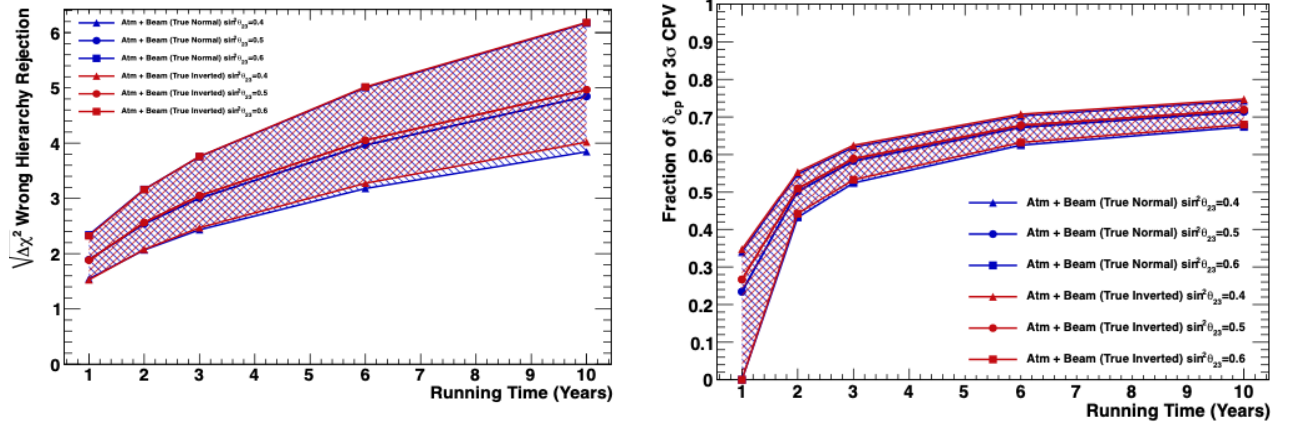

Figure 10.e.3. Sensitivity to measure neutrino mass hierarchy (left) and fraction of δ_{CP} phase space at which a 3σ observation of CP violation can be made (right) as a function of year for combined fit of atmospheric + beam neutrino data. Assuming $sin^2\theta_{23}$ = 0.4, 0.5 and 0.6 for normal and inverted hierarchy.
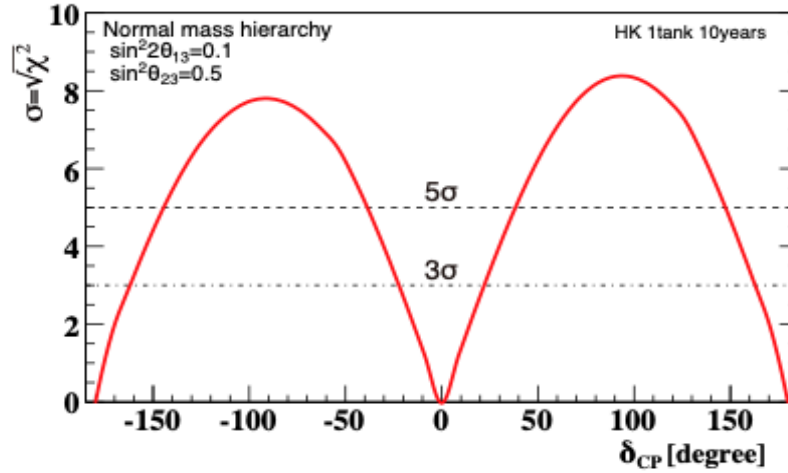
Figure 10.e.4. Expected significance to exclude $\delta_{CP} = 0, \pi$ in case of normal hierarchy. Mass hierarchy is assumed to be known.

Such competition is positively considered, since the comparison of results, obtained by different methods, provide the cross check and more precise and reliable combination.

10.e.ref References

[10.e.1] T2K collaboration, Constraint on the Matter-Antimatter Symmetry-Violating Phase in Neutrino Oscillations, 1910.03887.
[10.e.2] K. Abe et al., arXiv:1609.04111 [hep-ex].
[10.e.3] M. Jiang et al. (Super-Kamiokande), PTEP 2019, 053F01 (2019), arXiv:1901.03230 [hep-ex].
[10.e.4] F. An et al., Neutrino Physics with JUNO, J. Phys. G 43 (2016) 030401, arXiv:1507.05613.
[10.e.5] M. G. Aartsen et al. [IceCube Collaboration], J. Phys. G 44, no. 5, 054006 (2017) doi:10.1088/1361-6471/44/5/054006 [arXiv:1607.02671 [hep-ex]].
[10.e.6] M. G. Aartsen, et al., (IceCube-Gen2 Collaboration) and T. J. C. Bezerra, et al., (JUNO Collaboration), Phys. Rev. D 101, 032006 (2020).
[10.e.7] KM3NeT 2.0 Letter of Intent for ARCA and ORCA arXiv:1601.07459v1; Journal of Physics G 43 (2016) 084001.
[10.e.8] https://pos.sissa.it/358/1019/pdf
[10.e.9] A. V. Akindinov et al., arXiv:1902.06083 [physics.ins-det].
[10.e.10] K. Abe et al. (Hyper-Kamiokande Proto- Collaboration), eprint arXiv:1805.04163 (2018).

10.f Monte Carlo tuning

The charged-current (anti)neutrino–nucleus cross section is of special interest for reliable events reconstruction in the DUNE experiment and for its parameters optimization. The cross section is usually estimated by the sum of contributions from quasielastic scattering (QES), single-pion production (SPP) through nucleon and baryon resonances (RES), strange hyperon production for antineutrino reactions (QHP), and deep-inelastic scattering (DIS) and less essential but negligible contributions from coherent (COH) and diffractive (DIF) channels with an appropriate scratching of the phase space of the RES and DIS contributions comparable of magnitude within the few-GeV energy region. The problem is aggravated by the uncertainties in the knowledge of the simplest exclusive contributions: the description of the RES reactions is model-dependent and both RES and (Q)ES cross sections are very sensitive to the poorly known shape of the weak axial-vector form factors.

To describe the QES cross sections of neutrino charged current interaction with bound nucleons in any kind of nuclei at all energies of interest we propose an empirical notion of the effective ("running") axial-vector mass of the nucleon as a simple recipe for calculating the cross sections within the relativistic Fermi-gas model [10.f.1]. The approach is applicable to any nuclear target at all energies of interest and makes it possible to describe all available accelerator data on the total, differential, and double differential quasielastic cross sections by using only two adjustable parameters.

To describe the RES reactions we use an extended and updated version of the Rein–Sehgal (RS) model (KLN+BS) [10.f.2-10.f.4]. The RS model is based on the harmonic oscillator quark model in terms of the Feynman-Kislinger-Ravndal (FKR) relativistic formulation taking into account contributions from 18'th interfering low-lying nucleon and baryon resonances with invariant masses of final system of hadrons below 2 GeV, and non-interfering non-resonance contribution as the

43

background (NRB) of the resonance 1π production reactions. The model has been adapted to the calculation of the cross sections of $ν_τ$ and anti-$ν_τ$ by using a covariant form of the charged leptonic current with definite lepton helicity, keeping the hadronic current unchanged. The model took into account the pion-pole contribution to the hadronic axial current.

To describe the DIS cross sections we use the standard form of the cross section represented by the standard set of five structure functions (SF). Our careful calculation of SF is based on the parton distribution functions divided into "non-charm production" and "charm production" parts. In addition, we utilized some helpful technical methods of accurate calculation of the relations between SF. We have an opportunity to test the different models of parton distributions derived at the leading order and next-to-leading order approximation of the perturbative QCD.

To fine tune the values of phenomenological parameters of axial masses and kinematic bound on phase space of the RES and DIS contributions we examine in the advanced global likelihood analysis for all available experimental data on the QES [10.f.5], QHP [10.f.6], RES and DIS [10.f.7, 10.f.8] total, differential, and double differential CC cross sections obtained with a variety of nuclear targets in the accelerator experiments at ANL, BNL, FNAL, CERN, and IHEP, dating from the end of sixties to the present day.

For the recent NOvA analysis [10.f.9], neutrino interactions were modeled using GENIE 3.0.6 [10.f.10] updated with new models, which allows a user to test several predefined sets of the generator parameters (so-called tunes). In particular, GENIE 3 includes completely updated QES event generation procedure and well-known Valencia models for charged current QES and meson exchange currents (MEC) processes with fixed bugs [10.f.11]. Our previous analysis with JINR-model [10.f.12, 10.f.13] shows quite good agreement with ND data. The JINR-model is different from one used in the previous NOvA analysis [10.f.14, 10.f.15] mainly by the following. First, it includes the empirical "running axial mass" for simulation of QES+MEC events. Second, it uses the Berger-Sehgal model with resonance axial mass equal to 1.18 GeV (obtained from a global fit to available deuterium data) for SPP modeling (in the recent NOvA analysis Berger-Sehgal model is also used). As the empirical "running axial mass" enters in GENIE 3 among other models, it is quite easy to implement all settings for our analysis as a tune. We intend to include it in the official tunes list [10.f.16] to generate of a small batch of events with JINR-model (so-called miniproduction) in the full data tuning and processing chain of the NOvA experiment and use it for both modeling and interpretation of the data in the near and far detectors.

The SPP models currently implemented in GENIE does not account for interference between resonances and background contribution, which can lead to additional uncertainties in simulation that requires additional studying. For studying this issue, we are planning to implement SPP model [10.f.17], which utilizes an alternative NRB model (different from used in GENIE and Rein-Sehgal model) and takes into account interference between resonances. The model allows defining the angular distribution of the final state pions that can be studied in the DUNE experiment.

A superscaling model SuSAv2+MEC [10.f.18] will be included in the future version of GENIE soon. It is an alternative to the Valencia model to describe the CC0π channel in neutrino interactions and the full regime in (e, e′) reactions. In collaboration with Granada University we intend to implement in GENIE another superscaling model – SuSAM* [10.f.19] using a scaling

function extracted from a selection of the (e, e′) cross section data, and an effective nucleon mass inspired by the relativistic mean-field model of nuclear matter. This is a phenomenological model, which is technically much easier to implement, than SuSAv2+MEC and therefore we expect that such implementation will require less computing resources.

10.f.ref References

[10.f.1] I.D. Kakorin, K.S. Kuzmin and V.A. Naumov. An unified empirical model for quasietastic interactions of neutrino and antineutrino with nuclei (Accepted in PEPAN Letters).
[10.f.2] D. Rein and L.M. Sehgal. Annals Phys. 133, 79 (1981).
[10.f.3] K.S. Kuzmin, V.V. Lyubushkin and V.A. Naumov, Mod.Phys.Lett.A 19, 2815 (2004).
[10.f.4] C. Berger and L.M. Sehgal. Phys.Rev.D 76, 113004 (2007).
[10.f.5] K.S. Kuzmin, V.V. Lyubushkin and V.A. Naumov. Eur. Phys. J. C 54, 517 (2008).
[10.f.6] K.S. Kuzmin and V.A. Naumov. Phys. Atom.Nucl. 72, 1501 (2009).
[10.f.7] A. Gazizov, M. Kowalski, K.S. Kuzmin, V.A. Naumov and C. Spiering. EPJ Web Conf 116, 08003 (2016) (arXiv:1604.02092).
[10.f.8] K.S. Kuzmin, V.V. Lyubushkin and V.A. Naumov. Phys.Atom.Nucl. 69, 1857 (2006).
[10.f.9] K. Bays. Internal report. DocDB # 43581.
[10.f.10] C. Andreopoulos et al., The GENIE Neutrino Monte Carlo Generator, Nucl. Instrum. Meth. A614, 87 (2010).
[10.f.11] https://hep.ph.liv.ac.uk/~costasa/genie/releases.html
[10.f.12] I.D. Kakorin, K.S. Kuzmin and V.A. Naumov. Internal report. DocDB # 38061.
[10.f.13] I.D. Kakorin, K.S. Kuzmin and V.A. Naumov. Internal report. DocDB # 23018.
[10.f.14] P. Adamson et al. (NOvA Collaboration), Phys.Rev.Lett. 118, 151802 (2017).
[10.f.15] P. Adamson et al. (NOvA Collaboration), Phys.Rev.Lett. 118, 231801 (2017).
[10.f.16] https://hep.ph.liv.ac.uk/~costasa/genie/tunes.html
[10.f.17] M. Kabirnezhad. Phys.Rev.D 97, 013002 (2018).
[10.f.18] S. Dolan et al. Phys.Rev.D 101, 033003 (2020).
[10.f.19] I. Ruiz Simo et al. Phys.Rev. D 97, 116006 (2018).

10.g Detection of Supernova signal

10.g.1 Introduction

Core-collapse supernova (SN) explosion is expected to emit about 10^{58} neutrinos in a short burst with typical timescales of ~10s (Figure 10.g.1).
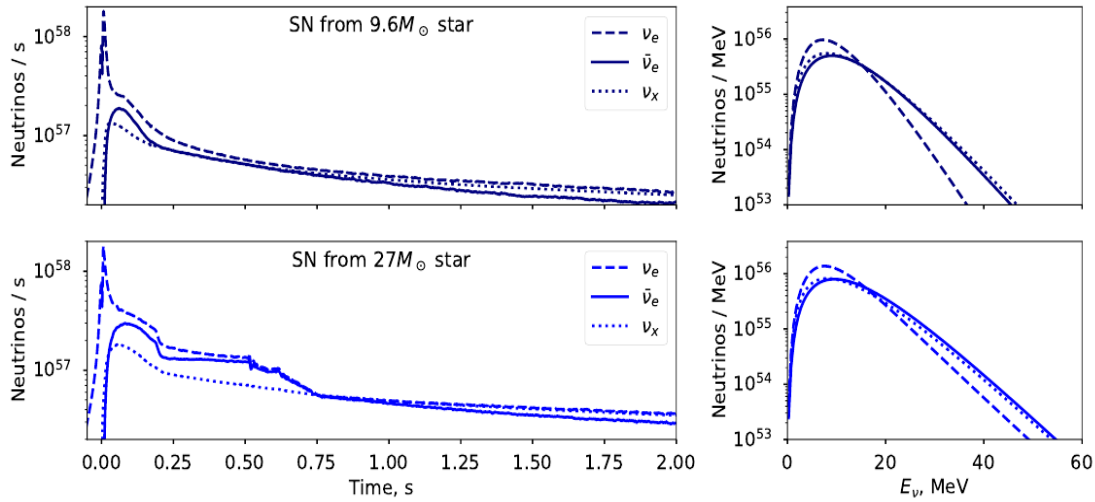
Figure 10.g.1. Expected neutrino production vs. time (left) and energy (right) from collapsing stars with a mass of 9.6 M_{sun}(top) and 27 M_{sun}(bottom), from the simulation by the Garching group [2]

Detection of neutrino signals from the core-collapse supernova would be a valuable source of knowledge about both neutrino properties and the supernova explosion process [10.g.1]. Along with many other neutrino experiments, NOvA is sensitive to such signals if the supernova occurs within our galaxy. However, since the estimated rate of such events in our galaxy is 1-3 SN/century, an experiment expecting to detect SN neutrino signals should implement a real-time triggering system, continuously monitoring the detector data and measuring the significance of presence of SN neutrino bursts.

10.g.2 Simulation of the supernova neutrino interactions

Development of the triggering system and, in particular, the algorithms for selection and reconstruction of the SN neutrino interactions require the detailed event-by event simulation of such interactions in the detector.

A dedicated software package named "GenieSNova" was developed to simulate interactions of supernova neutrinos inside the NOvA detectors. This new package generates neutrinos according to a supernova neutrino flux distribution including both the time structure and energy distributions. It then simulates neutrino interactions on the NOvA materials according to the detectors' geometry. The GenieSNova package interfaces models of supernova neutrino fluence from the Garching group [10.g.2] and the Supernova Neutrino Database [10.g.3] with the GENIE neutrino interactions generator [10.g.4] to accomplish this simulation. Figure 10.g.2 shows an example of such simulation for the NOvA Far Detector.
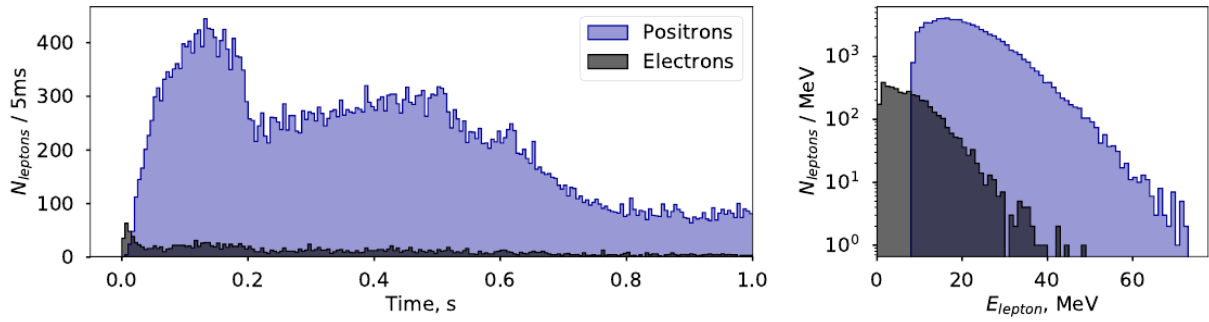
Figure 10.g.2. Results of GenieSNova simulation of SN neutrinos from a 27M$_{sun}$ progenitor star at 2 kpc distance, interacting in the NOvA Far Detector: time (left) and energy (right) distributions of secondary charged leptons.

The main interaction channel for the supernova neutrinos in scintillator detectors is the inverse beta decay process (IBD), producing the positrons, which can be selected by NOvA reconstruction algorithms.

10.g.3 Supernova trigger system in NOvA

NOvA's Data-Driven Trigger (DDT) system is used to perform fast data reconstruction online in order to decide which time ranges of data should be saved for further offline analyses. To achieve this, the data stream from the detector is sliced into 5 ms chunks (called "milliblocks") and, for supernova detection, data in these milliblocks are subjected to background rejection and neutrino interaction candidates' reconstruction procedures in more that 2200 parallel processes on NOvA Far Detector (170 for Near Detector), to count the number of potential supernova neutrino candidates in each 5 ms in real time.

Background suppression steps include rejection of signals from atmospheric muons and their decay products (Michel electrons), high energy cosmic ray showers, low-energy signals, correlated in time, and finally masking the noisy electronic channels. Also the fiducial volume cut is applied in order to reduce the background, originating from outside the detector and near its borders.

Figure 10.g.3 shows the resulting efficiency for the selection of the IBD positron signal after the background rejection and reconstruction procedures (right), and the expected spectrum of the positrons from the supernova neutrino signal (left).
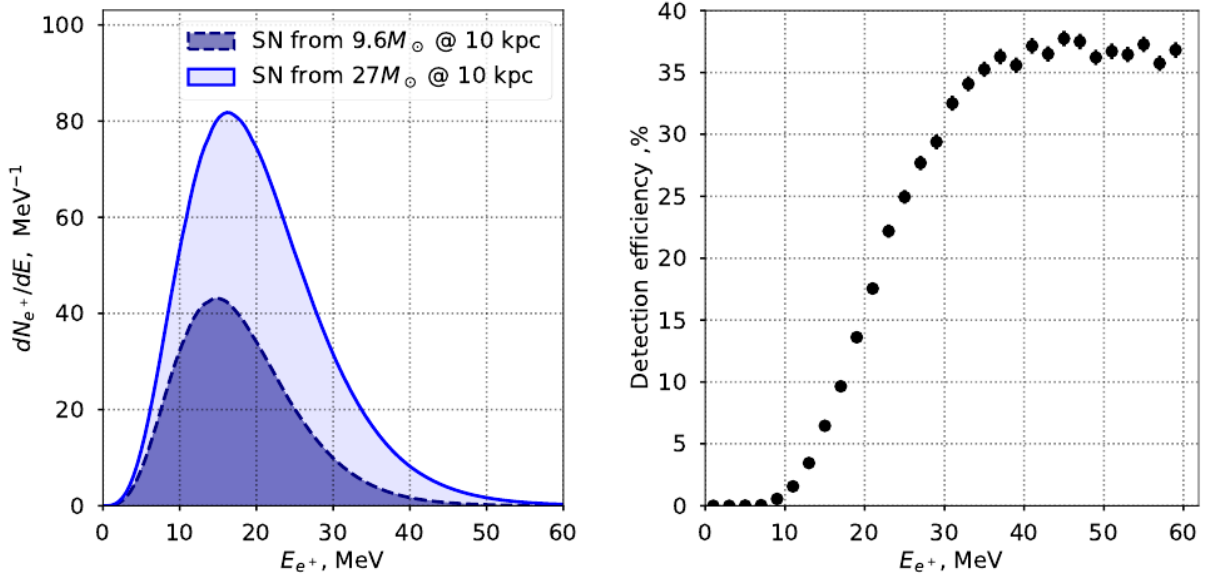
Figure 10.g.3. Positron spectrum from simulated supernova neutrino IBD interactions in the Far Detector (left) and efficiency of positron detection as a function of positron energy (right)

After the parallel DDT processes have performed searches for IBD interaction candidates, data on the candidate rate per 5 ms are sorted and accumulated in a time series. In order to decide if this time series contains a signal from a supernova, we scan the incoming data and test the "background-only" and "signal + background" hypotheses.

In order to perform such discrimination, we use the log likelihood ratio function for these hypotheses as the test statistics. This log likelihood ratio, depending on the signal hypothesis, in particular, the expected signal interactions rate vs. time, enhances the significance of the supernova signal detection. Figure 10.g.4 shows an example of such detection, calculating significance using three different shapes of the expected signal.

The supernova trigger alert is issued when the significance exceeds the threshold of z_0=5.645, which corresponds to an average false triggering rate of one per week. This threshold allows detection of the 27 M_{sun} at the distance 10.58 kpc (9.6 M_{sun} at 6.23 kpc) with 50% efficiency using the Far Detector of NOvA. Figure 10.g.5 shows the resulting coverage of the distribution of the galactic core-collapse supernova candidates by NOvA supernova trigger system.
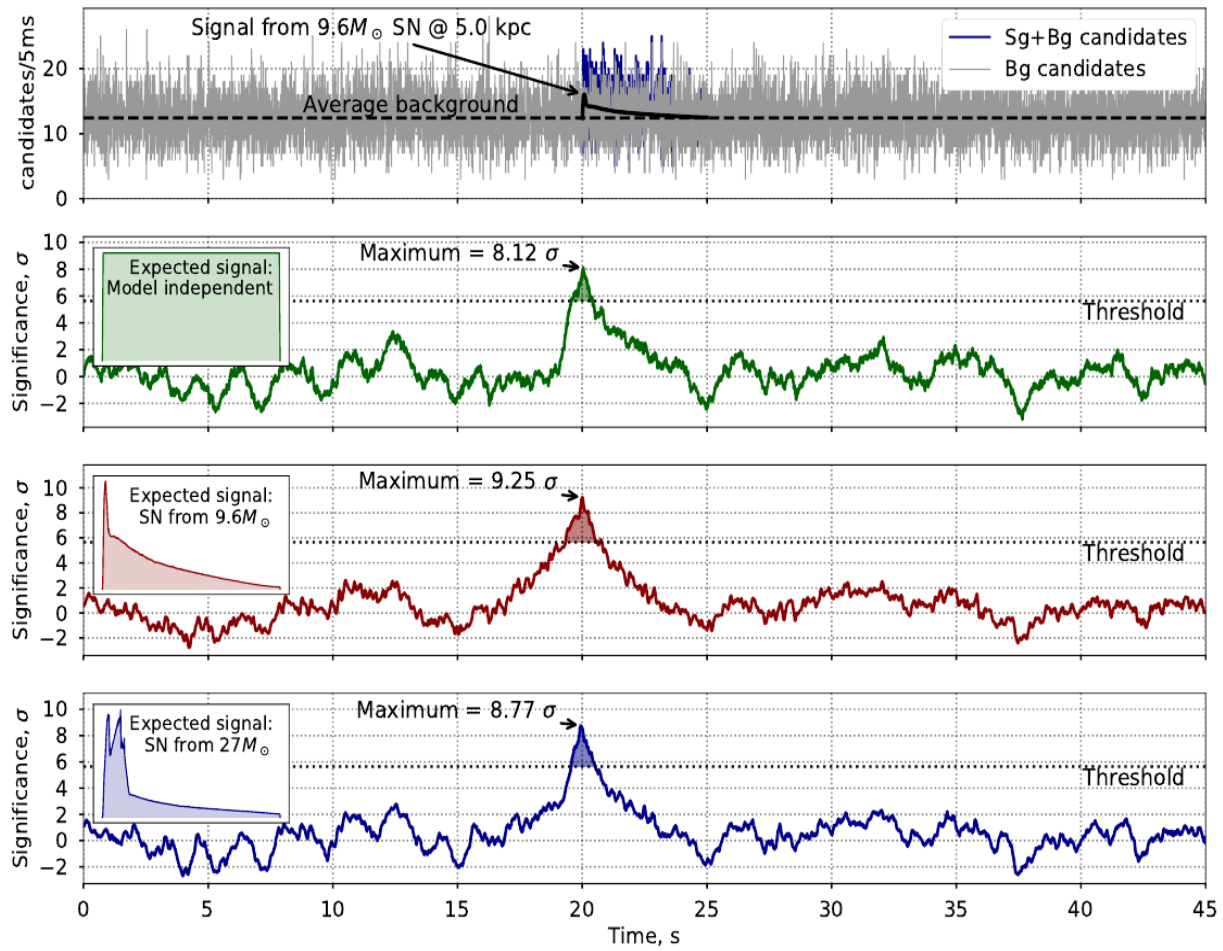
Figure 10.g.4. Example of the trigger system detecting a simulated supernova signal from a star 5 kpc away. The top time series of neutrino candidates per 5 ms bin in the NOvA Far Detector shows the location and size of an injected signal. The next three time series are the significance of the data matching the expected signal shape starting at that point in the time series. The injected signal is drawn from the middle model, causing it to match the best: but the other two templates still pick up the correct time (t = 20 s) with high significance.
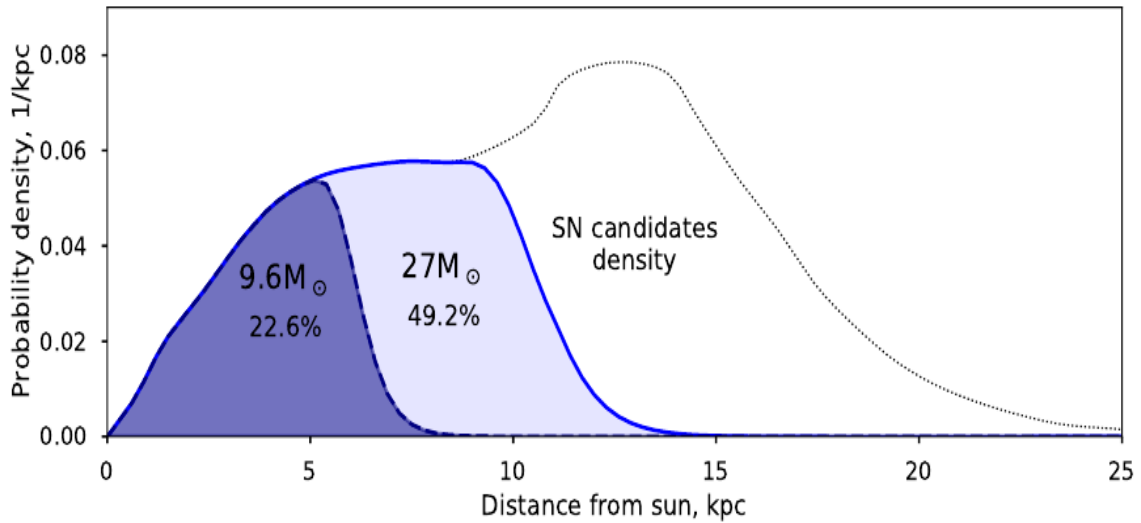
Figure 10.g.5. The NOvA experiment's sensitivity to galactic supernova vs. distance. The dark blue area is for a 9.6 M_{sun} progenitor, the light blue area from a 27 M_{sun} star. The dotted curve for supernova progenitor density is from [10.g.5]. Percentage is the fraction of SN candidates covered by the trigger, for the two cases of progenitor masses.

10.g.4 Future improvements and plans

Previously considered neutrino fluxes, provided by the simulation groups, do not include the neutrino oscillation effects. However, these effects, especially the oscillations in the stellar medium during the collapse, can significantly affect the observed event rates, signal shape and spectrum. These effects are discussed in [10.g.1,10.g.2].

Using the fact that the SN trigger system in NOvA is sensitive to the signal shape, it is feasible to estimate the sensitivity of NOvA to the neutrino oscillation parameters, in particular, neutrino mass hierarchy.

Currently SN triggering system in NOvA uses the triggers detectors in the "OR" mode: whenever near or far detectors observe the significance above threshold, the trigger signal is sent to the system, and the data within 45s around the peak time is saved for further more thorough offline analysis. However, a better result can be achieved by performing a meta analysis, based on the measured significance from two detectors. Such an approach should improve the total SN detection significance, increasing the reach of the SN trigger system.

Development of a real-time system for the significance combination and commissioning it on the NOvA detectors can have a broader use: for the global SuperNova Early Warning System upgrade, which is currently in development. Real-time metaanalysis of many detectors, sensitive to various interaction channels should provide a rich opportunity for sSN detection and study worldwide.

10.g.5 DUNE capacity for supernova neutrino detection

The 40 kton liquid argon far detector of the DUNE experiment is expected to be sensitive to the core-collapse SN neutrino signal [10.g.6] up to ~ Mpc distance, allowing a very precise measurement of the neutrino flux structure in case of a closer supernova. This could provide the opportunity to study the effects of the neutrino oscillations (see Fig.10.g.6), core-collapse shockwave instabilities, neutrino collective effects, and others [10.g.6, 10.g.7].

Moreover, DUNE will feature several detectors with various detection techniques, which would allow to study flavour composition of the SN neutrino signal, providing additional capabilities to study the core-collapse process and neutrino properties. In view of this, the development of the real-time combination system should also be useful, when applied to DUNE.
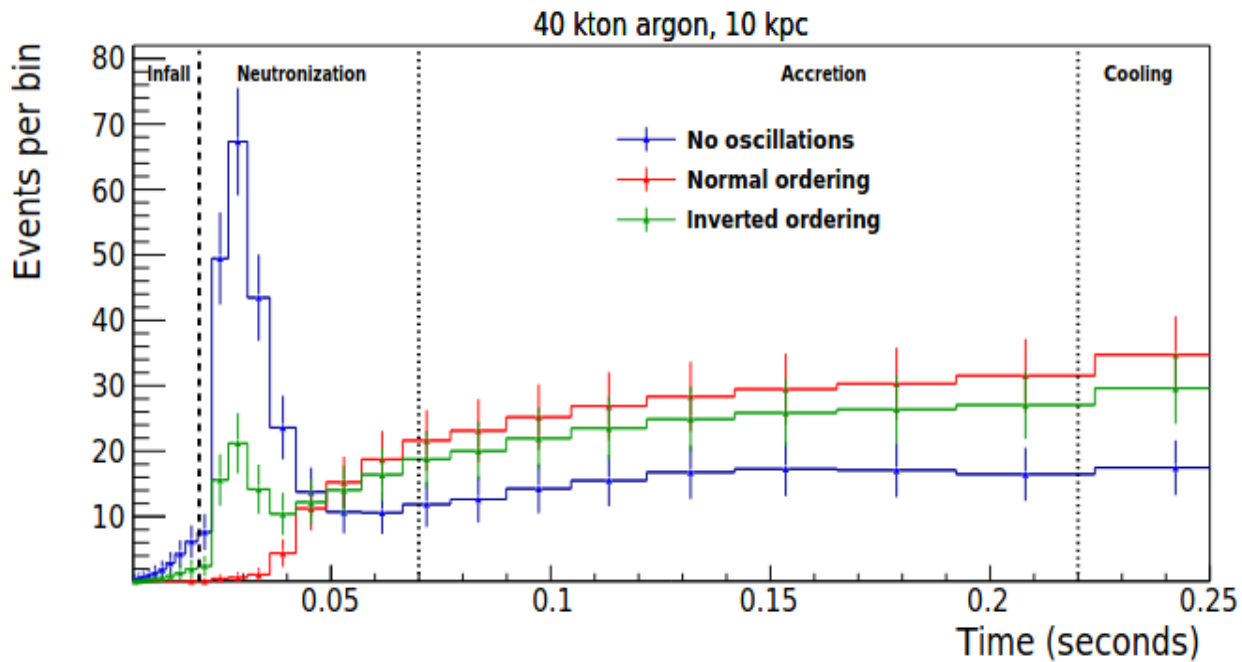
Figure 10.g.6. Figure from [10.g.6], expected number of supernova neutrino interactions from the core-collapse supernova at 10 kpc distance in the 40 kton DUNE detector. The effect of the oscillations in the stellar medium is significant.

10.g.ref References

[10.g.1] K. Scholberg, Supernova Neutrino Detection, Ann. Rev. Nucl. Part. Sci. 62 (2012) 81 [arXiv:1205.6003].
[10.g.2] A. Mirizzi, I. Tamborra, H.-T. Janka, N. Saviano, K. Scholberg, R. Bollig et al., Supernova Neutrinos: Production, Oscillations and Detection, Riv. Nuovo Cim. 39 (2016) 1 [arXiv:1508.00785].

[10.g.3] K. Nakazato, K. Sumiyoshi, H. Suzuki, T. Totani, H. Umeda and S. Yamada, Supernova neutrino light curves and spectra for various progenitor stars: From core colllapse to proto-neutron star cooling, The Astrophysical Journal Supplement Series 205 (2013) 2.

[10.g.4] C. Andreopoulos, A. Bell, D. Bhattacharya, F. Cavanna, J. Dobson, S. Dytman et al., The GENIE neutrino Monte Carlo generator, Nuclear Instruments and Methods in Physics Research Section A: Accelerators, Spectrometers, Detectors and Associated Equipment 614 (2010) 87

[10.g.5] A. Mirizzi, G. G. Raffelt and P. Serpico, Earth matter effects in supernova neutrinos: Optimal detector locations, JCAP 0605 (2006) 012 [astro-ph/0604300].

[10.g.6] Jost Migenda for the DUNE collaboration, Supernova Burst Observations with DUNE
        arXiv:1804.01877 [physics.ins-det]

[10.g.7] Artur Ankowski et al., Supernova Physics at DUNE, arXiv:1608.07853 [hep-ex]

10.h Monopole

10.h.1 Introduction

The NOvA Far Detector is on the surface, with a concrete and barite overburden of 3 m water-equivalent. It has the unique ability to search for subluminal exotic particles that would usually be absorbed by large shielding or overburdens of other experiments. One such particle, hypothesized in 1931 by Dirac [10.h.1], is the magnetic monopole. Recent theoretical work suggests a wide range of possible masses for monopoles [10.h.2, 10.h.3]. Searches over the past century have yet to find evidence of such a particle's existence. Significant fluxes of slow (β <0.01) GUT-scale monopoles ($m > \sim 10^{16}$ GeV) have been ruled out by underground experiments [10.h.4]. Weaker limits exist for slow monopoles in the range $10^5 < m < 10^{12}$ GeV from mountain-top experiments [10.h.5]. NOvA, a large low altitude surface detector, strikes a balance between these approaches. With its large size, it is able to set stronger flux limits for monopoles with $m > \sim 10^8$ GeV which are not absorbed by the atmosphere. However, compared to a dedicated underground detector, NOvA is not optimized for monopoles and must contend with a large cosmic ray background.

Using NOvA's data-driven trigger (DDT) system [10.h.6], the FD is able to isolate interesting physics signals among 150 kHz of cosmic rays. The event topology is a straight track traversing the FD with a speed that is a small fraction of the speed of light. This search has been optimized for $\beta = 10^{-3}$ magnetic monopoles, but has sensitivity to monopoles with $3 \times 10^{-4} < \beta < 6 \times 10^{-3}$.

10.h.2 Simulation

A monopole traversing the FD deposits visible energy in the liquid scintillator. NOvA's liquid scintillator is mostly composed of mineral oil (solvent) and pseudocumene (scintillant); its electron density is 2.9×10^{23} cm^{-3}. Although there is substantial theoretical uncertainty on the value of dE/dx, we use this nominal value to set limits in this search.

Geant4 [10.h.7] is used to simulate the detector's response to a monopole. In the absence of information about the distribution of the direction of the monopoles, the probability is assumed to be identical for monopoles coming from any direction. The monopole kinetic energy is very large relative to the energy lost in the detector, so it is assumed that the monopole's velocity remains constant.

The NOvA detectors were designed to measure energy deposition of particles with β near 1, which traverse each cell in the detector in under a nanosecond. No consideration was given in the design phase to particles depositing energy over as much as a microsecond, as monopoles at the lower end of our sensitivity would. In order to verify our simulation of the detector response to such slow signals, we performed a dedicated test stand measurement [10.h.8] which simulated monopole signals using light pulses generated by LEDs. The ratio of the measured signal to the simulation was 1.0±0.1.

Average APD channel response
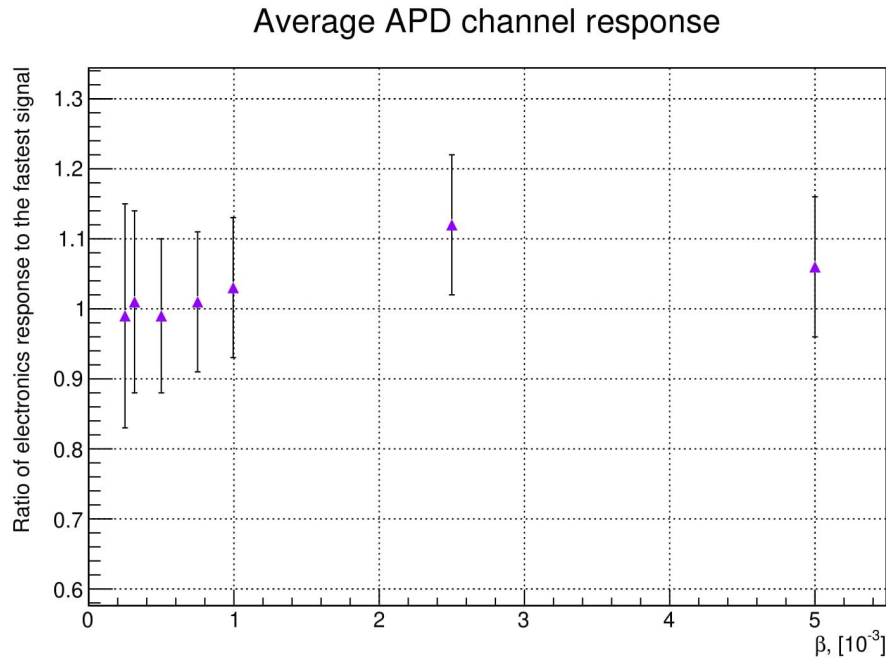
Figure 10.h.1. Average APD channel response vs betas

While this indicates no trouble, to conservatively account for the possibility that signals from slow energy depositions are overmodeled in our detector simulation, we reduce the signal by 10% in our simulation.

Each simulated monopole is combined with 5 ms of minimum bias data from the Far Detector. This results in an event that contains both the true monopole and real detector activity. This sample is used to measure how well the search algorithm can identify slow monopoles and differentiate them from the cosmic ray background.

10.h.3 Online trigger algorithm

The slow monopole trigger algorithm, initially inspired by IceCube's Slow-Particle-Trigger [10.h.9], identifies straight lines of hits consistent with a slow track. The trigger algorithm starts by considering pairs of hits on the surface of the detector for each 5 ms readout. It identifies hits that lie on a 20 cell wide "road" between the original surface hits (see Fig.10.h.2). The algorithm then looks for gaps between the hits on the road and identifies the maximum plane gap (along the z-axis) and the maximum cell gap (along the x- or y-axes). If there is a plane gap larger than 30 planes or a cell gap larger than 20 cells, the algorithm rejects the pair of hits. The procedure is then repeated for all of the pairs of hits on the detector surface.
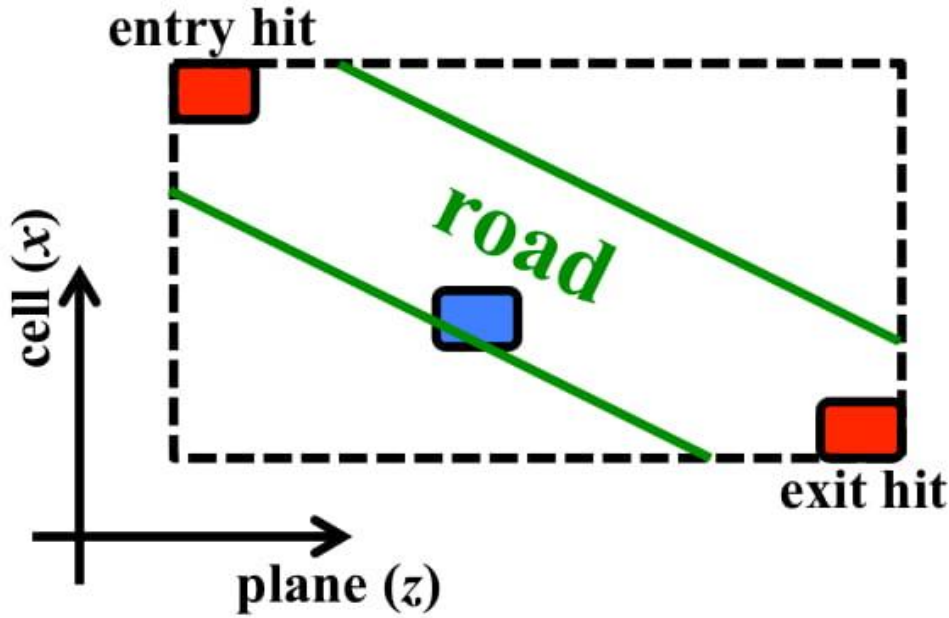
Figure 10.h.2. Schematic of the trigger algorithm. The hits on the detector surface are labeled entry and exit based on time. The algorithm looks for large gaps between hits on the road.

The trigger budget lacked the necessary CPU time to consider all possible pairs of surface hits, so only every tenth pair is checked. This sparsification method is efficient for monopole signals because a true monopole signal would have many pairs of surface hits. The pairs of surface hits must also have sufficient separation in space and time to originate from a track with a speed of $4\times10^{-5} < \beta < 5\times10^{-3}$. Monopoles with higher speeds are expected to be very heavily ionizing; a separate trigger not used in this analysis handles that case. If the algorithm identifies a pair of surface hits without large gaps, the event is written out to permanent storage.

10.h.4 Event selection

Data is acquired in two projected views separately, the xz- and yz-views. The y-direction is vertical while the z-direction points along the neutrino beam originating from Fermilab; x is approximately west. The first stage of event selection is monopole track reconstruction. This process begins by extracting two-dimensional information from each view and then combines this information into three-dimensional monopole tracks.

First, the algorithm identifies all of the speed-of-light tracks — primarily cosmic ray muons — and removes them. Since these tracks can overlap a potential monopole track, some true monopole hits may be removed at this step, somewhat reducing the search efficiency; this is the only significant downside to operating the detector on the surface. The algorithm then removes isolated as well as uncorrelated activity. The remaining energy depositions (hits) are reconstructed using the Hough tracking algorithm [10.h.10] to identify straight line objects. A line is fitted to each such collection of hits. The linear correlation coefficient, time gap fraction (defined below), and speed are

calculated for these candidate monopole tracks. A candidate must meet the following three basic requirements, as well as others described below:

1. There must be at least 20 hits in each view.
2. The track must cross at least 10 planes in each view.
3. The track must have a reconstructed length of at least 10 m.

Slow monopoles are not highly ionizing. The distinguishing characteristics used in this search are the straightness of their tracks and their consistent slow speed. The standard linear regression correlation coefficient (r^2) is calculated for hits in xt and yt separately. A true monopole track would have r^2 close to unity. The minimum of r^2_{xt} and r^2_{yt} is called r^2_{min}.

A potential background is caused by reconstruction failures in which two speed-of-light cosmic rays are identified as a single monopole track. Such monopole tracks have a cluster of hits occurring early in time, a large time gap, and then another cluster of hits occurring later. To remove such cases, the largest time gap between consecutive hits is required to be small. The quantities f_{xt} and f_{yt} are calculated for each track. For each view, f is the ratio of the largest time gap between hits in the track, ordered by time, and the total extent of the track in time. A high-quality track will have a value of f close to zero, whereas a track built from two unrelated cosmic rays will have a value of f close to unity. The maximum of f_{xt} and f_{yt} is called f_{max}.

To set selection criteria, small subsamples of NOvA data were examined under the assumption that such samples would contain no monopoles. Up to 10% of the data was used in this way. The remaining criteria for selecting an event as a monopole are:

1. $f_{max} \leq 0.2$
2. $r^2_{min} \geq 0.95$
3. $\beta < 10^{-2}$

10.h.5 Results

The triggered sample contained 10 447 881 events and none fell into the signal region. Figure 10.h.3 shows the distribution of the full sample. All data events are far from the signal region. The most signal-like events were reconstructed with β between 10^{-3} and 10^{-2} and r^2_{min} around 0.65. Upon visual inspection, these events proved to be caused either by two speed-of-light tracks in the same location at slightly different times, or by tracks formed out of fragments of high energy showers. In neither case would other events with the same characteristics easily be able to satisfy the requirement of > 0.95. We also expect that visual inspection of any such exceptional background event would unambiguously result in its rejection. A progression of hits moving slowly across the segmented detector is clearly distinguishable from all backgrounds we considered and all near-background events we observed.
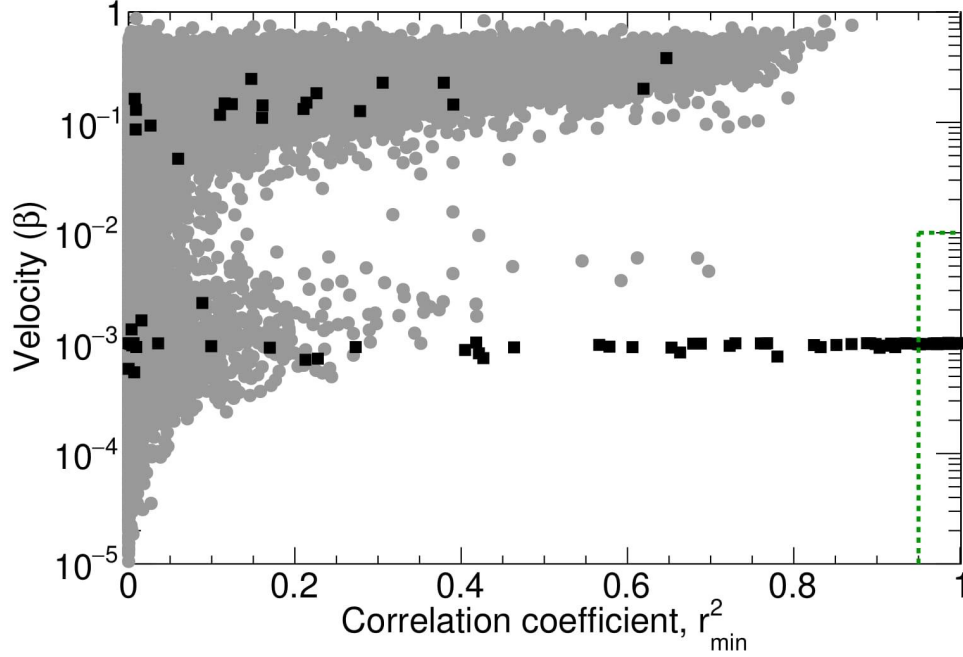
Figure 10.h.3. Reconstructed monopole speed and r^2_{min} for events passing all other selections. Data is shown as grey circles, and MC for $\beta = 10^{-3}$ as black squares. Events must be in the dashed box in the lower right to be selected.

Since the analysis is background-free, the 90% C.L. flux upper limit is $\Phi_{90\%} = 2.3/L$, where $L = \Omega\varepsilon At$ is the integrated acceptance, where Ω is the solid angle coverage, ε is the efficiency, A is the projected surface area of the FD visible to the monopole, and t is the integrated live time. Each quantity is detailed below.

Limits are reported for the two major coverage scenarios, half coverage where $\Omega = 2\pi$, and full coverage where $\Omega = 4\pi$. The coverage depends on the kinetic energy of the monopole, which is calculated from the monopole's speed and mass. If the monopole's energy is sufficient, it can traverse the entire planet. In this case, NOvA has 4π coverage. The half coverage regime occurs when the monopole has enough energy to make it through the atmosphere from above, but not enough to reach NOvA from below. Figure 10.h.4 shows the solid angle coverage as a function of monopole speed and mass.
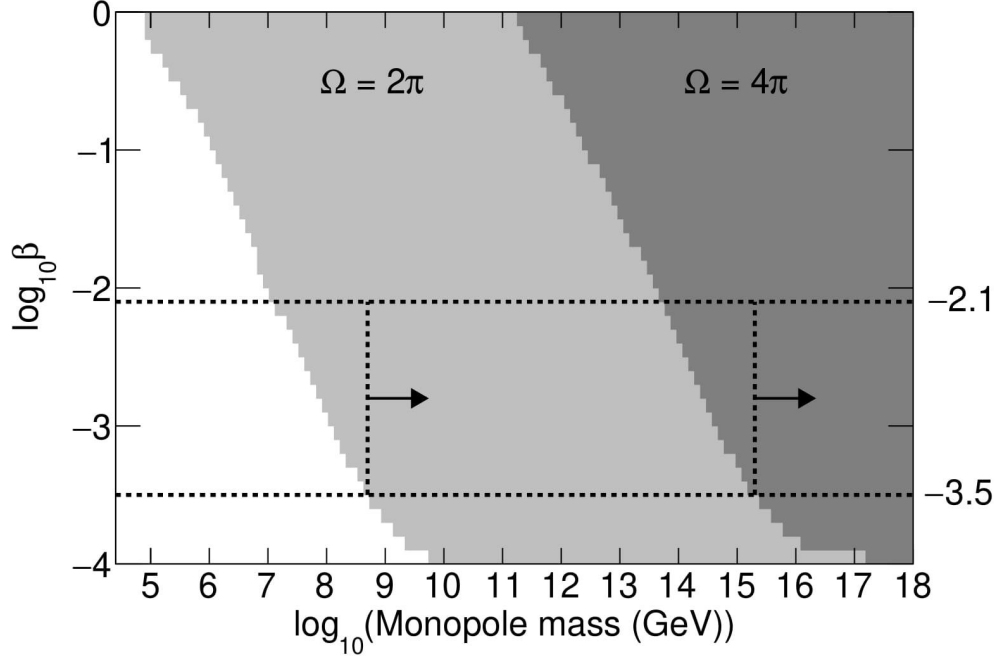
Figure 10.h.4. Figure 10.e.4. Expected significance to exclude $\delta_{CP} = 0, \pi$ in case of normal hierarchy. Mass hierarchy is assumed to be known. Solid angle coverage as a function of monopole speed and mass. Horizontal dashed lines indicate the boundaries of the search sensitivity in speed. Vertical dashed lines indicate the reference masses used to generate limits shown in Fig. 10.h.5.

We calculate the detector's projected area, A, for each simulated monopole's trajectory. The reconstruction efficiency also depends on the monopole's trajectory, so the product is determined event by event, $\varepsilon A \equiv \langle \varepsilon_i A_i \rangle$. The mean efficiency for detecting a monopole with $\beta = 10^{-3}$ which intersects the detector is 29%. For monopoles with a true crossing length of at least 10m which also cross at least 10 planes and 20 cells in each view (matching the basic requirements) the selection efficiency is 53%.

Data from 5 June 2015 through 12 October 2015 is used for this search. In these 129 days, good data was collected for 8.21×10^6 s. Only data which included the entire Far Detector and which passed all data quality checks was used. The DDT system was 99.9% efficient during this time period, where the small inefficiency is caused by the available time for the trigger to process incoming data being exhausted. The corrected live time is therefore 8.20×10^6 s (94.9 days).

Figure 10.h.5 shows limits as a function of β for two mass cutoffs. These represent slices through the coverage shown in Fig. 10.h.4. By taking other vertical slices through this figure, it can be seen that some sensitivity exists for masses as low as $\sim 2 \times 10^7$ GeV, but only for such monopoles at the upper end of the speed range, $\beta \approx 10^{-2.1}$.
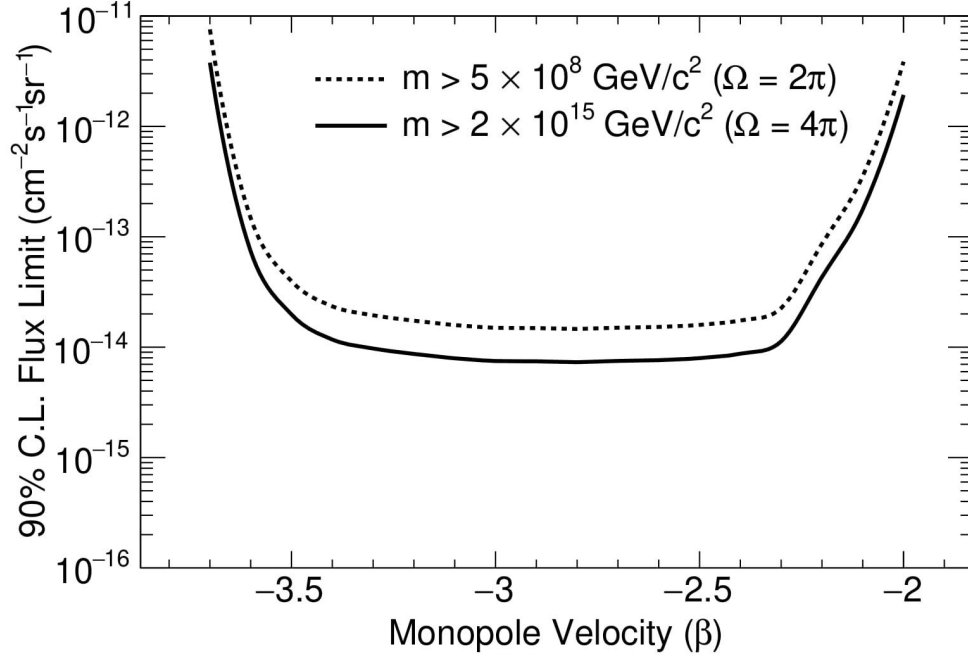
Figure 10.h.5. Upper limits on the magnetic monopole flux for the two coverage regimes. The sensitivity falls off at low β as the energy deposition of monopoles drops below the analysis threshold. At high β, the sensitivity is limited by the trigger design.

In terms of detector effects, these limits are conservative since they use the lower bound on hit efficiency as described before. A higher efficiency would extend the quoted limits slightly towards lower masses. Other detector-based systematic uncertainties are negligible. We considered uncertainties in live time and solid angle. Each is well under 1%. However, substantial theoretical uncertainty in slow monopole dE/dx feeds into an uncertainty on translating non-detection into a flux limit. As stated above, these limits use the nominal dE/dx of Ahlen and Kinoshita. Higher or lower energy depositions would modify the limits in the same way as changes in detector efficiency.

These limits assume a monopole with charge g. The limit weakens at low β because such a monopole does not deposit enough energy to pass the trigger or analysis selections. For a generic slow-moving particle with ionization dE/dx sufficient to pass these selections, the flux limits remain similar from $\beta = 10^{-3}$ down to ~4×10^{-5} the lower cutoff in the trigger. Below this speed, a particle cannot, in any case, reliably cross the detector within a single 5 ms trigger block. Because the trigger records 2.5% of the detector lifetime, some efficiency for very slow particles remains down to $\beta = 7\times10^{-6}$, at which point the particle does not travel even the required 10 m in 5 ms. At high β, regardless of ionization signal, the limits cut off near 10^{-2} because the trigger does not look for fast tracks.

10.h.6 Conclusion and future plans

By virtue of a large fine-grained detector on the Earth's surface, NOvA is uniquely sensitive to slow intermediate-mass monopoles which would not reach previous detectors such as MACRO [10.h.4]. We have constrained the flux of this population of monopoles in a large region of speed-

mass space which had previously been unconstrained. For heavier monopoles, our result confirms previous limits.

The results shown here represent less than 10% of the data the NOvA Far Detector has collected to date. Data following October 2015 was taken at a higher APD gain, allowing collection of fainter signals which will allow improved mass reach. We plan to continue slow monopole investigation with high APD gain.

10.h.ref References

[10.h.1] P. A. M. Dirac, Proc. Roy. Soc. Lond. A133, 60 (1931).
[10.h.2] T. W. Kephart and Q. Shafi, Phys. Lett.B520, 313 (2001), arXiv:hep-ph/0105237 [hep-ph].
[10.h.3] M. Tanabashi et al.(Particle Data Group), Phys. Rev. D98, 030001 (2018).
[10.h.4] M. Ambrosio et al. (MACRO), Eur. Phys. J.C25, 511 (2002), arXiv:hep-ex/0207020 [hep-ex].
[10.h.5] S. Balestra et al., Eur. Phys. J.C55, 57 (2008), arXiv:0801.4913 [hep-ex].
[10.h.6] A. Norman et al., Proceedings, 21st International Conference on Computing in High Energy and Nuclear Physics (CHEP 2015): Okinawa, Japan, April 13-17, 2015, J. Phys. Conf. Ser.664, 082041 (2015).
[10.h.7] S. Agostinelli et al., Nucl. Instrum. Meth.A506, 250 (2003).
[10.h.8] A.I.Antoshkin, Long signals measurements on Electronic test stand at JINR, Internal technote. DocDB # 40216.
[10.h.9] M. G. Aartsen et al. (IceCube), Eur. Phys. J.C74, 2938 (2014), [Erratum: Eur. Phys. J. C79, no. 2, 124 (2019)], arXiv:1402.3460 [astro-ph.CO].
[10.h.10] P. Hough, "Method and means for recognizing complex patterns," U.S. Patent No. 3,069,654 (1962).

10.i Atmospheric muons

10.i.1 Introduction

Far Detector of the NOvA experiment is located on the surface and due to large dimensions it detects 10^5 atmospheric muons per second.
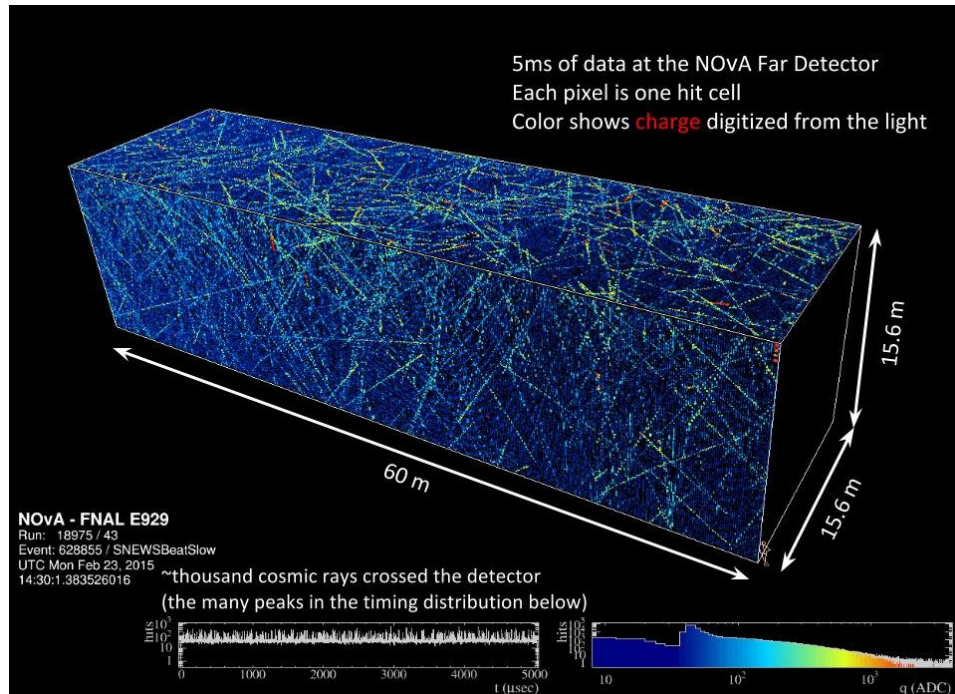
Figure 10.i.1. Event display of NOvA Far Detector with many cosmic ray tracks.

Based on this, NOvA Collaboration provides several researches connected to atmospheric muons, and has opportunities for some more. JINR team already participates in the measurement of the East-West asymmetry of secondary cosmic rays and in the study of very high-energetic muon events in the Far Detector. Also, NOvA members study seasonal variations of atmospheric muon flux (multi-muon event research was finished and printed in [10.i.1]) and events with high multiplicity parallel cosmic muons from Extensive Air Showers in the NOvA Far Detector.

10.i.2 High-energy cosmic-ray muons

Analysis of muons with the energies higher than 100 GeV, produced in the upper atmosphere, can provide information about the spectrum and composition of primary cosmic rays and the details of the interaction of hadrons with nuclei at energies inaccessible to current accelerators.

It is possible to estimate the energy spectrum of these high-energy muons using the method named 'parmeter' [10.i.2]. It is one of the methods of muon energy reconstruction, based on measuring the specific components of energy loss.
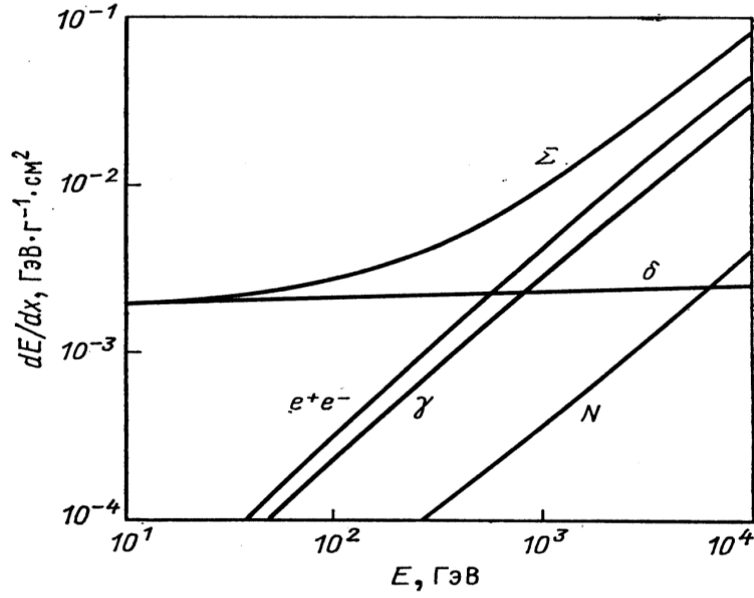
Figure 10.i.2. Energy loss components of muon (in iron). This picture is borrowed from [10.i.2].

Muon energy loss can be defined as *-(dE/dx)=a+bE*, where *a* is the ionisation energy (delta-electrons) loss and *bE* is the sum of e-pair production, bremsstrahlung, and photonuclear contributions (*a* and *b* are slowly varying function of the muon energy). Above 1 TeV energy loss is almost proportional to *E*.

The key point of the implementation of this method is the separation of relatively mild fluctuating loss on the e-pair formation and catastrophic collisions in the processes of bremsstrahlung and nuclear interactions. When we manage this, we will be able to estimate the muon energy from its energy loss.
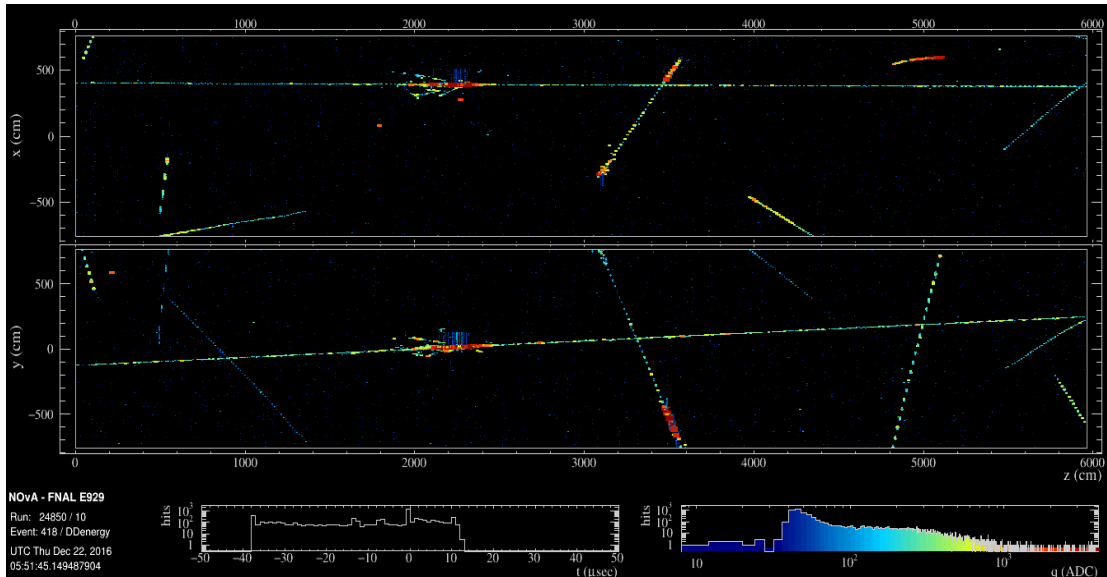
Figure 10.i.3. High-energy muon in real data of the Far Detector of NOvA.

10.i.3 East-west asymmetry

Measurement of the east-west asymmetry of cosmic muons can help with discrimination of the primary cosmic ray mass composition.

The phenomenon is based on the Lorentz force, that incline charged particles, moving in a geomagnetic field. In the Northern Hemisphere for the particles coming to a certain point on the Earth from the east, some of the trajectories are forbidden, and cosmic ray flux from east is smaller than from the west.
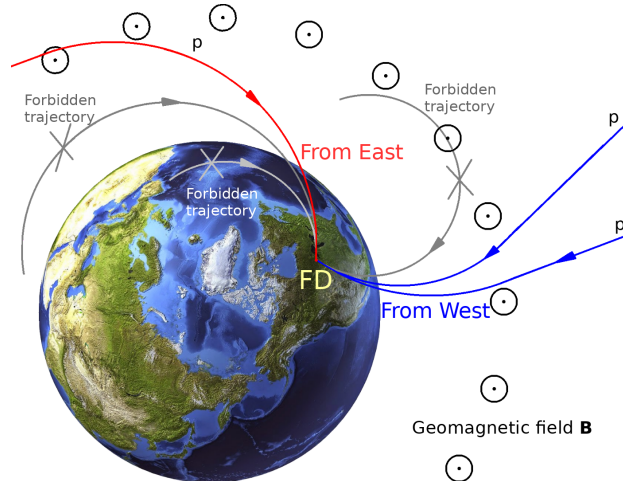
Figure 10.i.4. East-west asymmetry of cosmic rays for NOvA FD.

The study of east-west asymmetry in the Far Detector of NOvA is complicated by the fact that the overburden covering the detector and the rock surrounding it are also asymmetrical.
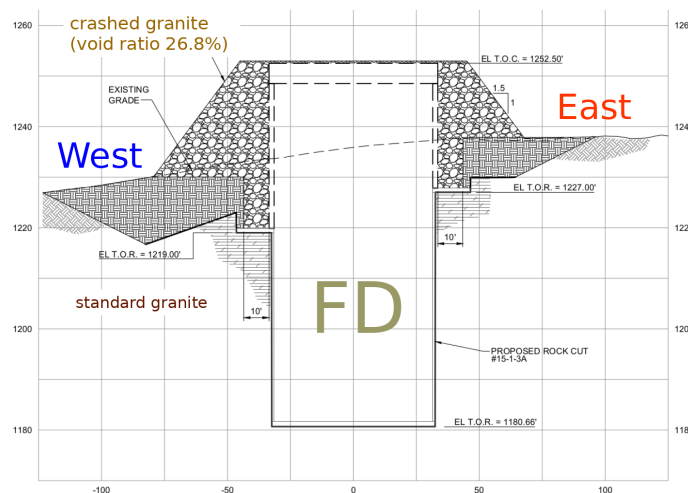
Figure 10.i.5. Asymmetry of the hill around Far Detector.

When corresponding corrections are applied, we will obtain the east-west asymmetry measurement at the NOvA Far Detector coordinates and improve the knowledge about the geomagnetic field and primary cosmic rays. It is planned to study how asymmetry depends on the zenith angle of muon direction and muon energy.

East-west asymmetry of atmospheric muon fluxes, detected in the NOvA Far Detector, was so far measured on 122 millions reconstructed tracks. The contribution of the anisotropic detector environment was previously estimated by using MC-generator CRY, where the geomagnetic effect of East-West asymmetry is not implemented.
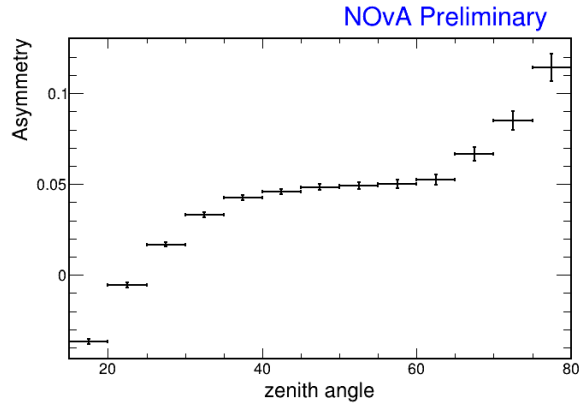
Figure 10.i.6.a. East-West asymmetry of atmospheric muons, stopped in the Far Detector of NOvA, without hill asymmetry correction. Asymmetry is defined as A=(W-E)/(W+E), where W is muon flux coming from West, E is one from East
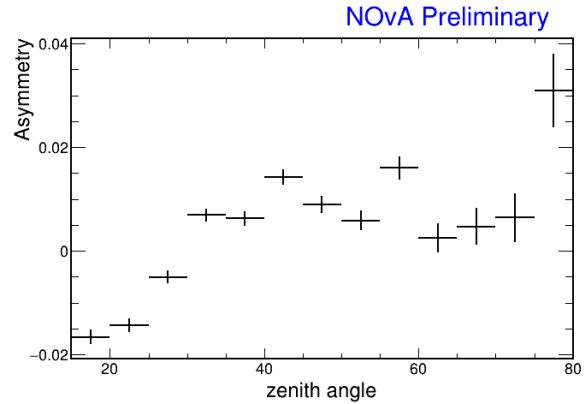
Figure 10.i.6.b. Geomagnetic asymmetry of atmospheric muon fluxes (first order correction)

As a first step, the reconstruction efficiency of muons stopping in the detector was estimated depending on the arrival direction: according to the expectation, the reconstruction efficiency of tracks aligned with the planes that make up the detector structure turned out to be significantly lower: about 60% and 50% for muons moving in +/-10 degrees from the vertical and horizontal, respectively, with efficiency in other areas of about 80%.
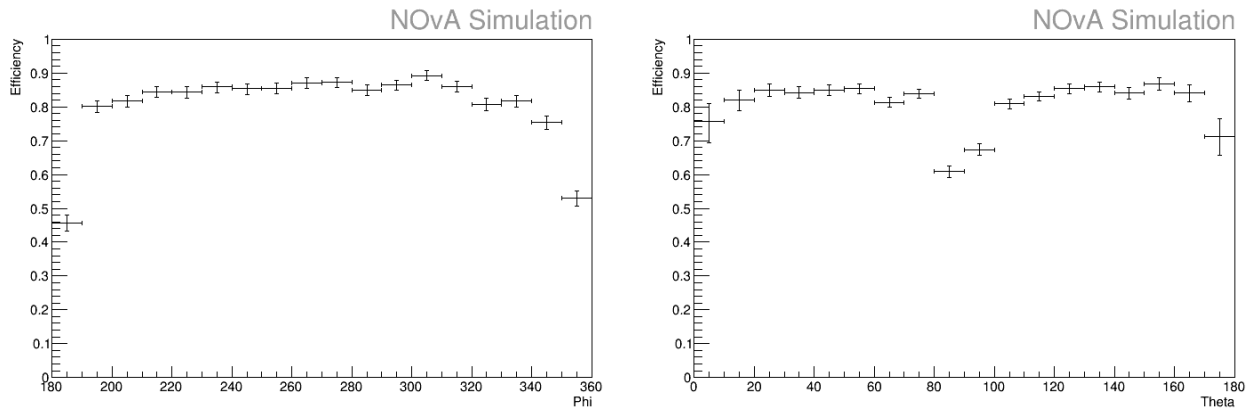
Figure 10.i.7. Reconstruction efficiency as a function of muon track direction angles.

Initial energy reconstruction of a stopped muon was made by four methods: based on the calorimetric energy of the track, with and without taking into account the dependence of energy loss on the particle energy and taking into account multiple Coulomb scattering in the detector material. The first method was found unsuitable for use.
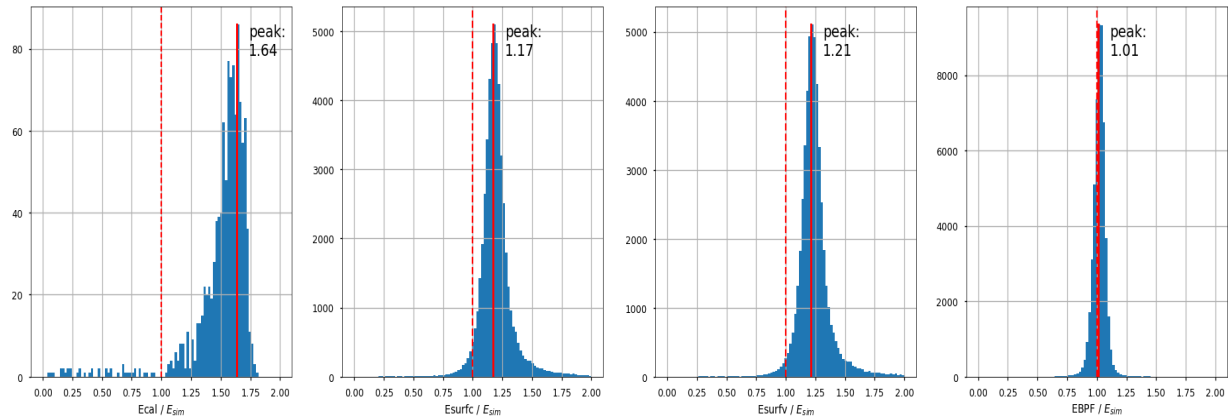

Figure 10.i.8. The accuracy of muon energy reconstruction, from left to right: 1) using the calorimetric energy method, 2) without taking into account the dependence of energy losses on the particle energy, and 3) taking it into account, 4) taking into account rescattering.

It is planned to calculate the efficiency of muon registration as a function of particle energy, the direction of motion and the position of tracks in the detector, including using a combination of methods to reconstruct the particle energy left inside and outside the detector.

To describe the absorption of muons in matter and the efficiency of muon parameter reconstruction, a Monte Carlo simulation of 10 million muon tracks has been created. The results were presented in

the form of multidimensional tables with a uniform partition of the allowable ranges of arrival angles, with uneven partition and with the allocation in the parameter space of areas of complex shape for uniform filling of each area with statistics. None of the methods of representation allows us to achieve such a description of the transformation of the flow from true to detectable so that the inverse transformation does not lead to instability of the result. Therefore in the future we are going to use the regularization of the inversion procedure according to the Tikhonov method.

10.i.ref References:

[10.i.1] NOvA Collaboration (M.A. Acero (U. Atlantico, Barranquilla) et al.) Observation of seasonal variation of atmospheric multiple-muon events in the NOvA Near Detector // Phys.Rev. D99 (2019) no.12, 122004.
[10.i.2] R. P. Kokoulin, A. A. Petrukhin, Phys. Part. Nucl. (Zh. Fiz. Elem. Chast. Atom. Yadra) (In russian), 21, no. 3, 774 (1990).

10.j Electronic Parameters Measurements for NOvA

10.j.1. NOvA electronic test stand

It was realized from the very beginning that the comprehensive understanding of the NOvA detector's operation will, in particular, require additional precise measurements of electronics parameters even after commissioning. For this reason, an electronics test bench was developed at JINR using the components of actual NOvA electronics. The NOvA test bench at JINR consists of a few parts (see fig 10.j.1).
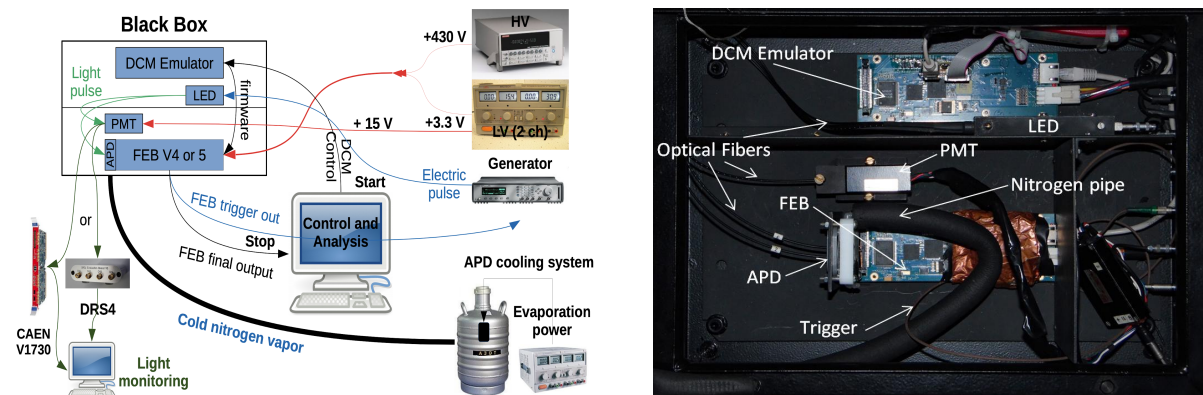

Figure 10.j.1. NOvA test bench. Schematic view - left, Black box - right.

First is the native NOvA electronics – Avalanche PhotoDiode and Front-End Board. Second is the special hardware – download cable, DCM-emulator, LED, Low and High Voltage Sources, Pulse generator and cooling system. Third is a PC with the necessary software. All sensitive devices were placed into a black metal box (fig 10.j.1. right). The black box allows one to perform all of the measurements with photodetectors, like APDs and PMTs, and screens all external electromagnetic noise. Because APDs in NOvA operate at -15° C we employ a cooling system based on Nitrogen evaporation flow. A pulse generator waits for the FEB trigger and sends the electric pulse to the

LED. Then the light pulse from the LED travels through the fibers to the APD, and the FEB reads the data.

Indeed, several important measurements were performed at the JINR NOvA electronics test bench, and more are planned.

10.j.2. Sag effect

An important characteristic of the electronics operation is a cross-talk between different channels. It can have several sources and should be adequately understood and described in the Monte Carlo simulation and calibration.

In fig 10.j.2 the event display in the NOvA FD is presented. One may notice some strange hit structures, which are called Flashes. The main feature of flashes is that sometimes the FEB channels in the same FEB produce signals over threshold simultaneously, but these events take place only if the primary signal is of very high amplitude. Understanding this effect is important for events with high-energy depositions, in particular, for the estimation of Cosmic Ray background and searches for Exotics.
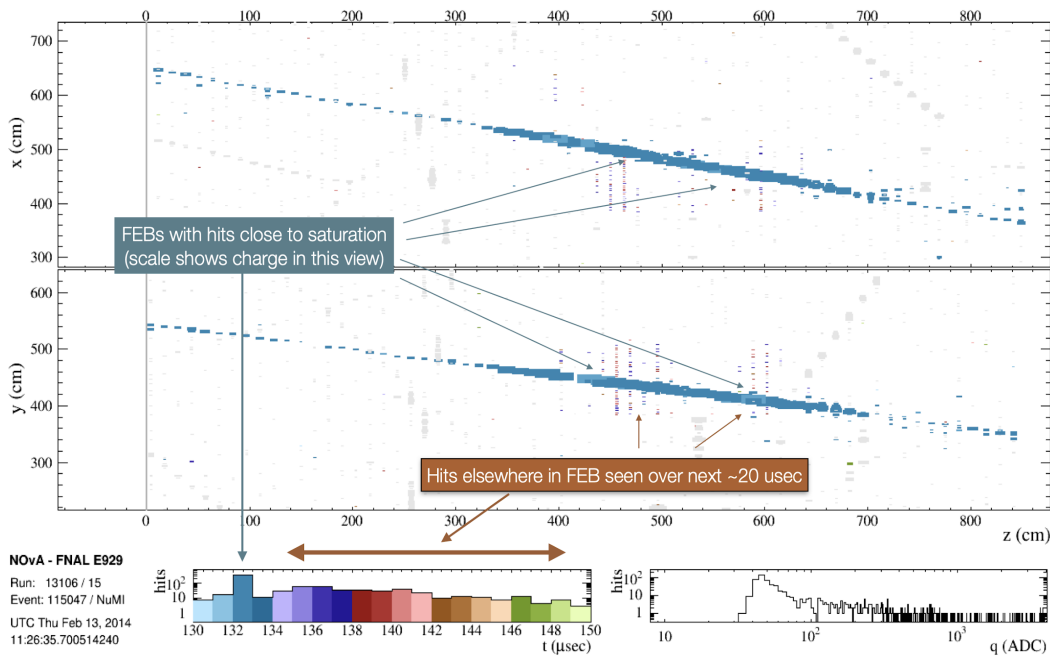
Figure 10.j.2. An example of the event in the Far Detector with Flashes.

After building the test bench we began studying the APD response to different light intensities. It was very important for understanding the detectors performance for high energy dissipations.

By sending very high intensity light into a single APD pixel, which saturates the ADC, we found that the same small inverted signals occur in most of the channels within the same FEB (sag-effect). But while checking the FEB by injecting a huge charge into a single FEB channel we observed only normal cross-talk in neighboring channels that drops exponentially.

The next step was to check the APD feeding chain. In the NOvA detectors all APDs operate with a gain of about 100. We also performed a measurement of APD gain with different temperatures to study APD operation voltage at different temperatures (see fig. 10.j.3.left).
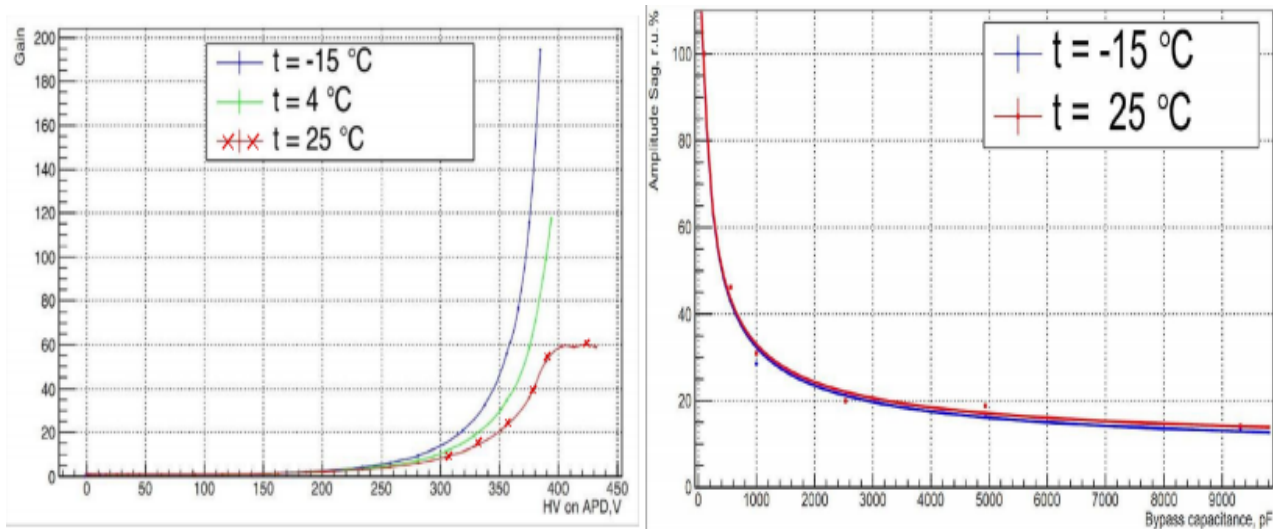

Fig 10.j.3. APD gain vs applied voltage with different temperatures (left). APD Sag dependence with respect to the primary effect vs bypass capacitance (right).

We tested different capacitance in the APD bias voltage chain and observed a change in the value of negative crosstalk pulse. It was suggested that the capacitance blocks a voltage drop, which was named the Sag-effect. The Sag was defined as a value of the amplitude of the inverted signal in the neighboring channels in the case of a huge amplitude in the primary one. We applied different amplitudes to the APD and measured the value of the Sag. The result was that the relative value of the Sag does not depend on the amplitude, and is equal to 1.89% for the original electronic circuit. The Sag does not depend on the temperature as well. It is the capacitance, which essentially drives the effect (see the right part in fig. 10.j.3). As an example, a replacement of the original 100 pF capacitor by a 9.4 nF one reduces the effect sevenfold.

After these measurements, which clarified the situation, the NOvA collaboration has adopted Sag as a useful option for dynamic range extension of electronics. In a case where the primary signal saturates a readout channel, the Sag amplitudes travel to the next channels, which are almost free of signals because of low event rate. And, finally, the primary signal's amplitude can be evaluated by many (up to 31) neighboring amplitudes. As a result, we can still estimate the primary signal with a reasonable precision. For more information about the results of the test bench activity see [10.j.1, 10.j.2].

10.j.3. Response to the long signal

An experimental setup was made to study the response of the electronics to long signals. In addition to the ordinary setup, a PMT and a stand-alone ADC were introduced. The PMT was used to monitor the shape of the initial light pulse and ADC with fast sampling to digitize PMT signals. The main idea was to send light with the same integral intensity, which corresponds to a constant charge. We also tried to generate rectangular-like light pulses. The ASIC shaper integrates the APD

pulse width and converts it into a rise time, and shaping parameters vary on pulse amplitude (Figure 10.j.4).
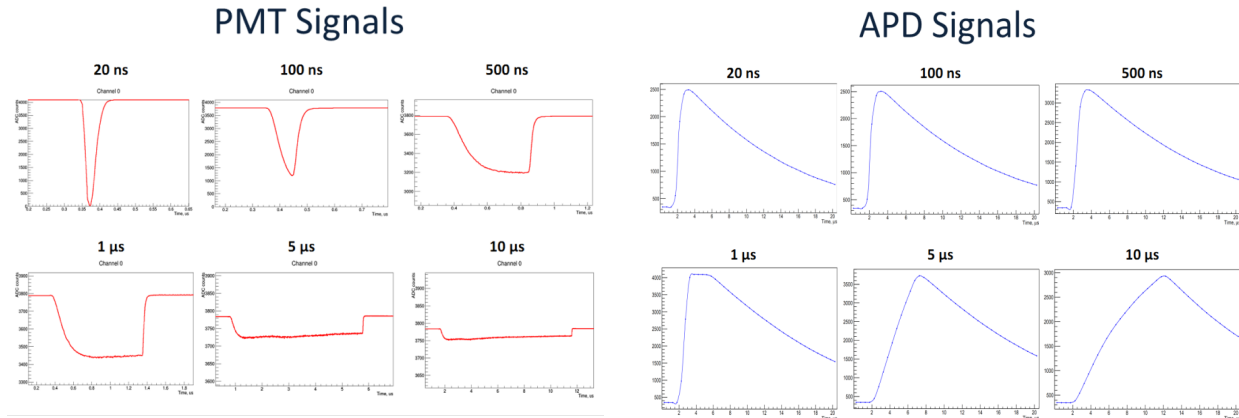

Figure 10.j.4. PMT signals on stand-alone ADC - left, APD signals on the NOvA electronics - right.

10.j.4. Shaping parameters

For simulation of the detectors' performance a request came from the NOvA collaboration to find precisely all the shaping parameters for both detectors. It was important for computer modeling and Monte-Carlo simulations. The scheme of the measurement was the same that aforementioned. The fall time was found to depend linearly on the amplitude (see Figure 10.j.5) and the rise time variation with amplitude was found to be negligible.
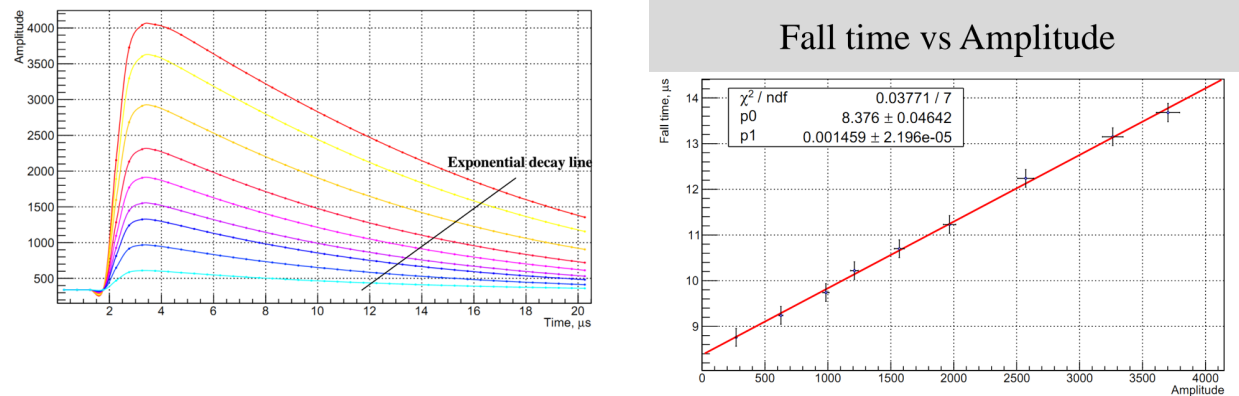
Figure 10.j.5. APD signals with different amplitudes-left. Fall time dependence on the amplitude of the signal-right.

10.i.ref References

[10.j.1]   A.Antoshkin, NOvA internal talk, DocDB #14261.
[10.j.2] A.I.Antoshkin, Long signals measurements on Electronic test stand at JINR, Internal technote, DocDB # 40216.

10.k Benchmarking of the NOvA scintillator at JINR

10.k.1. Scintillation quenching. Birks law.

A charged particle passing through a substance deposits its energy within. Part of this energy goes to photon production. For some substances (scintillators) this portion is significant, so that generated light can be detected and measured by photosensors or photodetectors. The spectrum and intensity of the light signal depends on the intensity of the energy release, and the type of passing particle and attributes of the scintillator, see [10.k.1] and [10.k.2]. Many scintillators, depending on radiation length, are sensitive not only to charged particles, but also to gamma-radiation and neutrons. These are the main attributes of scintillators: light yield, the spectral composition of radiation, energy resolution, decay time, radiation resistance, radiation length and quenching factors – Birks Law.

The scintillation response, S, of organic crystals depends on the nature and energy, E, of the incident ionizing particle, of residual range r. The specific fluorescence, dS/dr , is not in general proportional to the specific energy loss dE/dr . By considering the quenching effect of the molecules damaged by the particle by the "excitons" produced by it, it is possible to show that:

$$\frac{dS}{dr} = \frac{A\frac{dE}{dr}}{1+kB\frac{dE}{dr}} \quad \textbf{(g.1)}$$

Where A and kB are constants, which have been evaluated for scintillator from observations of S and E, and the range-energy data. The method used for evaluating the relative response is applicable to ionizing particles of any nature or energy, and also to the different organic scintillation crystals or liquids.

The quenching factor is a very important attribute of any scintillator [10.k.3]. If we do not know the quenching factor, we cannot say what kind of particle passed through the scintillator and what primary energy it had.

10.k.2. Measurement of the Birk's constant for NOvA scintillator.

In the case of NOvA we would like to measure Birk's coefficients for protons of MeV energy scale. But it is not so easy to deliver protons with this energy inside the scintillator. We have to use a neutron source and measure the energy of recoil protons. Recoil protons are produced in the liquid scintillator by neutrons emitted by Pu-Be source with continuous spectrum[1]. In the case of a continuous spectrum it is possible to use the time-of-flight method for selecting neutrons of a certain energy.

---

[1] We operate with radioactive sources in special premises in Radio-Chemical Laboratory. We very much appreciate the great help of V. Egorov, S. Kazartcev and V. Brudanin in preparation of these measurements.
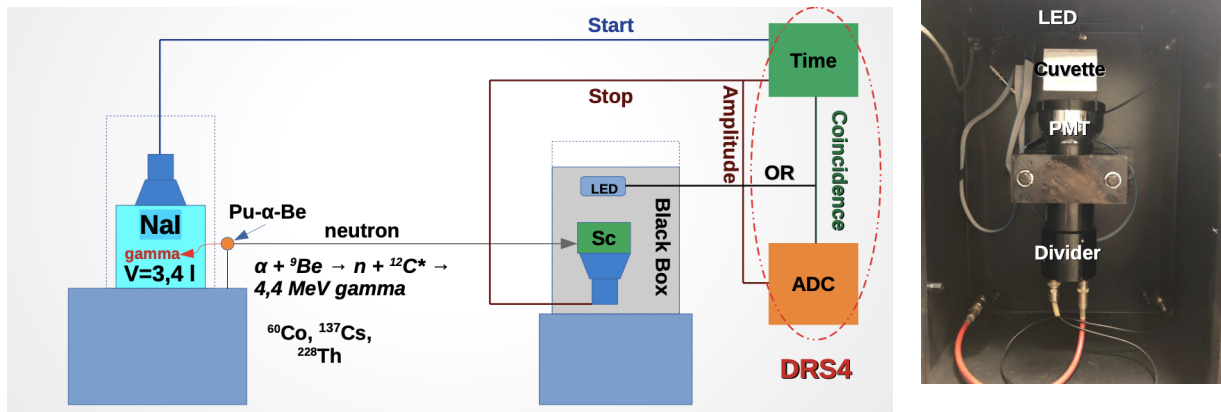
Figure 10.k.1. Schematic operation of the JINR scintillator test stand. Left - schematics of the scintillation stand operation. Right - inside the black box: the cuvette with LS readout by the PMT.

To measure proton response in the NOvA LS we used the Neutron time-of-flight (TOF) technique (fig. 10.k.1). A neutron is produced by an isotope PuBe-source simultaneously with γ-quantum, which triggers the start counter (NaI-crystal). The neutron produces a recoil proton in the LS sample in a transparent cuvette read out by a PMT, which generates the stop signal.

By measuring the neutron's TOF (length) one can obtain its real energy. On fig. 10.k.2 (left) a timing histogram of signals coming from different particles is presented. When γ-quantum backscatters in the NaI-crystal and then hit the scintillator cuvette (γ-γ coincidence) we can use this as a reference time by knowing distance and the speed of light. The same reference when neutrons interact in NaI-crystal and γ-quantum come to the cuvette, this time is peaking around γ-γ time peak (γ-n). A broad gap is splitting γ-γ(γ-n) interactions and neutrons time travelling to the cuvette because of the relatively slow speed of neutrons and the distance of 2 meters.

Selecting neutrons by time slicing we can extract recoil proton spectrum (fig. 10.k.2. right) and its edge defines maximum transferred energy which is equal to the primary neutron's energy which we know from TOF.
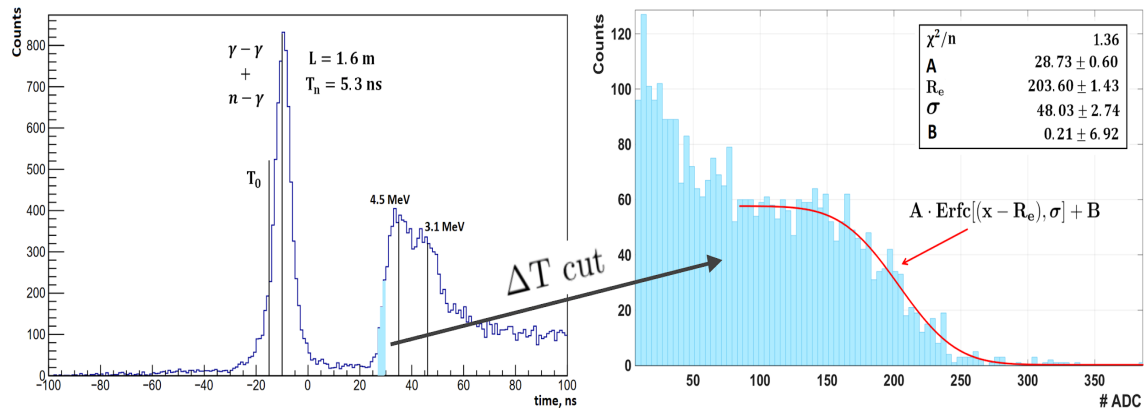

Figure 10.k.2: Timing histogram - left, selected recoil protons by neutrons time slicing - right.

Response from protons is calibrated with respect to gamma-sources ^{137}Cs, ^{60}Co, [228]Th (see fig 10.k.3 - left) assuming negligible quenching effect for fast electrons (Compton spectrum edge).
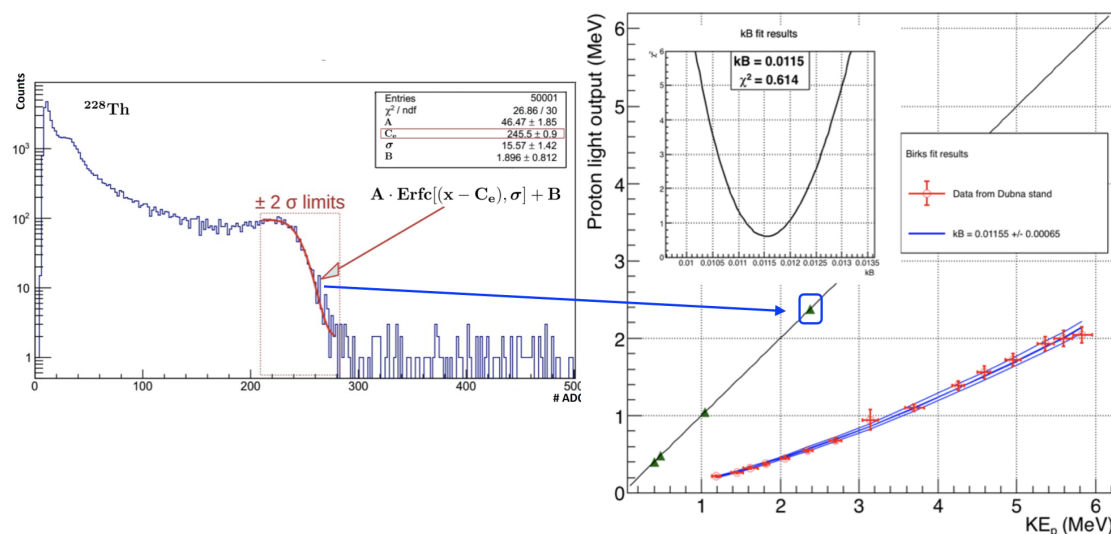

Figure 10.k.3. Left - [228]Th compton spectrum, Right - MC fit for measured dataset.

Finally, data were analysed by using NOvA simulation software based on GEANT deposit energies and custom simulation for light output (fig.10.k.3 right). The Birks coefficient is $k_B = 1.155$ +/- 0.065 [g/(MeV·cm^2)].

Calculations were cross-checked by numerical integration using NIST tables accounting for NOvA LS composition $k_B = 1.13$ +/- 0.07 [g/(MeV·cm^2)] which is in a good agreement with the MC fit [10.k.4].

10.k.3 Scintillator properties.

We exploit the idea to measure the volume with respect to distilled water in a thin-mouth tube with a scale at different temperatures. Water density was carefully checked by Density Meter DMA 5000 M (precision is 10^{-6}, temperature stability is 10^{-3}C). Volume uncertainty is about 2.5ul/10ml = 0.03%. Then by knowing a volume of the tube one can precisely measure the density of another liquid (NOvA scintillator). We use a thermal-chamber to adjust stable temperatures to different values. Results are presented in Table 10.k.1.

T *C	10	15	20	23	25	30
Rho	0.8603	0.8575	0.8547	853	0.8519	0.8491

Table 10.k.1. Scintillator density Rho dependance vs Temperature T.

10.k.ref References

[10.k.1] Birks J. B. The Theory and Practice of Scintillation. Counting, Pergamon Press, 1964.
[10.k.2] Kharzheev Yu.N. Scintillation counters in modern experiments at high-energy physics. Physics of elementary particles and atomic nuclei. Issue 4. Dubna : JINR, 2015.
[10.k.3] Birks J. B. Scintillation counters, 1955.
[10.k.4] A.I.Antoshkin, Test bench for measurements of scintillators (NOvA, LAB-based etc.) properties, Internal technote, DocDB # 31369.

10.l Future plans for NOvA scintillator measurements

We are planning to measure the contribution of the cherenkov light in the NOvA LS which is important for the NOvA detectors simulation. Aiming the task we are going to build up a new scintillation stand (see fig.10.l.1). The general idea is to use monochromatic γ-source (ex. ^{137}Cs). A photon scatters in the cuvette by a certain angle dissipates the certain energy by producing an electron. By selecting angles of γ-qunta with a second detector (in coincidence) one can measure scintillator response on different electron's energies. For NOvA LS with refractive index of n=1.46 the cherenkov threshold is about 190 keV. By means of analyzing scintilator's responses on energies below and above the threshold we can extract the cherenkov contribution [10.l.1].
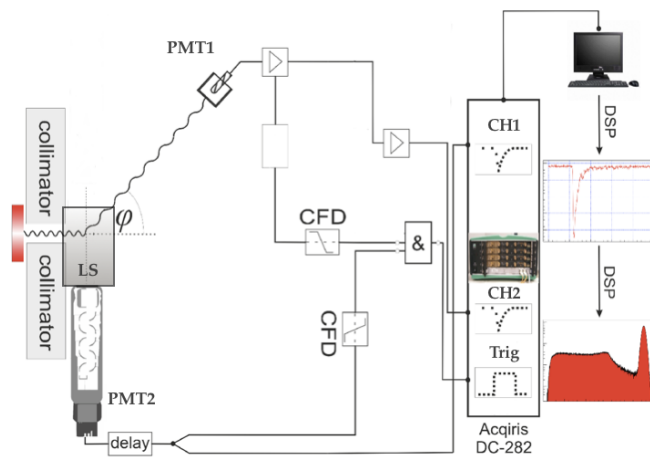

Figure 10.l.1. Schematics of the scintillation stand for Cherenkov light measurements.

We have to prepare a radioactive premise to perform this measurement. Purchase PMTs, NaI-crystals, radioactive sources and materials.

10.l.ref References

[10.l.1] N.Anfimov et.al, Nova Benchmarking at JINR, Internal talk, DocDB # 43461.

10.m Light collection system for the DUNE Liquid Argon Near Detector

10.m.1 Introduction

DUNE is a next-generation accelerator neutrino oscillation experiment [10.m.1, 10.m.2]. DUNE will utilize an intense beam of predominantly muon (anti)neutrinos produced at Fermilab, will sample the unoscillated beam on the Fermilab site, 574m from the proton target and 62m underground, and then will sample the oscillated beam 1300km away and 1.5km underground, at the Sanford Underground Research Facility (SURF) in South Dakota, using four 10 kt liquid argon (LAr) target modules. By using LAr time projection chambers (TPCs), DUNE benefits from the exquisite precision to look at the particles escaping the nucleus, and measuring the neutrino energies with unparalleled accuracy. An extensive research and development (R&D) program is currently ongoing to deliver detectors capable of fulfilling DUNE's physics goals.

As the DUNE Far Detectors have LAr targets, there will also be a major LAr component for the DUNE near detector (ND) suite, in order to minimize cross section and detector systematic uncertainties for oscillation analyses [10.m.1, 10.m.2]. However, the intense neutrino flux and high event rate at the ND makes traditional, monolithic, projective wire readout TPCs unsuitable, which has motivated a program of R&D into a new LAr TPC approach, suitable for such a high rate environment, known as ArgonCube [10.m.3] (see fig 10.m.1). ArgonCube utilizes detector modularization (7x5 modules) to improve drift field stability, reducing high voltage (HV) and the LAr purity requirements; it uses a pixelized charge readout [10.m.4, 10.m.5], which provides unambiguous 3D imaging of particle interactions drastically simplifying the reconstruction; and new dielectric light detection techniques with Light Collection Modules (LCMs), which can be placed inside the field cage to increase light yield, and localization of light signals.
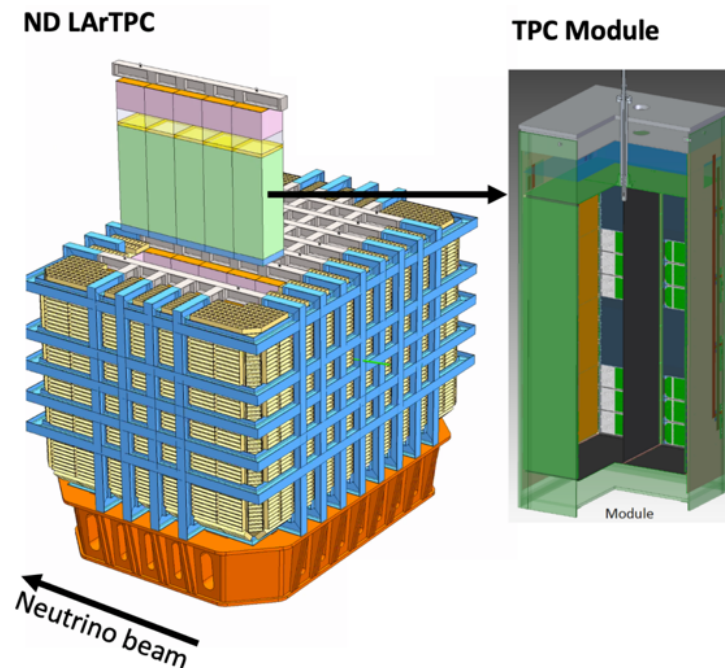

Figure 10.m.1: Illustration of the Near Detector modularized Liquid Argon TPC

With the various technological developments demonstrated with small-scale TPCs, the next necessary step in the ArgonCube program is to demonstrate the scalability of the pixelized charge readout and light detection systems, and to show that information from separate modules can be combined to produce high quality event reconstruction for particle interactions. To that end, a mid-scale (1.4m×1.4m×1.2m) modular TPC, dubbed the ArgonCube 2x2 Demonstrator (fig.10.m.2), with 4 independent LAr TPC modules arranged in a 2x2 grid has been designed, and is currently under construction in Bern. We propose moving the ArgonCube 2x2 Demonstrator into the NuMI on-axis neutrino beamline at FNAL, to serve as the core of a prototype for the ND.

10.m.2 ArgonCube 2x2 Demonstrator module

The basic principle of ArgonCube is a detector made of self-contained TPC modules sharing a common cryostat. Each module is made of a rectangular box with a square footprint and a height to be optimized in order to meet the physics goals and/or sensitivity constraints. The ArgonCube 2x2 Demonstrator module will be housed within an existing liquid nitrogen (LN2)-cooled and vacuum-insulated cryostat, shown in Figure 10.m.2, which is ~2.2 m in diameter, and ~2.8 m deep, for a total volume of ~6 m . The size of the cryostat sets the dimensions of the modules for the demonstrator. The square base of each module will be 0.67 m × 0.67 m, and the height will be 1.81 m. This makes the modules comparable in size to, but slightly smaller than, the proposed ArgonCube DUNE ND modules, which will have a base of 1 m × 1 m, with a 3.5 m height; optimized in order to meet the physics goals and sensitivity requirements.

Individual modules can be extracted or reinserted into a common LAr bath as needed, as is illustrated in Figure 10.m.2. This feature will be demonstrated during a commissioning run at Bern, but is not intended to be part of the detector engineering studies in the MINOS-ND hall. Pressure inside the modules is kept close to the bath pressure putting almost no hydrostatic force on the module walls, which allows them to be thin, minimizing the quantity of inactive material in the walls. The purity of the LAr is maintained within the modules, independent of the bath, as will be described below. The argon surrounding the modules needs not meet as stringent purity requirements as the argon inside. Under normal operation conditions all modules are inserted with only clearance distances of 1.5mm between modules. Cooling power to the bath is supplied by LN2 circulated through lines on the outer surface of the inner cryostat vessel.
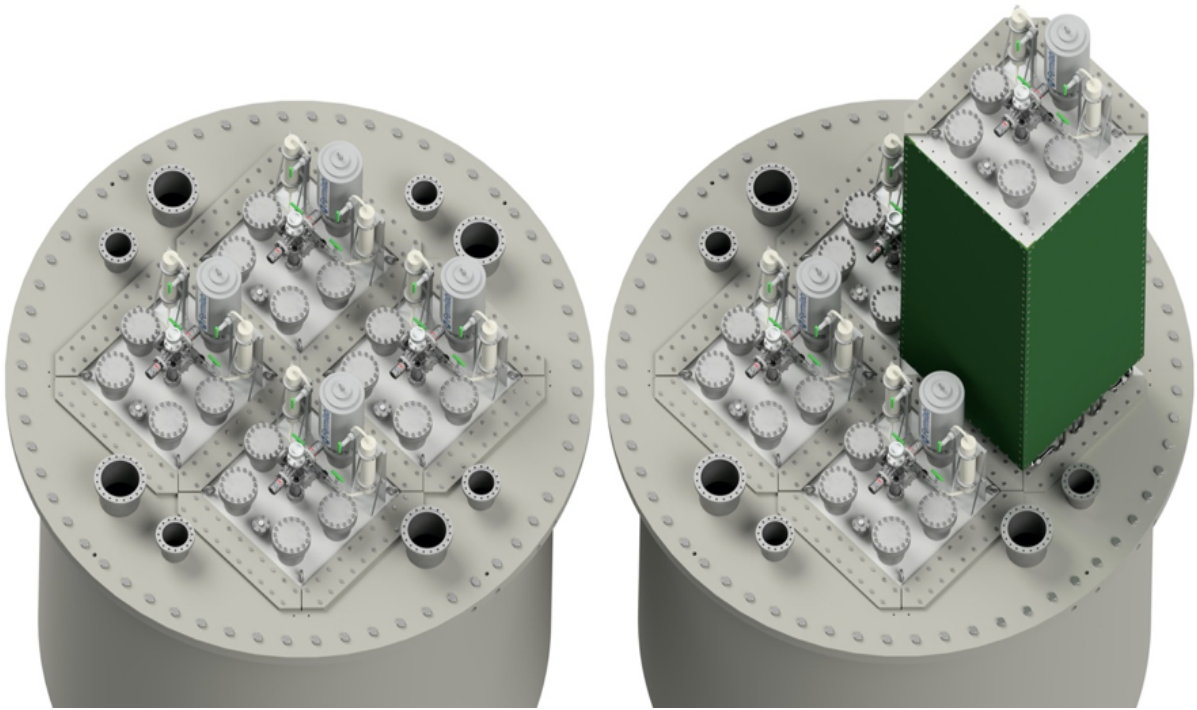
Figure 10.m.2. Illustration of the ArgonCube 2x2 Demonstrator module. The four modules are visible, with one of them is partly extracted, on the right.
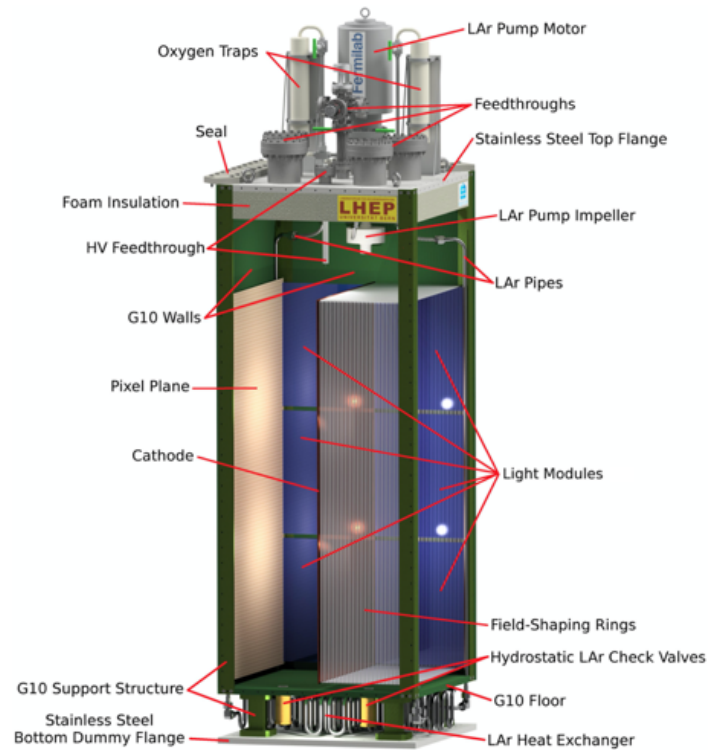

Figure 10.m.3. Cutaway drawing of a 0.67 m × 0.67 m × 1.81 m ArgonCube module for the 2x2 Demonstrator module.

A cutaway drawing of an individual 2x2 module is shown in Figure 10.m.3. The side walls of each module are made from 1 cm G10 sheets, to which the resistive field shell is laminated. G10's electromagnetic radiation length (X0 = 19.4 cm) and hadronic interaction length (λint = 53.1 cm) [10.m.6] are both comparable to LAr (14.0 cm and 83.7 cm respectively), making G10 structures in LAr almost transparent for passing particles, allowing for a performance comparable to a monolithic detector. G10 provides a strong dielectric, capable of 200 kV cm^{-1} at 1 cm thick [10.m.7]. This dielectric shielding eliminates the need for a clearance volume between the TPCs and the cryostat, while also shielding the TPC from field breakdowns in a neighbouring module.

The module is split into two TPCs by a central cathode made of an additional resistive layer on a G10 substrate. The segmented drift length does not require a high cathode voltage, and minimizes stored energy. For the 2x2 module footprint of 0.67 m × 0.67 m and an electric field of 1 kV cm^{-1} a cathode potential of only 33 kV is required. Operating a LArTPC at this voltage is feasible without a prohibitive loss of active volume [10.m.8].

The detector is oriented such that the cathodes are parallel to the beam. This minimizes the load on the readout electronics by spreading the event over more channels and reducing the required digitization rate for hit channels. In turn, this reduces the heat load generated at the charge readout and prevents localized boiling.

ArgonCube offers true 3D tracking information using the LArPix cryogenic ASIC [10.m.5] pixelated charge readout. LArPix ASICs amplify and digitize the charge collected at single-pixel in the cold to mitigate the need for analogue signal multiplexing, thus producing unambiguous 3D information. 64 pixels can be connected to a single LArPix ASIC. The baseline design is for the 2x2 is a 5 mm pixel pitch, corresponding to 40k pixels/m^2. Pixelated anode planes are located on the two module walls parallel to the cathode, each plane is 1.2 m × 0.6 m^2. The total area across all four modules is 5.8m2, which corresponds to 232k pixels. The readout electronics utilize two FPGA boards per module, connected to a single Ethernet switch. It should be noted that the pixel pitch may be reduced as prototypes develop, but this can be accommodated in the readout design.

The charge readout window (drift time) of 137μs is long compared to the 10μs [10.m.9] beam spill length in the NuMI and LBNF beams. For 1 MW beam intensity, the expected rate of neutrino interactions at the DUNE ND is roughly 0.5 per spill per ArgonCube module. With LArPix, reconstruction issues are greatly simplified compared to a projective readout TPC. Tracks and connected energy deposits will frequently overlap in any 2D projection, but can be easily resolved with a full 3D readout. However, disconnected energy deposits, such as those from photon conversions or neutron interactions in the detector, cannot be easily associated with a specific neutrino interaction. This problem can be solved by incorporating fast timing information from the prompt scintillation light emitted in LAr. The module's opaque cathode and walls contain scintillation light within each TPC (half module), improving the detection efficiency of the prompt component of the scintillation light. Furthermore, attenuation due to Rayleigh scattering, 6.6×10^{-1} m in LAr [10.m.10], is mitigated by the maximum photon propagation lengths of only 0.3 m. It is desirable to have a large area photon detection system to maximize the utility of scintillation light signals in the detector. To minimize any dead material within the active volume, it is also desirable that the light detection be as compact as possible. The solution pursued for the ArgonCube effort is Light Collection Modules (JINR) or ArcLights (Bern University) [10.m.11], which is a very

compact dielectric light trap that allows for light collection from a large area, inside high electric fields.

10.m.3 Light Detection

10.m.3.1. Liquid Argon Scintillation

Liquid noble gases, in particular, argon and xenon are widely used scintillator materials in particle detectors aiming to detect rare events. Due to their high scintillation efficiency, the possibility to be cleaned to a high level of purity, and their scalability to large detector volumes they are a very attractive detector medium for neutrino physics. Pure liquid argon scintillates almost exclusively in the vacuum ultraviolet wavelength region. The scintillation of pure liquid argon is restricted almost exclusively to an intense emission band in the vacuum ultraviolet (127 nm peak wavelength, 7.4 nm full width at half maximum).
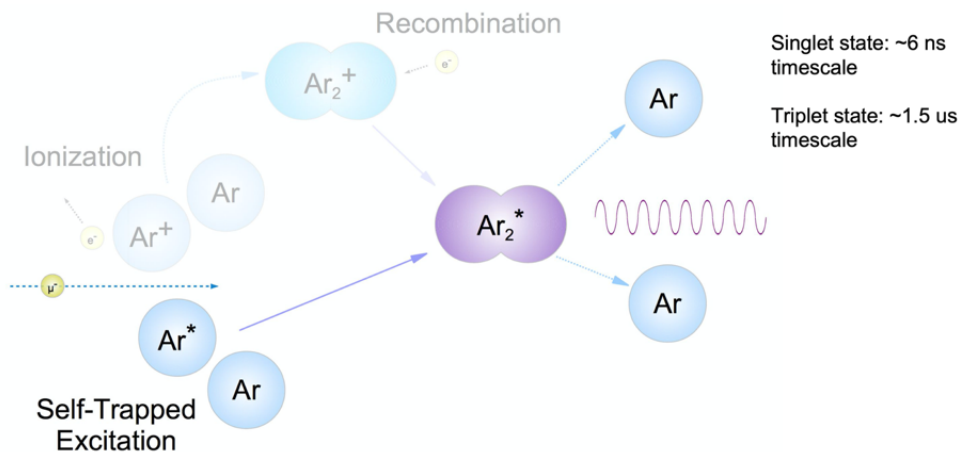

Figure 10.m.4. Illustration of the Liquid Argon scintillation mechanism

An incident particle which interacts with argon atoms leads either to ionized or excited atoms Ar^* (fig. 10.m.4). If the gas is very dilute, there is a low density of argon atoms and the optical transition probability of the excited atoms to undergo a transition to the ground state is high compared to the collision probability with another argon atom. Therefore, the excited atoms decay back to the ground state thereby emitting the characteristic resonance emission [10.m.12] at wavelengths of 104.8 and 106.7 nm [10.m.13]. Increasing the density leads to an increasing collision rate of excited argon atoms with atoms in the ground state. This increased collision rate can lead to the formation of strongly bound two-atomic argon molecules which are bound in the excited state ArAr or Ar^*_{-2}. These molecules are called excited dimers or shortly excimers. The excimers exist in two states (singlet $Ar*2[1\Sigma+u]$ or triplet $[Ar*2[3\Sigma+u]$ states). The excimer molecules are formed in different vibrationally excited states before they decay to the ground state ($Ar*2[1\Sigma+g]$). The decay time differs in tree orders of magnitude for singlet (~6 ns - fast components) and triplets (~1500 ns - slow components) excimer states. Transitions near the minimum form the so-called second continuum which is the dominant feature in the emission spectra centered at ~ 127nm (see with a width of 7-10nm (depending also on temperature [10.m.14]) for argon. After the transition to the repulsive ground state the molecule separates into

two neutral argon atoms. This mechanism provides excellent transparency of LAr because of excimers absence in unionized liquid. Light at higher wavelengths (mostly in the near IR) is also produced from transitions between highly excited argon atomic states. The production times of the triplet and singlet states and their production ratio vary with argon density and also depend on the type of projectile, e.g. electron, α-particle or fission fragment. However, the decay times are not affected.

10.m.3.2 Light collection system

The basic principle for Light collection and ArcLight modules is the same. Scintillation VUV-light produced in liquid argon (LAr) must be shifted from 128 nm to visible wavelengths in light detection systems. Light collection systems have employed tetraphenyl butadiene (TPB) coatings which is the most efficient scintillation material excited by VUV light. The emission spectrum of TPB is broad with the peak intensity around 425 nm (violet light). Then re-emitted light is trapped with the second re-emision to green light (see fig. 10.m.5).

ArcLight (fig.10.m.5 left) module which is developed by Bern University uses the ARAPUCA principal of the light trapping. The general idea is to let the violet light go in the shifter bulk and produce a reflective coating for the green light on all sides but the photosensor window. On the TPB side a dichroic filter which is transparent for the violet light and reflective for the green is used. All other sides are coated with conventional mirror film. The green light, hence, is trapped may come out from the small windows and readout by Silicon Photomultipliers – SiPM. The current size of ArcLight is 300x300x10 mm^3.
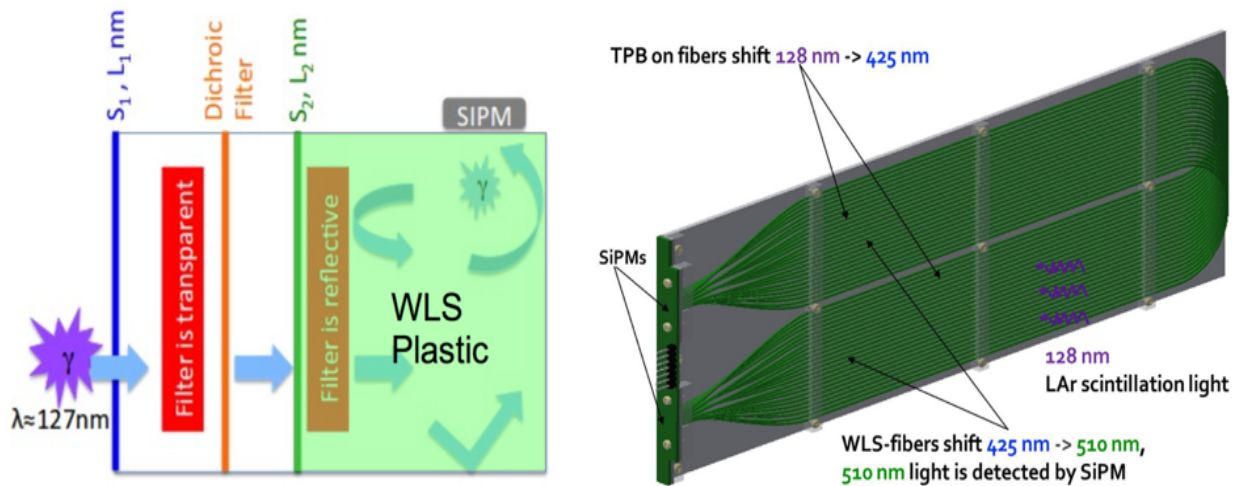

Figure 10.m.5. Two approaches in light detection. Left – ArcLight, Right – LCM.

The Light collection module (LCM) prototype is a frame cantilevered by the PVC plate that holds WLS-fibers which are bent into two bundles readout with two SiPMs light sensors. (Fig 10.m.5. Right). Fibers are grouped and held by spacer bars with holes which are tightened to the PVC plated by means of polycarbonate screws in order to unify thermal contraction of different materials. The PVC plate with WLS-fibers are coated with TPB that re-emit a VUV liquid argon light (127 nm) to the violet (~425 nm) which is shifted inside multi-cladding ∅=1.2 mm Kuraray Y-11 fibers to the

green light (~510 nm), then trapped by total internal reflection and finally, transported to the SiPMs. The current size of LCM is 100x300x10 mm^3.

The SiPMs are put on the Printed Circuit Board (SiPM PCB). The PCB with mounted SiPMs is shown on fig. 6 left. This PCB is attached to the LCM by means of polycarbonate screws. On the other side the PCB has 2 double-pin connectors to plug it to the Readout PCB (E-PCB) The E-PCB drawing is shown on fig. 6 right. Each E-shape supports 3 LCMs (6 SiPMs) or 1 ArcLight module (6 SiPMs). To gain signal from the SiPM a LMH6624 preamplifier from Texas instruments is used. The E-PCB contains 6 preamplifiers to provide signal transition through the long coaxial signal line (up to 2 m). Each preamplifier dissipates around 30-40 mW in a range of 1 V and BW of ~30 MHZ (~10 ns rise time). Such an energy dissipation leads to LAr bubbling and requires E-PCB displacement outside the active volume behind the anode pixel plane. Since there are two TPC semi-chambers in each module we need left and right E-PCB (fig 10.m.6. right) to provide consistent mechanical mock-up.
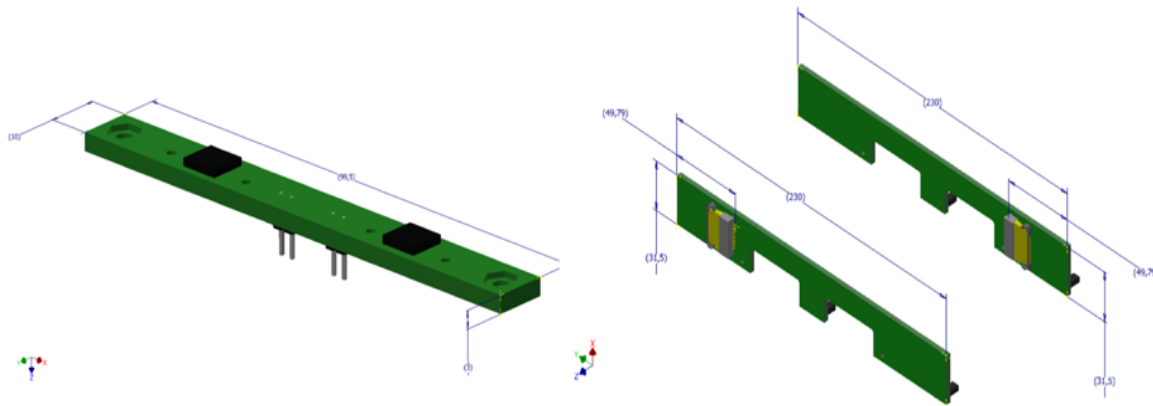

Figure 10.m.6. General view of the SiPM PCB and the E-PCB.

To connect all 16 E-PCBs in a single TPC-module we use 4 cables of 87 inches (2,2 m), 4 cables of 80 inches (2,0 m), 8 cables of 60 inches (1,5 m). Each cable is a cable assembly of 20 micro-coaxial cables FCF8-20-01-L-XX.XX-S type where XX.XX - is a length specified in inches. Cables are plugged into the E-PCB by means of FCS8-20-01-L-S-A-TR connector (see fig.10.m.6 right). On another side (at feed-through cryostat panel) cable is interfaced with the same FCS8-20-01-L-S-A-TR connector. Both cables and connectors are manufactured by Samtec company.

10.m.3.3   SiPM power supply

There are two possibilities to bias SiPM with reverse voltage. Schematically for some particular SiPM it is shown fig.10.m.7. All values of the component are used just for demonstration. The first approach is to use unipolar power and apply voltage from one side fig.10.m.7 (left) and the second one applies bipolar voltage from different sources from both sides fig.10.m.7 (right).
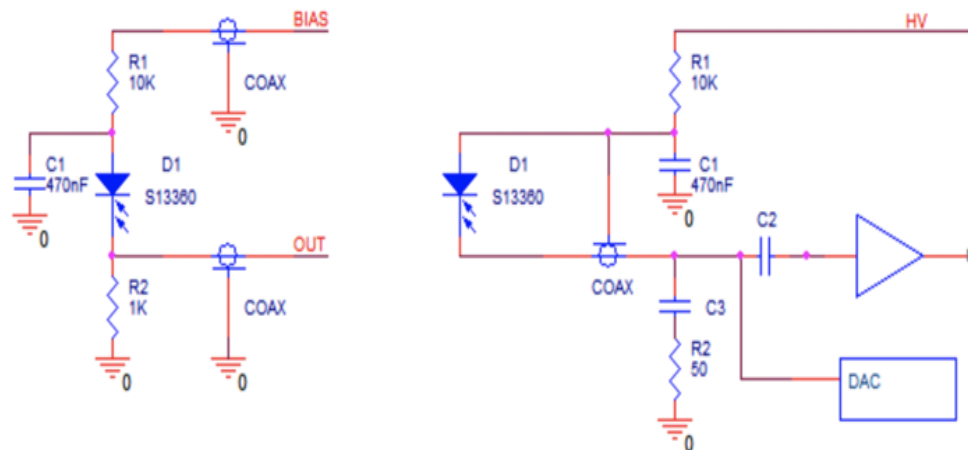
Figure 10.m.7. Schematics of a SiPM biasing. All values of the component are just for indication. Left - biasing from one side with unipolar voltage source. Right - biasing from two sides with two sources.

The first approach has a great advantage of DC-coupling for the readout circuit. The second one needs AC-coupling and brings additional nuisances for high loads and long pulses. HVSys company [2] introduced power (bias) systems of detectors whose architecture is aimed at low cost ($\approx (20-30)$\$/ch) along with absolute sufficiency of their characteristics.

1.   System modules serving up to 127 biasing cells. The system module includes a power supply and microcontroller. It is connected to the mains, and through the communication line is connected to the host computer. Devices constructed as a desk-top design are housed in plastic cases or as a module in the standard of EUROMECHANICS-6U 20 mm width.

2. A system bus that connects system modules to high-voltage cells. The system bus is made of a flat cable containing 10 lines located with a step 1.27 mm (0.050") and IDC connectors.

3. Multichannel cells generating high voltage for detectors biasing. They are made as a small size box or printed circuit board incorporating a connector for connection to the system bus and an output connector to the detector.
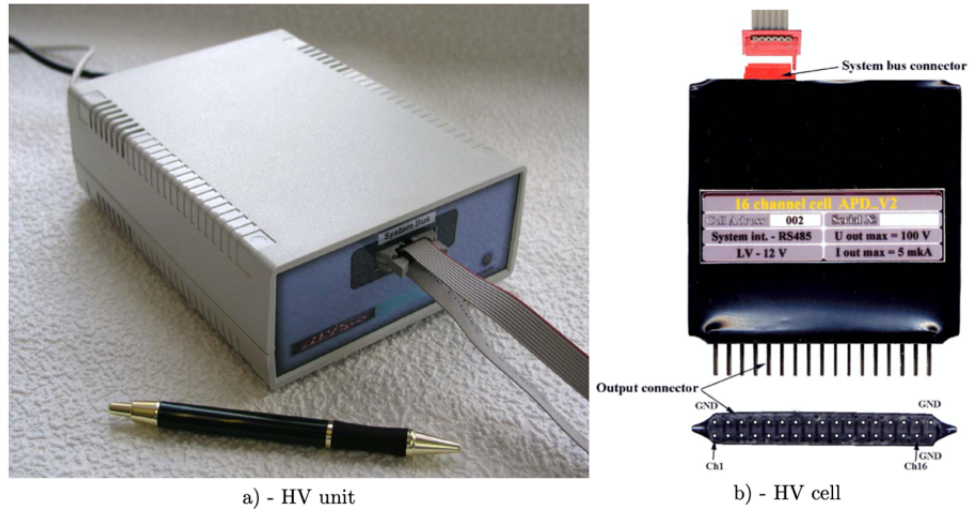
a) - HV unit

b) - HV cell

Figure 10.m.8. SiPM power supply HV-sys company

Following the second approach fig. 10.m.7(right) we develop a prototype by using 16 channel Digital-to-Analog Converters (DAC) which can produce voltage up to 40V (Texas Instruments DAC81416) see. Fig.10.m.9. All 16 channels share a common current of 25 mA. Each channel supplies a single SiPM array with adjustable voltage within 16 (or 12) bits of dynamic range ($\pm$1V, $\pm$2.5V, $\pm$5V, $\pm$10V,$\pm$20V, 40V). On another side we supply all SiPM with single voltage in order to add bias to SiPM operation point. Each of DAC is controlled by a micro-PC via SPI interface. Using this schematics we are able to control common current and cannot monitor each array individually. Main advantage of such schematics is a very low cost $\approx (5-10)$\$/ch.

b) - DAC81416EVM by TI
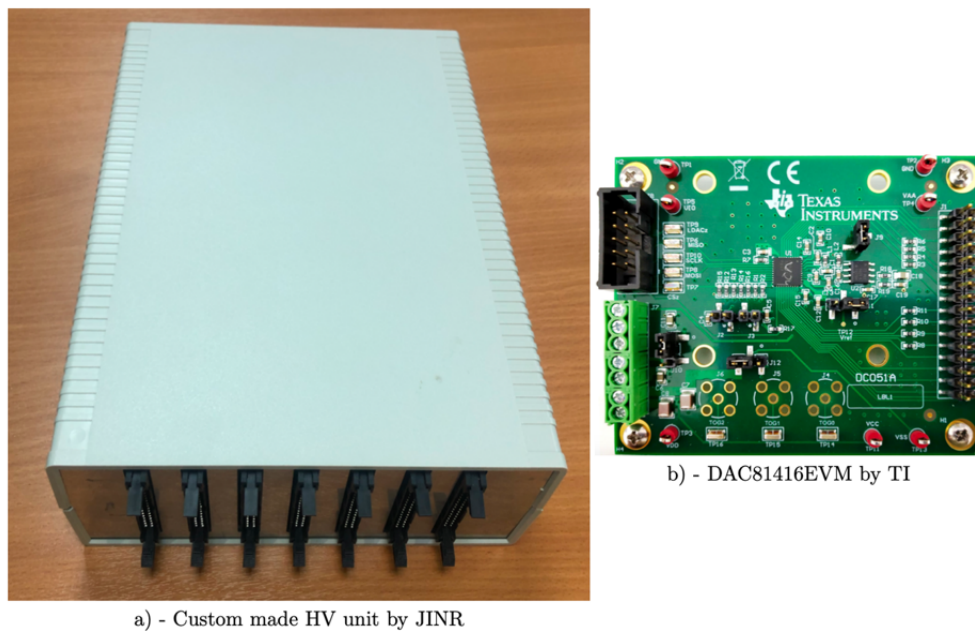
a) - Custom made HV unit by JINR

Figure 10.m.9. 7x16 modules prototype of SiPM power supply based on Texas Instruments DAC

We also develop a slow control software prototype which allows us to adjust voltage at each DAC pin. This software is split by two parts. First is a demon (resident program), which continuously queries DAC and take/put parameters into MySQL database. Second is written on Java-script and presents parameters given in the database. It is installed on Apache server and could be accessible from everywhere via internet browser. The software GUI is shown in fig.10.m.10.

Figure 10.m.10. Software GUI for the JINR power supply prototype.

10.m.3.4 Front-End

On the warm side of the cryostat we place a metal box which is a block of driver amplifiers AD8139 that interfaces unipolar signal from coax cable to differential para-phase signal on screened ribbon twisted pair cable. We are also going to put six DAC81416 16-channel 16-bit boards and Thinker board microPC to control SiPM power via SPI interface. 16 micro coaxial cable assemblies are plugged at the warm side of the feedthrough flange to the standard FCS8-20-01-L-S-A-TR connector. In the metal box we split assembly and solder it to the six 40 pins connectors. Three are for signals and another three for SiPM power supply. From the metal box 3 bundles of ribbon twisted pair cables are going to the rack with ADCs. In the rack upstream to ADCs a 19" unit with VGAs (Variable Gain Amplifiers) - LMH6521-type is placed to adjust dynamic range from Single photoelectrons (SiPM calibration) to high amplitude MIP signals. To digitize analogue signals from SiPM we are using ADC64 100 MHz 10-bit 64-channel (differential signals, full range ± 1.25 V) ADC produced by JINR VBLHEP electronic group(fig.h.11)[10.m.3]. This ADC streams UDP/TCP data packets via M-link MStream protocol that provides 10 Gbps optical link. To readout ADCs we purchase a network PCI-E card with two SFP+ transceivers, so we need a PC with fast PCI-E bus and fast disk drive. We also purchased 14 SFP+ ports 10 Gbps fast D-Link Switch to scale up to 14 ADCs boards (896 channels). The ADCs could be synchronized via White Rabbit protocol with 1 ns timestamp. For the prototype test we synchronized them by means of splitting sync-signal using one channel in each of two ADCs.
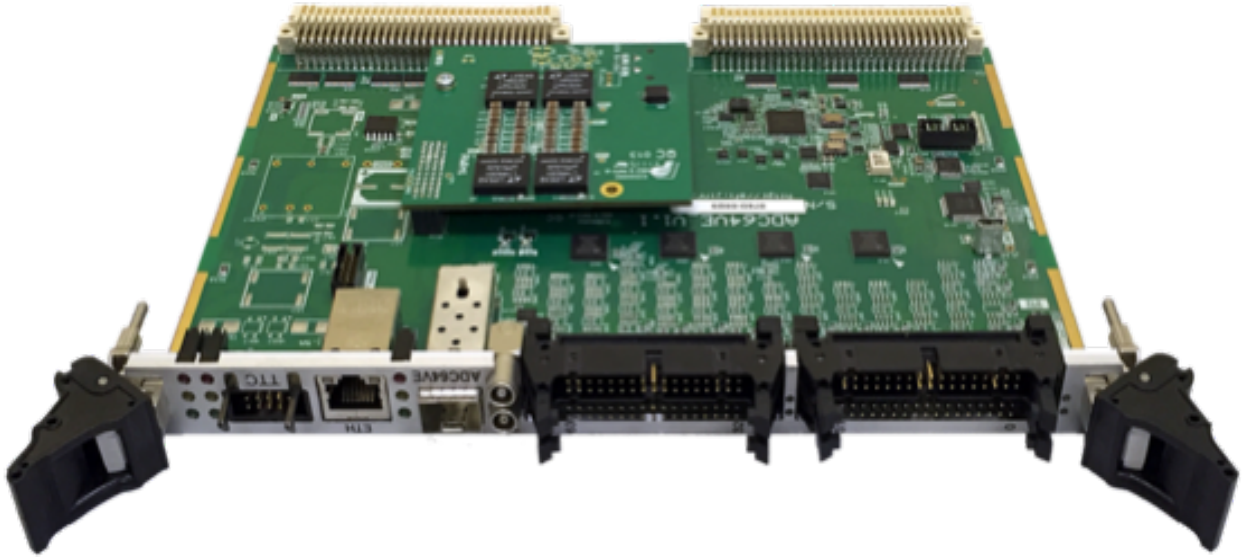
Figure 10.m.11. JINR ADC64 100 MHz 10-bit 64-channel prototype.

10.m.4 Tests of the Light Collection System

To perform preliminary tests with the light collection system a dedicated setup that allows cryogenic studies was designed and produced at DLNP JINR. The general view and schematic of the setup is shown on figure 10.m.12. The setup allows conducting relative studies either at room conditions or at cryo temperatures. It consists of a cylindrical cryostat with a special flange that works as a feedthrough for cables and also holds a rod with the light detector together with the alpha particle source (see fig.10.m.12). The DAQ, cables and electronics that were used in the tests are described above.
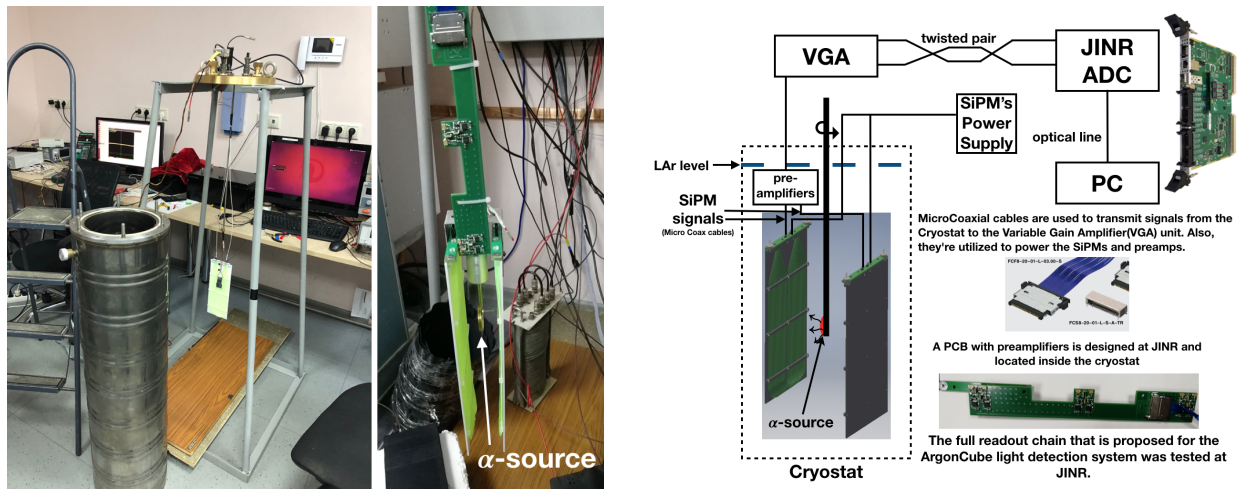

Figure 10.m.12. JINR setup for the light collection system study. Left - general view of the setup. Right - schematic view

First preliminary studies were dedicated to get the performance of the light collection modules at liquid argon temperatures and to study LCMs with different WLS-fibers coatings(TPB,bis-MSB). Performed tests show that LCM performance at cryo temperatures is reliable, module construction is rigid and the coating technique by the brush painting is preferable. As for the different dopants, the TPB coating is 40% more efficient in comparison with the bis-MSB. The absolute photon detection efficiency of the light collection module with TPB-coating is a 1% level. These first tests were performed using the alpha particle source and cosmic muons. By using the LED source we got the calibration spectrum which is shown in figure 10.m.13. This measurement gives the absolute value of the spectrometric channel in photoelectrons, thus, allows to get the LCM PDE thereafter. Average physical signals' waveform of alpha source and cosmic muons that were obtained during the studies in liquid argon are depicted in figure 10.m.14. Also, in the LAr tests a time spectra between the SiPM signal of the LCM and trigger signal were drawn(see fig.10.m.15). Future studies in our laboratory and upcoming tests at Bern University allow us to get comprehensive results of the whole light collection system including ArcLight modules, DAQ, and electronics.
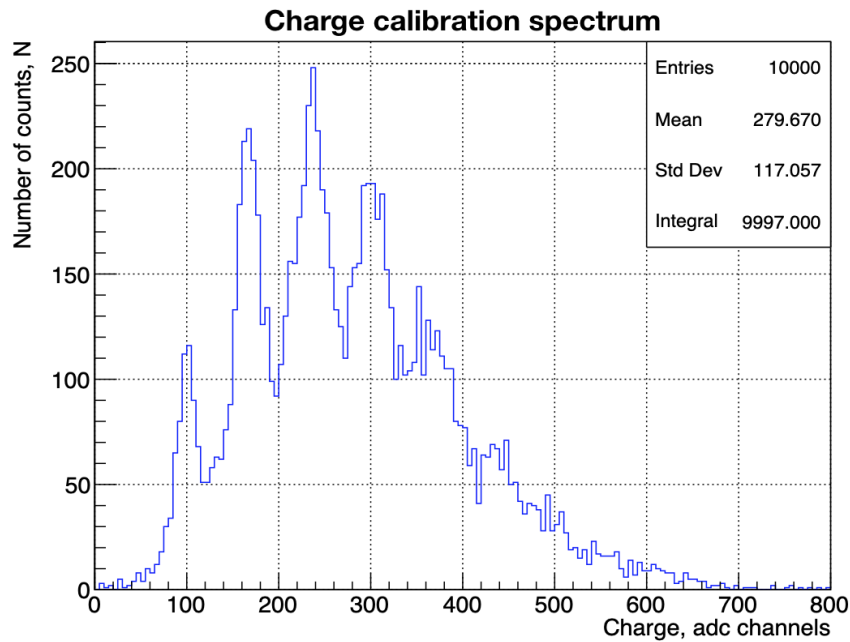

Figure 10.m.13. Typical calibration charge spectrum from the LCM using the LED source.
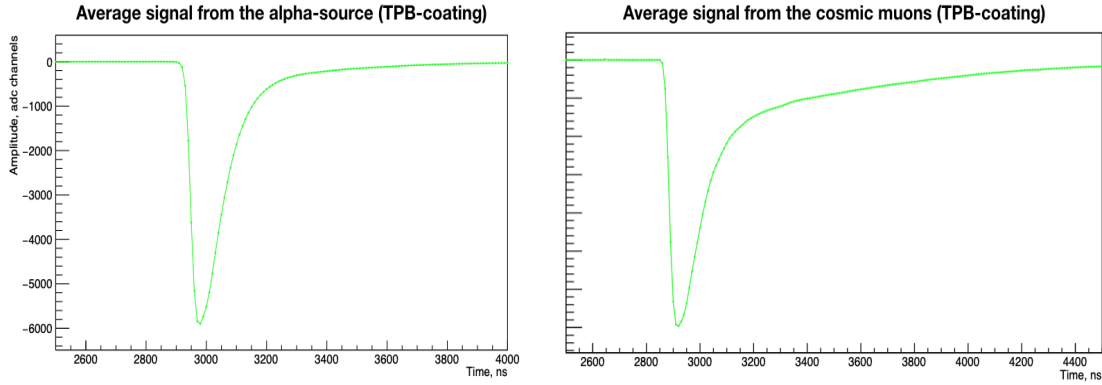
Figure 10.m.14. Waveforms of the signals from the light collection module during performance tests in liquid argon from alpha-particle source and cosmic muons.
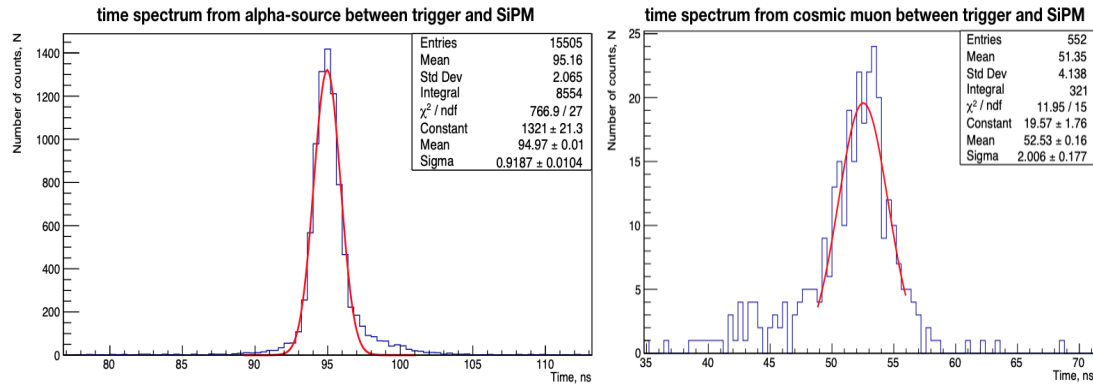

Figure 10.m.15. Time spectra obtained in LAr test from alpha-source and cosmic muons.

10.m.5   Future plans.

Currently, we have prepared all the components for the Light system for an upcoming test of a single TPC module which is planned and will be held at Bern University this summer. We require resources to prepare the 2x2 demonstrator test which will be held at Fermilab NuMi beam line next year. It is necessary to provide 384 of readout channels for this test: 7 ADC, 4 Power supply units, 384 SiPMs, preamplifiers, 384 VGAs, 192 Light modules.

An integration with the charge readout system requires data synchronization. Pursuing this goal we have to negotiate with VLHEP electronic group to implement PPS (pulse per second) or White Rabbit time synchronization module into the ADC.

We also plan to make a simulation on improvement of time resolution by optimizing impedance of preamplifiers and changing ADC with faster sampling frequency. This timing can improve neutrons identification in antineutrino interactions.

To identify all physical signal delays: cables, amplifiers, ADCs we must build up a time calibration system based on a fast light source. This system introduces light fibers inside the TPC chamber that

deliver light from a picosecond laser. Another approach is to use physical calibration by using cosmic or beam muons that trigger fast scintillation counters.

Developing of data acquisition software for data taking: data format, concatenation with charge readout, data packets synchronizing. Data monitoring: data sampling and presenting online results for system operation and data quality check.

We are also developing a technology of the shifter covering trying different dopants (TPB, bis-MSB, etc) and methods of the application (painting, spraying, evaporations ,etc). To increase detection efficiency and reliability of the light shifting we are trying to develop technology based on uncladded (naked) fiber with shifting dopants which require money for side-contracts.

Development of the longer modules up to 50 cm for the DUNE ND LAr TPC which has larger TPC modules with the size of 1000x1000x3500 mm: simulation of a new mechanical mock-up, optimization of the light collection (different dopant concentration in fibers), This might also require an upgrade of the cryogenic stand: new cryostat

Production of the light system for the DUNE ND LAr TPC which requires purchasing of materials, production and assembly for ~ 4000 (8000) 50 cm LCM modules: 160 (320) km of fibers, 16 k SiPMs, 16 k channels of Front-End Electronics and Power Supplies, 256 ADC modules. Electronic items might need readout optimization and channel reduction which requires additional studying and simulation.

10.m.ref References

[10.m.1] R. Acciarri et al. "Long-Baseline Neutrino Facility (LBNF) and Deep Underground Neutrino Experiment (DUNE) Conceptual Design Report Volume 1: The LBNF and DUNE Projects". In: (2016). arXiv: 1601.05471 [physics.ins-det].
[10.m.2] R. Acciarri et al. "Long-Baseline Neutrino Facility (LBNF) and Deep Underground Neutrino Experiment (DUNE) Conceptual Design Report Volume 2: The Physics Program for DUNE at LBNF". In: (2016). arXiv: 1512.06148 [physics.ins-det].
[10.m.3] C. Amsler et al. ArgonCube: a novel, fully-modular approach for the realization of large-mass liquid argon TPC neutrino detectors. Tech. rep. CERN-SPSC-2015-009. SPSC-I-243. Geneva: CERN, Feb. 2015. url: https://cds.cern.ch/record/1993255.
[10.m.4] J. Asaadi et al. "First Demonstration of a Pixelated Charge Readout for Single-Phase Liquid Argon Time Projection Chambers". In: (2018). arXiv: 1801.08884 [physics.ins-det].
[10.m.5] D. A. Dwyer et al. "LArPix: Demonstration of low-power 3D pixelated charge readout for liquid argon time projection chambers". In: (2018). arXiv: 1808.02969 [physics.ins-det].
[10.m.6] W.-M. Yao et al. "Review of Particle Physics". In: Journal of Physics G 33 (2006), pp. 1+. url: http://pdg.lbl.gov.
[10.m.7] E. Tuncer et al. "Electrical Insulation Characteristics of Glass Fiber Reinforced Resins". In: IEEE Transactions on Applied Superconductivity 19.3 (June 2009), pp. 2359–2362. issn: 1051-8223. doi: 10.1109/TASC.2009.2018748.
[10.m.8] M. Zeller et al. "First measurements with ARGONTUBE, a 5m long drift Liquid Argon TPC". In: Nuclear Instruments and Methods in Physics Research Section A: Accelerators, Spectrometers, Detectors and Associated Equipment 718.Supplement C (2013). Proceedings of the

12th Pisa Meeting on Advanced Detectors, pp. 454–458. issn: 0168-9002. doi: https://doi.org/10.1016/j.nima.2012.11.181. url: http://www.sciencedirect.com/science/article/pii/S0168900212015288.

[10.m.9] P. Adamson et al. "The NuMI Neutrino Beam". In: Nucl. Instrum. Meth. A806 (2016), pp. 279–306. doi: 10.1016/j.nima.2015.08.063. arXiv: 1507.06690 [physics.acc-ph].

[10.m.10] E. Grace and J. A. Nikkel. "Index of refraction, Rayleigh scattering length, and Sellmeier coefficients in solid and liquid argon and xenon". In: Nucl. Instrum. Meth. A867 (2017), pp. 204–208. doi: 10.1016/j.nima.2017.06.031. arXiv: 1502.04213 [physics.ins-det].

[10.m.11] M. Auger et al. "ArCLight—A Compact Dielectric Large-Area Photon Detector". In: Instruments 2.1 (2018), p. 3. doi: 10.3390/instruments2010003. arXiv: 1711.11409 [physics.ins-det].

[10.m.12] A. Fedenev et al. "Applications of a broadband electron-beam pumped XUV radiation source". J. Phys. D Appl. Phys. 37 1586, 2004.

[10.m.13] Kramida, A., Ralchenko, Yu., Reader, J. and NIST ASD Team. "NIST Atomic Spectra Database (version 5.2)". National Institute of Standards and Technology, Gaithersburg, MD. online: http://physics.nist.gov/asd, 2014.

[10.m.14] T. Heindl et al. "Table-top setup for investigating the scintillation properties of liquid argon". JINST 6 P02011, 2011.